HIGH TEMPERATURE CONDUCTIVITY OF GROWN STANNIC OXIDE SINGLE CRYSTALS

By

HOWARD FRANKLIN KUNKLE JR.

Bachelor of Arts
Washington and Jefferson College
Washington, Pennsylvania
1959

Master of Science
Oklahoma State University
Stillwater, Oklahoma
1961

Submitted to the Faculty of the Graduate School of
the Oklahoma State University
in partial fulfillment of the requirements
for the degree of
DOCTOR OF PHILOSOPHY
May, 1966

HIGH TEMPERATURE CONDUCTIVITY OF GROWN STANNIC OXIDE SINGLE CRYSTALS

Thesis Approved:

Thesis Adviser

Dean of the Graduate School

This research was supported by the

Office of Naval Research under

Contract No. Nonr-2595(01)

ACKNOWLEDGMENT

The author wishes to express his deepest gratitude to Dr. E. E. Kohnke for his patience and guidance throughout the execution of this work, to the Office of Naval Research for sponsoring the research, to the U. S. Department of Health, Education and Welfare for financial aid in the form of an N.D.E.A. Fellowship and to the Oklahoma State University Research Foundation for their administrative assistance. He is also indebted to H. Hall and W. Adkins for their help with the design and construction of experimental equipment, to Dr. J. Yahia and Dr. J. E. Houston for their helpful suggestions and stimulating discussion, and to Dr. R. Freeman for the loan of equipment. And finally the author wishes to recognize his wife, Carol, as his inspiration and for her labor in typing and proofreading.

TABLE OF CONTENTS

LIST OF TABLES

LIST OF FIGURES

CHAPTER I

INTRODUCTION

Metal Oxides

Although a vast amount of experimental work has been done on metal oxides, there still exists considerable confusion as to their fundamental electrical properties. This is understandable under the circumstances since overall sample preparation of oxides is difficult and the effects of past thermal and mechanical treatment are increasingly recognized as playing a significant role in property determination. Past investigations have been scattered over many forms of specimens, i.e., pressed powders, sintered ceramics, polycrystalline thin films, crystalline thin films, natural and synthetic single crystals. Reviews of typical work can be found in articles by Verwey[1] and Gray[2,3]. It now seems reasonable to hope that with refined growth techniques providing single crystals of controlled purity, work on oxides in general will soon produce a degree of understanding comparable to that which now exists for germanium and silicon.

In the past decade, efforts in the area of crystal growth have become more fruitful in the oxides as well as in metals, organic semiconductors, and intermetallic compounds. Oxide crystal growth has, in general, properties that distinguish it from other growth and which require special methods as well as equipment. These can be mostly attributed to the fact that oxides have high melting points -- usually

above 1000°C -- making it hard to find materials for crucibles and furnaces. Further complications such as partial decomposition or evaporation of the material may rule out certain standard growth techniques. As a result of these difficulties, controlled sample purity has been very hard to attain. However, the list of available research grade oxide crystals has been growing at an accelerated rate.

A significant portion of the electrical work on oxides has been done on TiO_2 [4] and ZnO [5]. Others widely studied have been NiO, CuO, Cu_2O and SiO_2 as well as the refractory oxides. Of particular pertinence to the work described in this report is the fact that another rutile structure oxide, SnO_2 has been studied in a number of sample forms. A review is presented in the next section of this chapter.

In investigating the electrical properties of solids it is found that both the bulk and surface influence the results. It therefore becomes desirable to separate their individual contributions by specific experiments or experimental techniques. One method is to regulate the size of the sample such that different surface-to-volume ratios can be examined. Another is to note the result of gaseous ambient changes which would be expected to have their principal effect on surface-sensitive properties. It has been noted that adsorption of gas on oxide surfaces affects such things as photo-conductive response[6], dark conductivity[7] and catalytic activity[8]. However, most of the work in this area has been done on pressed powders and/or ceramics characterized by large surface areas.

It seems reasonable to suspect that similar surface control of electrical properties can exist in high purity single crystals having large forbidden energy gaps and evidence will be presented later in this report showing that this is true in the case of flux-grown SnO_2 crystals.

Tin Oxide Review

SnO_2, the main constituent of natural tin ore, is the material about which this study is centered. It has a bipyramidal ditetragonal crystal structure with lattice dimensions of a= 4.73727Å and c= 3.186383Å [9]. In its natural crystalline form it is called cassiterite. Thin films have been investigated by Bauer[10] and Fisher[11] who reported resistivities of 10^{-2} ohm-cm, 6 cm^2/volt-sec for Hall mobility and 10^{20} cm^{-3} for free election concentration. From dark conductivity vs temperature their results indicated activation energies of 0.02 ev near 100°K and 0.05 ev near room temperature. Films were also studied by Ishiguro et al.,[12] who reported 10^{-2} ohm-cm, 15-35 cm^2/volt-sec and 10^{19} to 10^{20} cm^{-3} for resistivity, mobility and electron concentration respectively. Le Blanc and Sachse[13] have reported resistivities for sintered samples of around 10^8 ohm-cm at room temperature whereas reports on pressed powders and sintered samples by Guillery[14] gave 10^4 to 10^8 ohm-cm at low temperatures. After spraying $SnCl_4$ onto a hot substrate to get a thin film of SnO_2, Miloslavskii[15] obtained activation energies of 0.12 ev from conductivity data in the temperature range from 150°C to 200°C, room temperature resistivities from 10^2 to 10^3 ohm-cm and electron densities of 10^{19} to 10^{20} cm^{-3}. Foex[16], working with pressed powder prepared by precipitating SnO_2 from an acid solution and heat treating it in air at 1200°C, obtained data that can be analyzed to calculate activation energies of 0.77 ev and a forbidden gap of 4.0 ev in the 20°C to 1200°C temperature range. Kohnke[17] reports values of 0.72 ev for natural crystalline samples of SnO_2 having 10^{14} -10^{15} carriers/cm^3 at room temperature. From the short wavelength cutoff in transmission data he reports a gap of 3.54 ev compared to that gotten from the maximum of the photoconductivity spectral response data

of 3.44 ev by Hurt[18]. Loch[19] compares some of the results of mobility in sintered cold pressed powders with those above showing reasonable agreement.

Work has been limited on synthetic SnO_2 crystals due to lack of samples. Reed and Roddy[20] report having grown sample size SnO_2 using a vapor growth technique. MacAvoy and Marley[21] using a more refined system have produced good quality specimens. The result of their electrical measurements on grown samples will be reserved until later for comparison purposes. Houston[22] has recently completed a comprehensive photoelectronic analysis of flux-grown crystals produced locally. He proposes an energy scheme for as-grown samples, reporting donor levels at 0.21, 0.50, 0.60, 1.00, 1.30 and 1.80 ev below the conduction band and an acceptor level at 0.33 ev above the valence band. He reports also that the 0.21 and 0.50 ev levels are totally compensated whereas the 0.60 ev level appears to be only partially compensated. These results are further substantiated by dark conductivity measurements.

Scope of the Present Study

The results of a threefold investigation are presented in these pages. First, a method of growing sample-size synthetic crystals from a Cu_2O flux is described. Secondly, optical studies were made on these crystals and encompassed transmission measurements from the intrinsic cutoff to 9 microns for comparison with natural samples. A Polarizing microscope was used in conjunction with X-ray studies for identification and orientation purposes. Further optical work was coupled with dark conductivity results to investigate the source of certain transmission spectrum changes in the 6 to 8 micron wavelength range. The third category involves a dark conductivity and thermoelectric power analysis.

Due to the geometry and purity of these crystals, their conductivity was found to be surface controlled. Hence the analysis has been intentionally directed toward emphasizing the effect of surface conditions on the conduction process.

The results and their various implications are used to propose a model explaining the phenomena noted on these crystals. It is so constructed as to include all work to date on flux-grown samples and to serve as a source of suggestions for future work.

CHAPTER II

CRYSTAL GROWTH AND IDENTIFICATION

Background on Oxide Growth in General

In the past ten to fifteen years much effort has been concentrated in the area of crystal growth with the result that it now forms the basis of a rather large industry. As mentioned before, the growth of oxide crystals provides particular challenges which may necessitate the invention of new as well as the remodeling of old growth techniques.

In general, crystal growth can be accomplished by the following methods:

(1) Solid polycrystal ⟶ solid single crystal or polycrystal, of larger grain size

(2) Gas ⟶ Crystal

(3) Melt ⟶ Crystal

(4) Chemical reaction ⟶ Crystal

(5) Solution ⟶ Crystal

An example of method (1) is the grain growth which occurs during the annealing of cold-worked metals. Although it has been used for growth of certain single crystals, this method has not as yet been used for oxides. Some oxides have been grown by a technique classified as either method (2) or (4), which means the mechanism for the growth is not clearly understood. Vapor-phase growth falls into one or the other of these categories. When it involves transport by a carrier gas from the metal to crystal oxides it is definitely (4), but when the starting composition

or nutrient is the oxide itself in polycrystalline form both methods are possible at the same time. Since a good many oxides decompose before they melt, method (4) is particularly inviting because growth in the oxide form is possible in a temperature range in which the oxide is a stable composition.

Of all the methods, (3) is the most desirable since in this case only one constituent is present and the possibilities of contamination are greatly reduced. With oxides this method has its problems since melting points are usually high and crucible materials and furnaces capable of withstanding high temperatures and caustic ambients are at a premium. Recently commercial units for extremely high temperatures have been developed. In cases where induction heating is possible and the crucible can be made of the material to be melted, instrumentation problems are more easily overcome.

If an added component does not interact strongly with the crystal but does permit it to grow at a temperature below its melting point, it is convenient to consider growth from solution, method (5). Such growth may occur at normal temperatures and pressures or, as in hydrothermal crystal growth, at rather high temperatures and pressures. The solvent may be water, an inorganic salt, or an oxide at or above its melting point.

Some of the more prominent modifications of the above named methods will be discussed in terms of their direct applicability to oxide growth. Consider for example the Czochralski, or crystal pulling techniques. This is cataloged under the heading of method (3) and has been used to grow crystals of silicon and germanium, as well as the tungstates and molybdates of calcium and strontium. The apparatus consists of a furnace -- usually induction heated -- a noble metal crucible of platinum, gold or

rhodium holding the melt, and a seed which is normally rotated. The mechanically rotated seed is slowly withdrawn from the melt and since the temperature falls off sharply above the crucible, the liquid freezes on the seed as it is extracted. By controlling a variety of parameters such as temperature profile, pulling rate, pulling direction and melt purity, single crystals can be produced. If it is desired to dope the crystal using this method the oxide of the dopant is added in the proper ratio to the melt. This method has the possibility of an added modification which may have usefulness in the near future; pulling from a flux melt instead of the crystal melt itself. By using the proper combination of solvent to solute, good crystal growth can occur provided the solvent has a high separation coefficient, i.e., provided that it will produce very little contamination.

The second of four methods important for oxides in general and one which will be referred to later with regards to stannic oxide in particular, is that of hydrothermal growth. The essential constituents are the pressure vessel, solvent, seeds, nutrient and furnace. Usually the nutrient has the same composition as the seed and is placed in the bottom of the pressure vessel. The bomb is cylindrical in shape and has seeds hanging along its axis. By controlling solvent concentration, primarily hydroxide solution, and proper temperature gradient along the pressure vessel, the seeds will be washed with the dissolved nutrient into the growth zone of the cylinder and crystal growth can occur. For quartz crystal growth, a typical density of solvent at 400°C is 0.8 g/cc which can produce pressures in the bomb of 20,000 p.s.i.

A third technique is that of growing oxides from the vapor-phase which, as was stated previously, can be considered under either method

(2) or (4) depending on the mechanism for growth. Apparatus in this case can be varied but usually consists of a tube furnace capable of controlled axial temperature gradients. The furnace tube is divided into two zones, the growth zone and the nutrient zone. In the nutrient zone powder of the same composition as the crystals to be grown is heated to a temperature at which either decomposition occurs or the vapor pressure approaches atmospheric. A carrier gas made of a combination of an inert gas such as nitrogen or helium with oxygen is blown over the nutrient transporting the growth constituents to the growth zone where either seeds are placed or nucleation of seeds occurs naturally. This zone is at a substantially lower temperature and is regulated to cause recrystallization. Again, as is the case for most crystal growing techniques, many variables must be controlled in order to get desired results. In many cases only a few combinations of these variables can produce sizeable crystal growth to say nothing of achieving nearly imperfection-free samples.

Another method with widespread use in the oxide growth industry is the Verneuil, or flame fusion technique. Powder of the crystal to be grown is poured through an oxy-hydrogen flame and is melted. The flame is focussed on a seed crystal which is slowly lowered as growth occurs, producing in some cases large boules of crystals. Varied purity can be attained depending on the purity and composition of the starting powder.

This concludes a cursory review of the methods used for oxide growth in general. However, these with their various modifications provide the bulk of oxide growth techniques. A review of the literature shows that any one crystal can usually be grown in a variety of ways. A good example is ZnO which has been grown by vapor-phase reaction[23], from a flux melt of lead fluoride[24], and by a hydrothermal process[25]. Other

examples are contained in the following list which is by no means complete.

Vapor-phase growth:	ZnO[23], SnO_2[20,21]
Melt or flux growth:	Al_2O_3[28], ZnO[24], SnO_2[31], Fe_2O_3[29]
Hydrothermal growth:	ZnO[25], SnO_2[32], SiO_2[33], Al_2O_3[30], GeO_2[32]
Verneuil growth:	TiO_2[26], Al_2O_3[27] (Sapphire)

Tin Oxide Growth

Within the past four years stannic oxide, SnO_2, has been grown by three methods, vapor-phase[20,21], flux[31], and hydrothermal[32] This laboratory investigated all three with positive results in two of the techniques.

Vapor-Phase Growth - A vapor-phase growth technique suggested by Reed[34] is a simplification of the method described in the previous section. It used a quartz container approximately two inches in diameter with one closed end and the other connected to a one-quarter inch diameter chimney. Around the periphery and slightly above the closed end, holes were punctured allowing natural convection of air to pass through the crucible, over molten tin, and up through the chimney. Figure 1a shows the placement in the furnace. The temperature gradient was necessary for air convection as well as vaporization of the tin or its oxide and subsequent recrystallization near the chimney area. It was not known exactly what the temperature gradient was but the bottom of the crucible was heated to 1300°C. Reed suggested that the reaction $SnO(g)+\frac{1}{2}O_2 \rightleftharpoons SnO_2$ portrays the mechanism for growth[20].

Results in this laboratory were sporadic as were those of Reed. However, the crystals grown were not as large. Reed reported needle

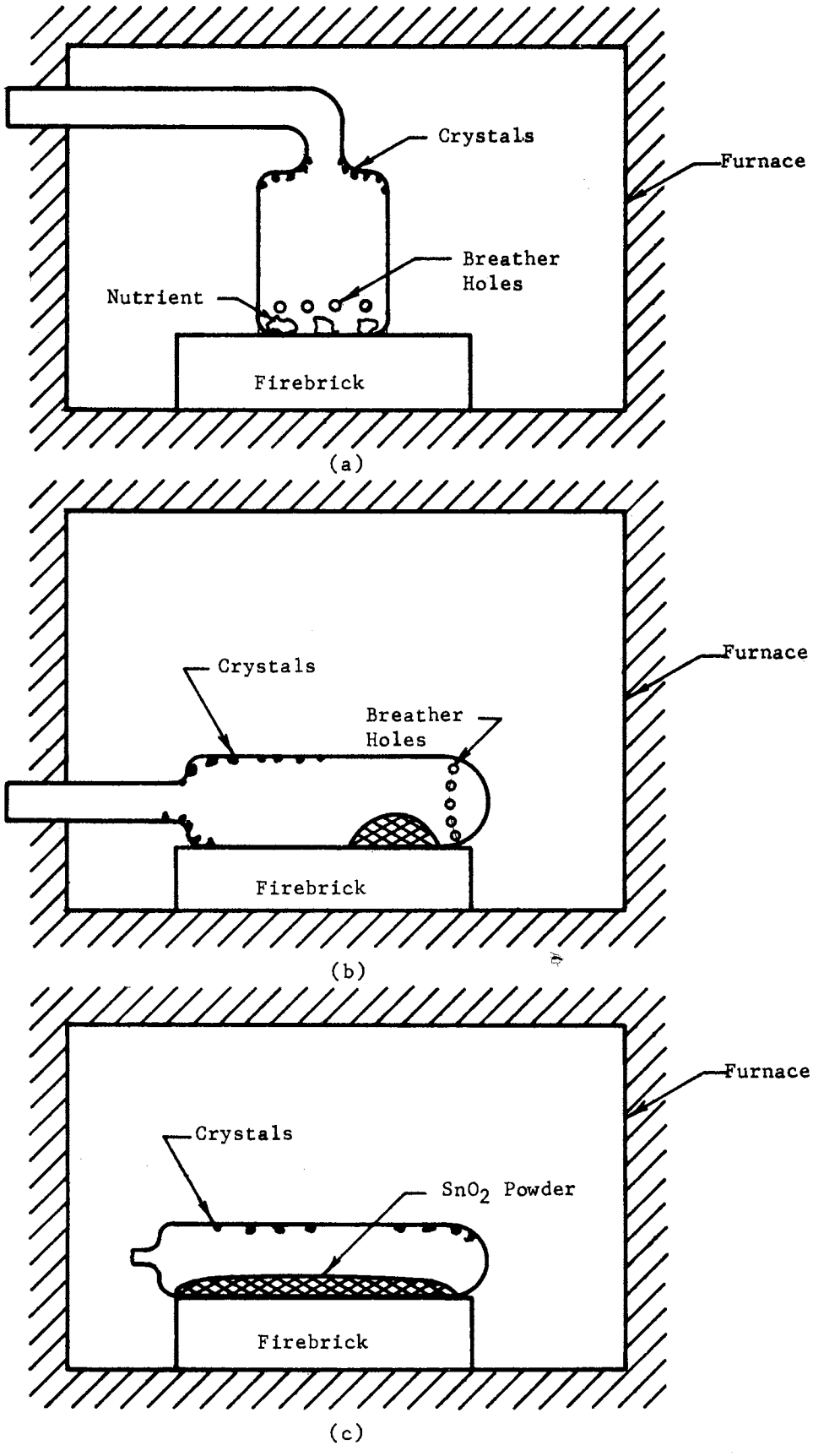

Figure 1. Arrangement of Crucibles in the Furnace for Vapor-Phase Growth Technique.

growth, centimeters long and tenths of a millimeter wide but with the set up described above only very small crystals were obtained locally, being at most one tenth of a millimeter long. Two modifications of the above design were attempted. Due to the geometry of the furnace the first employed a quartz crucible constructed from two inch vitreous tubing with a chimney and a closed end as before (Figure 1b). In this case the air convection was horizontal passing through the holes in the rear of the closed end of the crucible over the nutrient and out the chimney that protruded from the furnace door. Instead of the tin metal as nutrient, commercially available reagent grade stannic oxide powder was used. However, by varying the amounts of powder, breather hole size, and furnace temperature, crystals of no better quality and size than before were obtained.

Figure 1c shows a third apparatus employing a quartz crucible. In this case it was constructed as before with the exception of the holes and chimney. A port was attached so that a rough pump vacuum could be pulled subsequent to covering the bottom with reagent grade SnO_2 powder. The port was then sealed off and the crucible placed in the furnace. Runs to near 1300°C using this configuration produced crystals somewhat larger than before in the same growth period. It must be emphasized again that although in this case quality crystals were produced with very well defined faces and apparently flawless bulks they were microscopic in size making them too small for research samples. About the same time an elaborate system was constructed by Marley and MacAvoy[21] after a comprehensive study of the vapor-phase technique and very good sample size crystals produced by this method became available. Consequently, it seemed reasonable to search for an alternative growth procedure and this

direction of the research was abandoned.

Hydrothermal Growth - Chronologically the hydrothermal method was the first tried in this laboratory and was the subject of a M.S. thesis[35]. Its use was prompted by the fact that quartz and cassiterite are found in the same rock formations, presumably the result of a natural hydrothermal growth process. The technique was in essence that previously discussed for oxides in general with a temperature range from 200 to 400°C and pressures of 15,000 to 20,000 p.s.i. Repeated runs were made varying temperatures, percent of fill, and concentrations of NaOH with no apparent solubility of the nutrient SnO_2 powder. Thus no crystal growth was gotten either on the natural cassiterite seeds or the walls of the autoclave. Lack of time and facilities for working at higher pressures forced the abandonment of this project. During the past year, however, Roy[32] has been able to grow crystals with 2 x 2 x 4 millimeter dimensions using growth periods of one week. With two-molar KOH as solvent, other parameters were a temperature of 700°C and 45,000 p.s.i. bomb pressure.

Flux Growth - A flux growth technique developed in this laboratory has produced the sample-sized crystals necessary for the electrical and optical studies described in this report. In Figure 2 a schematic of the apparatus for the experimentation is seen. It consists of a Harper Electric Company Model HL-7610 globar muffle furnace, capable of temperatures to 1500°C; a Leeds and Northrup Speedomax H control unit and recorder using a platinum-platinum (90%) rhodium (10%) thermocouple sensing device. The crucible is made of platinum and is the 50cc Model 201, purchased from Englehard Industries. In the trials discussed below it was found when using operation temperatures above 1275°C alloying of copper and/or tin with platinum

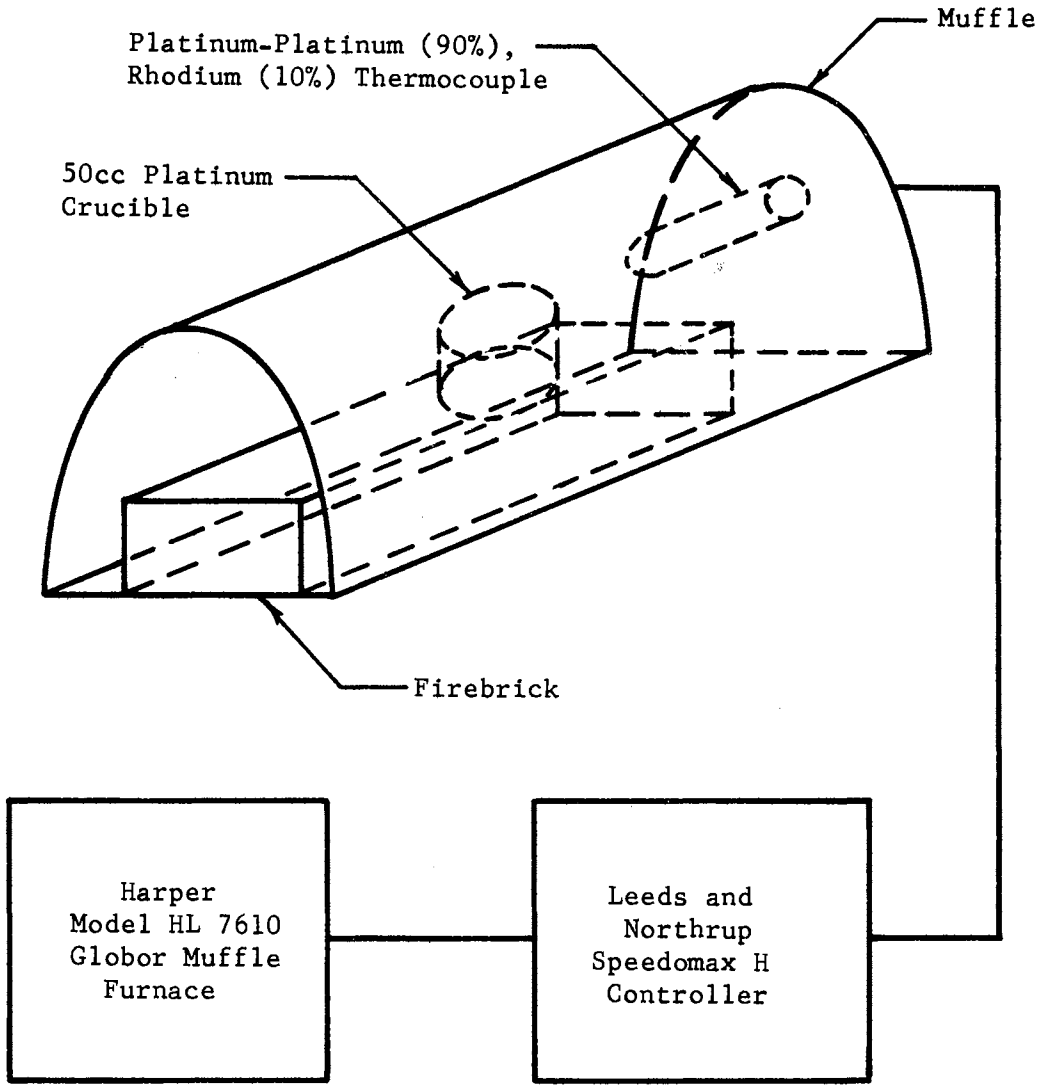

Figure 2. Flux Growth Apparatus Schematic Diagram.

occurred by a reaction in the melt. This reaction seems to be a rate process dependent on temperature. At most, the life of a crucible seems to be about three runs at growth temperature for one week when low temperatures are used, possibly indicating that alloying is present at all temperatures at which the melt is liquid. If high temperatures are used one run is possible.

When considering the use of flux growth techniques, it is advantageous to have phase diagrams of system combinations with the substance to be crystallized. This laboratory started a literature search for systems containing SnO_2. Two such diagrams were found, one with PbO[36] and the other with Al_2O_3[37]. Different combinations of PbO and SnO_2 powder were extensively studied. Heating and cooling rates were varied in the temperature and composition range where crystallization might occur as indicated by the diagram. In all situations it was found that an intermediate compound -- presumably a lead stannate -- formed on cooling the flux.

It was not feasible to attempt the use of Al_2O_3 since the operation temperature range for supersaturation is well above that attainable with the present experimental system.

A statement made in Mellor[38] about the possibility of growing stannic oxide crystals from a cuprous oxide melt finally led to a fruitful investigation in this area. The first attempt at growing SnO_2 from a Cu_2O melt produced crystalline needles approximately one centimeter long by less than one tenth of a millimeter wide possessing a square cross sectional area. Repeated runs using different ratios of SnO_2 to Cu_2O by volume were investigated. Along with the various ratios, trials were made with the powders separated and mixed as well as combinations of both.

Seeding with both crystals of cassiterite (the natural crystalline species) as well as with synthetic tin oxide was tried. Along with the different mixture combinations another very important aspect of the growth process was examined, that of heating and furnace control when at and near the growth temperature.

The prime concern has been to grow the largest crystals possible by controlling the above mentioned variables. It is found that a mixture of two parts Cu_2O to one part SnO_2 by volume works equally well whether the constituents are mixed together or placed separately in the 50cc platinum crucible. The importance of seeding has not yet been definitely established. Seeding near the walls by placing small seed crystals in the melt itself provides no larger growth at the periphery of the crucible than occurs during a good run in which seeds are left out. It has never been noticed that seeding in the middle of the melt enhances crystal growth in this region. The conclusion reached, then, is that the cooling mechanism at the surface has more of an effect on growth than does the seeding. It is not intended to say that seeding the melt would not help growth, only that seeding in the above manner seems to have little effect. Efforts to introduce an externally cooled seed would appear to be the next logical extension.

Before describing the effects of the other variables mentioned, it is well to discuss the appearance of the slug as taken from the crucible subsequent to a run of one week or better. All visible evidence leads one to believe that the ingredients have melted homogeneously. The surface of the slug when cool is very smooth and appears to have a metallic look. Since cuprous oxide is moderately soluble in hydrochloric acid, the slug and crucible are placed in this acid bath because the slug adheres to the walls. As the solvent material is eaten away the crystals, being chemically

inert in acids, protrude as needles positioned near the slug surface and spread randomly throughout its bulk. Secondly, platelets sometimes apparently forming the sides of unfilled rectangular parallelopipeds of SnO_2 crystals, are found deeper in the slug and are more concentrated at the walls of the crucible. Finally the rods or bars with square cross-sectional area are found at the slug-crucible interface and are positioned at about half depth in the slug, which itself after cooling only half fills the crucible. An interesting pattern of growth is followed by the rods. They seem to nucleate at the crucible wall and extend along it in all directions. Growth of rods is very seldom found protruding perpendicular to the wall into the bulk. The SnO_2 powder that does not participate in the larger growth settles to the bottom of the crucible. As might be expected, it does not remain in the powder or submicroscopic crystalline form but appears as a mass of small nucleation crystals which can easily by examined with a standard laboratory stereomicroscope.

Last but not least in importance is the temperature control. Cu_2O is listed as having a melting point of 1235°C but in the present case when mixed with SnO_2 is known to exist in a liquid state to near 1150°C. Although the phase relationships have not been a subject of study it appears that operation is in the range of temperature and composition above a eutectic point. When the crystal growth range was established at approximately 1175°C to 1300°C, two different types of procedures were employed when near the temperature control point. The first was cycling over 20 to 50 degrees above and below the control point and the second, close control at this point. (It must be remembered that the temperatures mentioned here are those seen by the recorder whose thermocouple is not contact with the crucible, Figure 2). From these trials it has been

concluded that cycling has the effect of producing much larger crystals than close control, as might be expected if this process is one of a solvent - solute situation where heating and subsequent cooling cause supersaturation resulting in precipitation of SnO_2.

With the limitations imposed by the apparatus used and the temperature control that is employed it is probable that crystal sizes have reached their maximum. Suggestions for modifications aimed at obtaining larger specimens will be presented in a later section.

Impurity Analysis

A spectrographic analysis was made of some of the larger crystal pieces.* Quantitatively two impurities were found. In 1.2 grams of crystals, 0.0021% by weight of cupric oxide and 0.02% silicon dioxide were detected. It is actually suspected that both of these numbers are too high to be indicative of the average crystals used in the experimental studies. Due to the size of the crystals quite a number of them had to be collected to weigh 1.2 grams and unfortunately the crystals that had to be used contained some inclusions that were visible veins or bubbles having a reddish to black appearance. Since the melt is of a similar color it was concluded that these flaws contained some of its ingredients. Although the crystals were ground up and washed in aqua regia and hydrofluoric acid in order to dissolve these impurities and were subsequently rinsed in acetone and methanol and washed in distilled water before drying, it is virtually certain that the detected impurity content is too high in comparison with sample crystals which have very

*Analysis by the Bruce Williams Laboratory, Joplin, Missouri.

few visible flaws. An agate pestle was used to grind the crystals into powder which may account for the high silica content. This often happens for samples prepared for analysis in this way. An interesting consequence of the analysis is that although the flux is made up of cuprous oxide, the inclusion report shows cupric oxide. As stated previously, a chemical reaction is suspected since copper and/or tin alloys with the platinum crucible. The change of cation valency supports this type of speculation.

Crystal Identification

To substantiate the belief that the flux-grown crystals were stannic oxide the Debye-Scherrer X-ray powder pattern photograph method was used. The identification had originally been accomplished by merely comparing the photographs of the unknown to that of a known standard in this case, reagent grade SnO_2 powder.

The apparatus used consists of a Norelco type 12045/3 X-ray unit equipped with a copper target and nickel filter. The camera is the conventional circular 114.6 millimeter diameter type depicted in Figure 3. Film placement followed the Straumanis arrangement in which the two free ends of the film are located halfway between the X-ray entrance and exit ports of the camera.

Sample preparation for crystals and powder consisted of grinding them in an agate pestle until the contents could be vibrated into a glass capillary having an outside diameter of approximately one millimeter. This capillary was then placed in its slot at the center of the camera and aligned with a special magnifying eyepiece that is inserted in the exit port.

Before presenting the results, a cursory review of the powder pattern

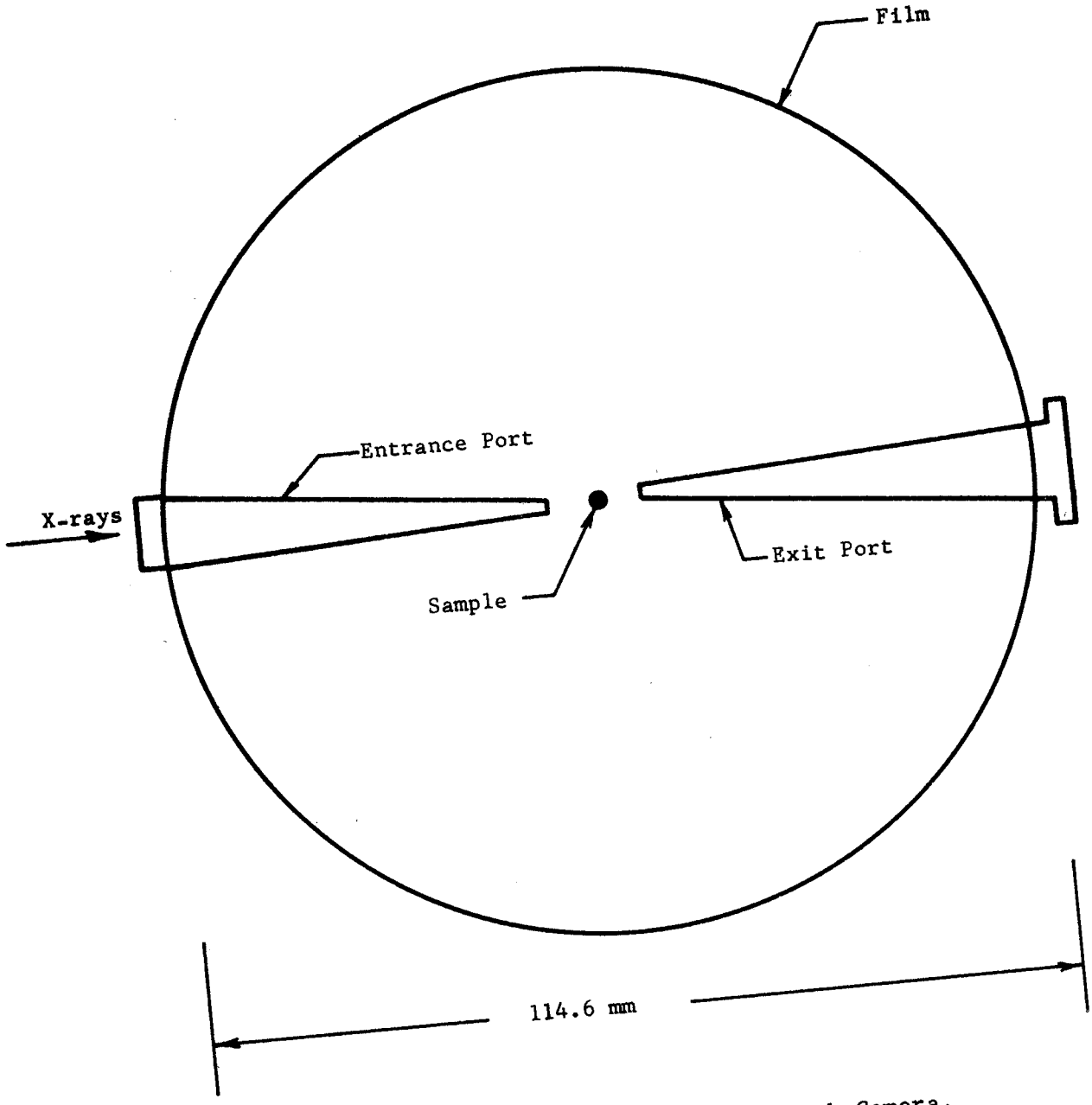

Figure 3. X-ray Powder Photograph Camera.

principles will be helpful. The X-ray beam is defined by the entrance port and is focused onto the sample which is then rotated about its axis. As the beam passes through the powder sample it encounters thousands of powder grains, each a small crystal in random orientation. Among these orientations there are many that are so positioned that the appropriate glancing angle θ for a given set of planes (Miller indices h,k,l) is made with the X-ray beam. This reflection occurs such that its direction makes an angle $2\theta^{o}$ with the X-ray path. The locus of beams that come from planes with appropriate glancing angles form a cone of X-rays cutting across the photographic film inscribing on it circular arc patterns. This behavior follows the Bragg equation:

$$\theta = \sin^{-1} \left(\frac{\lambda}{2} \frac{n}{d_{hkl}}\right) \qquad (1)$$

where θ is the glancing angle, λ the wavelength of X-radiation, n the order number associated with the reflection and d_{hkl} the planar spacing for a given set of planes (h,k,l).

Two types of results were gotten from this study on the grown samples. First in importance was the fact that in the photographic comparison of grown sample to standard it was shown that the crystals were definitely stannic oxide. Secondly from these photographs the interplanar spacings for given sets of crystallographic planes were calculated and related to preceeding work.

As a result of the camera geometry as seen in Figure 3, one can calculate the glancing angle θ from the equation:

$$4\theta = S/R \qquad (2)$$

where S is the distance between corresponding circular arcs produced by the

same cone of X-rays, R is the film radius and 4θ the cone-opening angle. The camera is conveniently constructed such that its 114.6 millimeter diameter allows one to measure S in millimeters giving a direct correspondence of one millimeter to one half the Bragg angle, 1/2 θ.

These measurements were made on a General Electric Fluoroline Model film reader capable of accuracies to better than a tenth of a millimeter. This involves securing the film in the reader and recording the distance in millimeters to arcs corresponding to the same cone of X-rays. A computer program* (Appendix A) for the I.B.M. 1620 was used to take this data as recorded along with the X-radiation wavelength and compute the d_{hkl} values using Equation 1. As was stated previously, the target on the X-ray unit is copper, determining the wavelength used. For the front reflection lines (θ between 0° and 45°), $\lambda = 1/3(K_{\alpha_2}+2K_{\alpha_1})=K_{\alpha}$. This is an intensity weighted sum of two strong emission lines that have very nearly the same wavelength. For copper, $K_{\alpha_2} = 1.54434$Å, $K_{\alpha_1} = 1.54050$Å which makes $K_{\alpha} = 1.5418$Å. The reason for the weighted wavelength in the front reflection direction is that the resolving power of the apparatus is such that these two lines are responsible for essentially the same cone that is photographed. In the back reflection direction (θ between 45° and 90°), since resolving power increases with glancing angle, these two wavelengths produce separate lines and in this case the appropriate λ is used in the computer program. The nickel filter blocks out other prominent shorter wavelengths that would only clutter up the photograph.

Another constant that is needed in the program is the shrinkage correction factor. This is computed from the photograph by taking an

---

*Written by Dr. Robert Gebelt, Chemistry Department, Oklahoma State University.

average of the centers of a number of line pairs for both forward and back reflection lines. If the distance between the two centers is not 180 millimeters corresponding to 90° then the correction factor is defined as $= \frac{\text{distance between centers (mm)}}{180}$. Errors can develop if the film size after development is not considered. Reasons for shrinkage or elongation -- the latter being the more likely case -- are hanging while drying after development and heat expansion while held in the film reader where the film is in contact with a piece of glass that is heated and lighted by a fluorescent bulb.

Figure 4 shows an indexed powder X-ray photograph of an SnO_2 crystal. Note the symmetric pairs of lines in both the forward and back directions as well as the doublets in the back reflection picture. The line identification was done by comparing d_{hkl} values with those gotten by Swanson and Tatge[41] for given h,k,l (Table I). In this study no attempt was made to calculate or measure intensities of the lines other than to visually estimate the relative intensities as compared to the previous work.

Table II lists the d_{hkl} values and the corresponding lattice planes for comparison with Table I. Notice that every line that was identified in the work in 1953 is also present in the work done in this laboratory except for one line which is reported to be very faint. Table III shows the comparison on the back reflection data of separating the doublet into its corresponding wavelengths K_{α_1} and K_{α_2}. As can be seen, there is very close agreement leading one to conclude that these are doublets and not independent reflections.

Crystal Orientation

The orientation of the flux-grown stannic oxide crystals was accomplished using the Laue Back Reflection X-ray pattern and a polarizing

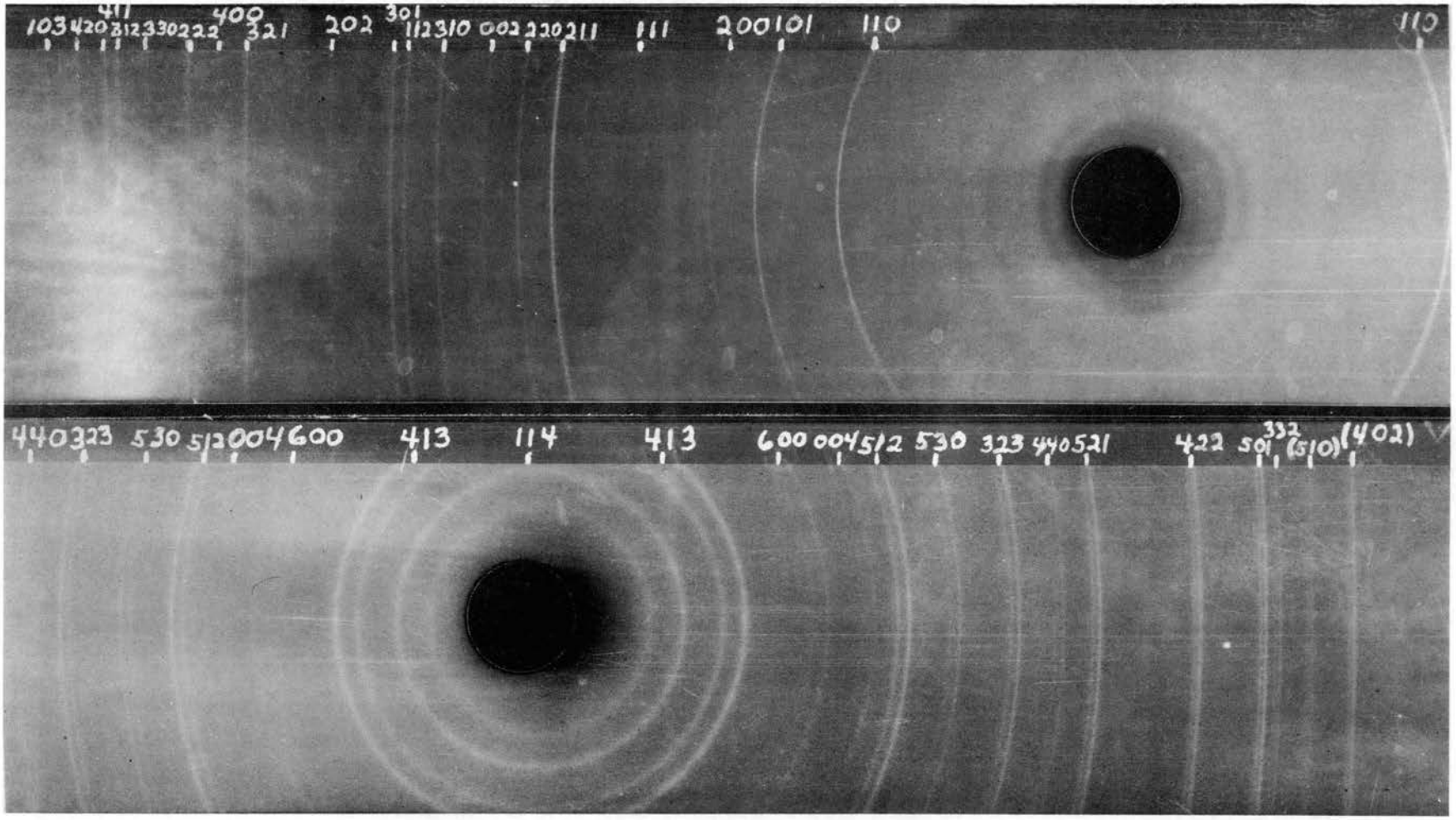

Figure 4. X-ray Powder Pattern Photograph of Flux Grown SnO_2 Crystals.

TABLE I

COMPARISON OF LINE INTENSITIES AND d_{hkl} FROM SnO_2 POWDER PATTERNS BY VARIOUS AUTHORS*

hkl	1929 Natta and Passerini Fe, 1.9360 A		1932 Weiser and Milligan Mo, 0.7093 A		1938 Boldyrev Mo, 0.7093 A		1938 Hanawalt, Rinn, and Frevel Mo, 0.7093 A		1942 Harcourt Cu, 1.5405 A		---- Harcourt; Boldyrev Mo, 0.7093 A		---- British Museum Cu, 1.5405 A		---- United Steel Co, 1.7902 [a] A		1953 Swanson and Tatge Cu, 1.5405 A, 26°C	
	d	I	d	I	d	I	d	I	d	I	d	I	d	I	d	I	d	I
	A		A		A		A		A		A		A		A		A	
110	3.27	mw	3.41	100	3.337	50	3.35	100	3.33	100	3.34	80	3.31	80	3.36	80	3.351	100
---	-----	----	------	---	-----	----	-----	----	-----	----	-----	----	2.92	20	-----	-----	------	---
101	2.606	s	2.68	100	2.636	50	2.65	63	2.63	100	2.64	80	2.63	80	2.65	80	2.644	81
200	-----	----	2.35	50	2.367	40	2.36	18	2.35	33	2.36	60	2.35	60	2.37	50	2.369	24
111	-----	----	------	---	-----	----	-----	----	2.28	8	2.28	30	------	---	2.31	20	2.309	5
210	-----	----	------	---	-----	----	-----	----	2.11	5	2.11	20	1.95	50	-----	-----	2.120	2
211	1.754	vs	1.77	100	1.764	100	1.75	63	1.75	100	1.75	100	1.75	100	1.76	100	1.765	63
220	-----	----	------	---	1.675	70	1.67	10	1.668	33	1.67	70	1.67	60	1.67	60	1.675	63
002	1.583	mw	------	---	1.590	20	1.58	5	1.58	17	1.58	50	1.59	50	1.59	50	1.593	8
---	-----	----	------	---	1.529	10	-----	----	-----	----	-----	----	1.57	40	-----	-----	------	---
310	1.491	----	------	---	1.500	80	1.495	10	1.49	33	1.49	70	1.50	60	1.50	60	1.498	13
112	1.430	s	1.43	70	1.438	70	1.438	10	1.43	33	1.43	70	1.44	60	1.44	60	1.439	17
301	1.409	s	------	---	1.413	70	1.415	15	1.408	33	1.411	70	1.41	60	1.41	60	1.415	15
---	-----	----	------	---	-----	----	-----	----	-----	----	-----	----	1.35	20	-----	-----	------	---
202	-----	----	1.32	20	1.323	40	1.318	6	1.318	17	1.321	50	1.32	40	1.32	50	1.322	7
321	1.211	vs	1.21	70	1.216	80	1.215	10	1.211	33	1.213	80	1.22	70	1.21	60	1.215	11
400	-----	----	------	---	1.185	30	1.182	2	1.181	8	1.183	40	1.19	20	1.18	40	1.184	3
222	1.150	s	1.16	20	1.155	70	1.152	6	1.151	17	1.153	60	1.16	60	1.15	60	1.155	8
---	-----	----	------	---	-----	----	-----	----	-----	----	1.141	30	------	---	-----	-----	------	---
330	1.114	ms	------	---	1.118	60	1.112	3	1.113	17	1.115	60	1.12	60	1.12	50	1.117	3
312	1.087	s	1.10	40	1.092	70	1.087	8	1.088	33	1.090	80	1.09	80	1.09	60	1.092	8
411	1.078	s	------	---	1.081	80	-----	----	1.077	33	1.079	80	1.08	80	1.08	60	1.081	8
420	1.058	ms	------	---	1.060	70	1.059	3	1.057	17	1.059	70	1.06	50	1.06	50	1.059	3
---	1.049	mw	1.05	10	-----	----	-----	----	-----	----	1.047	70	1.05	40	-----	-----	------	---
103	1.035	ms	------	---	1.037	40	1.037	2	1.033	17	1.035	50	1.04	40	1.04	50	1.036	4
---	-----	----	------	---	-----	----	-----	----	-----	----	-----	----	1.01	20	-----	-----	------	---
402	-----	----	------	---	-----	----	0.950	8	0.947	50	0.947	80	------	---	0.951	80	0.9505	8
510	-----	----	------	---	-----	----	.931	1	.928	17	.928	60	------	---	.931	70	.9291	3
332	-----	----	------	---	-----	----	-----	----	.914	17	.914	60	------	---	.916	70	.9143	3
501	-----	----	------	---	-----	----	0.907	4	.907	33	.907	70	------	---	.910	80	.9081	8
422	-----	----	------	---	-----	----	.882	4	.881	50	.881	80	------	---	-----	-----	.8819	7
303	-----	----	------	---	-----	----	-----	----	-----	----	-----	----	------	---	-----	-----	.8814	6
521	-----	----	------	---	-----	----	0.847	2	0.848	50	0.848	80	------	---	-----	-----	.8480	6
440	-----	----	------	---	-----	----	-----	----	.838	17	-----	----	------	---	-----	-----	.8375	1
323	-----	----	------	---	-----	----	-----	----	.826	33	-----	----	------	---	-----	-----	.8261	4
530	-----	----	------	---	-----	----	-----	----	.813	8	-----	----	------	---	-----	-----	.8125	2
441	-----	----	------	---	-----	----	-----	----	.807	33	-----	----	------	---	-----	-----	------	---
512	-----	----	------	---	-----	----	-----	----	-----	----	-----	----	------	---	-----	-----	0.8026	6

[a] Weighted Kα.

*Reproduced from Swanson, H. E. and Tatze, E., Natl. Bur. Standards (US) Circ. 539, Vol I (1953).

TABLE II

d_{hkl} VALUES AND BRAGG ANGLES CALCULATED FROM SnO_2 POWDER PATTERN

hkl	Bragg Angle, θ	d_{hkl}
	K_α = 1.54180Å	
110	13.42°	3.321Å
101	17.08	2.624
200	19.12	2.353
111	19.61	2.297
210	-----	-----
211	26.04	1.756
220	27.51	1.668
002	29.08	1.586
310	31.09	1.493
112	32.52	1.434
301	33.12	1.411
202	35.78	1.318
321	39.51	1.212
400	40.75	1.181
222	42.04	1.151
330	43.81	1.114
312	45.11	1.088
411	45.56	1.080
420	46.76	1.058
103	48.26	1.033
	K_α = 1.54050Å	
402	54.27	.9489
510	56.08	.9282
332	57.50	.9133
501	58.10	.9073
422	60.88	.8817
303	-----	-----
521	65.33	.8476
440	66.94	.8371
323	68.90	.8256
530	71.54	.8120
441	-----	-----
512	73.73	.8024
004	75.23	.7966
600	77.32	.7895
413	80.96	.7799
114	83.67	.7749

microscope. These X-ray pictures were taken on a General Electric Model XRD Unit that had a copper target and no filter. The microscope was a Bausch and Lomb Model LI.

TABLE III

COMPARISON OF BACK REFLECTION DOUBLETS USING THEIR CORRESPONDING WAVELENGTH CALCULATED FROM SnO_2 POWDER PATTERN

	K = 1.54434Å		K = 1.54050Å	
hkl	Bragg Angle	d_{hkl}	Bragg Angle	d_{hkl}
402	54.45°	.9490	54.27°	.9489
510	56.26	.9285	56.08	.9282
332	57.69	.9136	57.50	.9133
501	58.27	.9078	58.10	.9073
422	61.12	.8818	60.88	.8817
521	65.63	.8477	65.33	.8476
440	67.25	.8372	66.94	.8371
323	69.21	.8259	68.90	.8256
530	71.90	.8123	71.54	.8120
512	74.22	.8024	73.73	.8024
004	75.80	.7965	75.23	.7966
600	77.93	.7896	77.32	.7895
413	81.92	.7799	80.96	.7799
114	85.15	.7749	83.67	.7750

Since SnO_2 is birefringent with the optical axis parallel to the c-axis or (001) direction, this orientation in the crystal is readily determined using a polarizing microscope. The sample crystals grow such that they have a square cross-sectional area and a long axis parallel to the direction of fastest growth. It turns out that the long axis corresponds to the c-axis in all samples studied. Identification of the growth surfaces is then somewhat simplified since one direction in the crystal is known.

The arrangement for the back-reflection technique is shown in Fig. 5. This setup is similar to the Laue transmission method for crystal structure determination except that the photographic film is located between the X-ray source and the specimen. The film to specimen distance is the universally accepted value of three centimeters and the film size 3 1/2 x 5 inches. The white X-radiation passes through a collimating system, then through a hole in the photographic film, strikes the crystal, and is

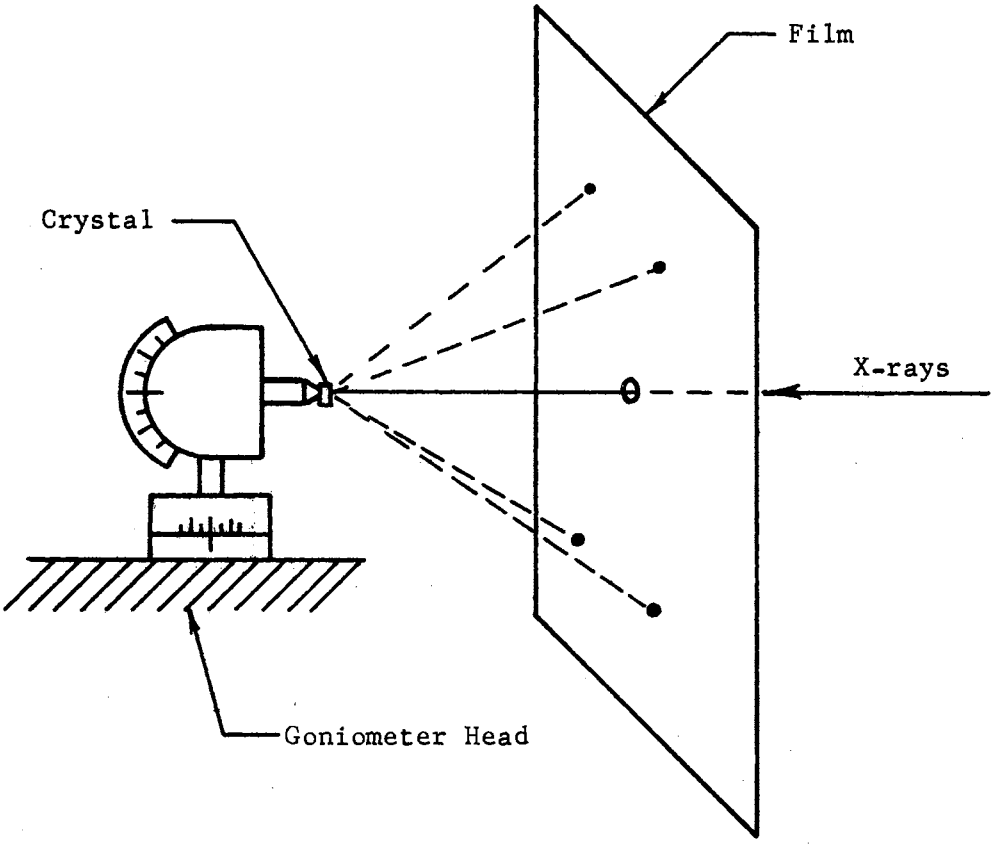

Figure 5. Laue Back-reflection Technique Schematic Diagram.

diffracted back onto the film. Spots appear on the film which represent X-ray beams "reflected" by the atomic planes in the sample.

Once the photographs are taken the task of identifying the planes responsible for the spots begins. This may be accomplished in many different ways. In the present situation, since one direction in the crystal was known, and it was suspected that the as-grown faces were either (100) or (110) planes, calculating the interplanar angles was simplified. As it turned out, the latter assumption was correct. The alignment of the crystal in the goniometer head was such that the c-axis was parallel to an axis corresponding to the length of the film. Likewise the as-grown face was parallel to the film surface in one case and rotated 45° about the axis in the second because the (100) and (110) planes have an interplanar angle of 45° in the tetragonal system.

In the tetragonal system or any framework using a coordinate system consisting of three mutually perpendicular axis, the angle between two planes is equal to the angle between the perpendiculars or normals to these planes. Therefore using the equation:

$$\cos\varphi = \frac{\frac{1}{a^2}(h_1h_2+k_1k_2)+\frac{1}{c^2}(l_1l_2)}{\sqrt{\left[\frac{1}{a^2}(h_1^2+k_1^2)+\frac{l_1^2}{c^2}\right]\left[\frac{1}{a^2}(h_2^2+k_2^2)+\frac{l_2^2}{c^2}\right]}} \qquad (3)$$

where φ is the angle between the normals to the lattice planes with Miller indices (h_1,k_1,l_1) and (h_2,k_2,l_2), interplanar angles can be calculated. The lattice constants a= 4.73727 and c= 3.186383 as reported in Wyckoff[9] were used in this equation. Pertinent planes and their associated angles with the (100) and (110) planes are tabulated in Table IV. In comparing these calculated planar angles to those which can be determined from the photograph, two methods may be used. The first is to measure distance and calculate by triangulation and the second is to use a Greninger plat[39].

This is a hyperbolic polar coordinate net that can be placed on the photograph such that interplanar angles can be read off directly. It is designed for use with the 3 cm sample-to-film distance apparatus.

TABLE IV

ANGLES BETWEEN CRYSTALLOGRAPHIC PLANES RESPONSIBLE FOR PROMINENT SPOTS IN FIGURES 6 AND 7

Projection Plane (HKL)	Plane (hkl)	Angle	Zone Axis
(110)	(541)	14°30'	$1\bar{1}1$
	(431)	18 24	$1\bar{1}1$
	(321)	24 58	$1\bar{1}1$
	(221)	27 44	$1\bar{1}0$
	(530)	14 2	001
	(210)	18 26	001
(100)	(501)	16°34'	$0\bar{1}0$
	(301)	26 22	$0\bar{1}0$
	(510)	11 18	001
	(310)	18 26	001
	(210)	26 34	001
	(611)	16 37	$0\bar{1}1$
	(411)	24 8	$0\bar{1}1$

Therefore, by comparison of the various angles calculated by the equation to those gotten from the photographs, Figures 6, 7, and 8 were identified. Lattice directions or zone axes associated with the prominent lines of spots are indicated. Once determination is completed two cross checks can be made. The first uses the following equation:

$$\cos \rho = \frac{a^2(u_1u_2+v_1v_2)+c^2w_1w_2}{\sqrt{[a^2(u_1^2+v_1^2)+c^2w_1^2][a^2(u_2^2+v_2^2)+c^2w_2^2]}} \qquad (4)$$

where $[u_1v_1w_1]$ and $[u_2v_2w_2]$ are the indices of zone axes or lattice directions. Therefore ρ is the angle between these lattice directions. The second is to use Equation 3 and the Greninger plat to check angles between identified spots. A few of the prominent lattice directions as indicated on Figures 6, 7 and 8 are presented in Table V.

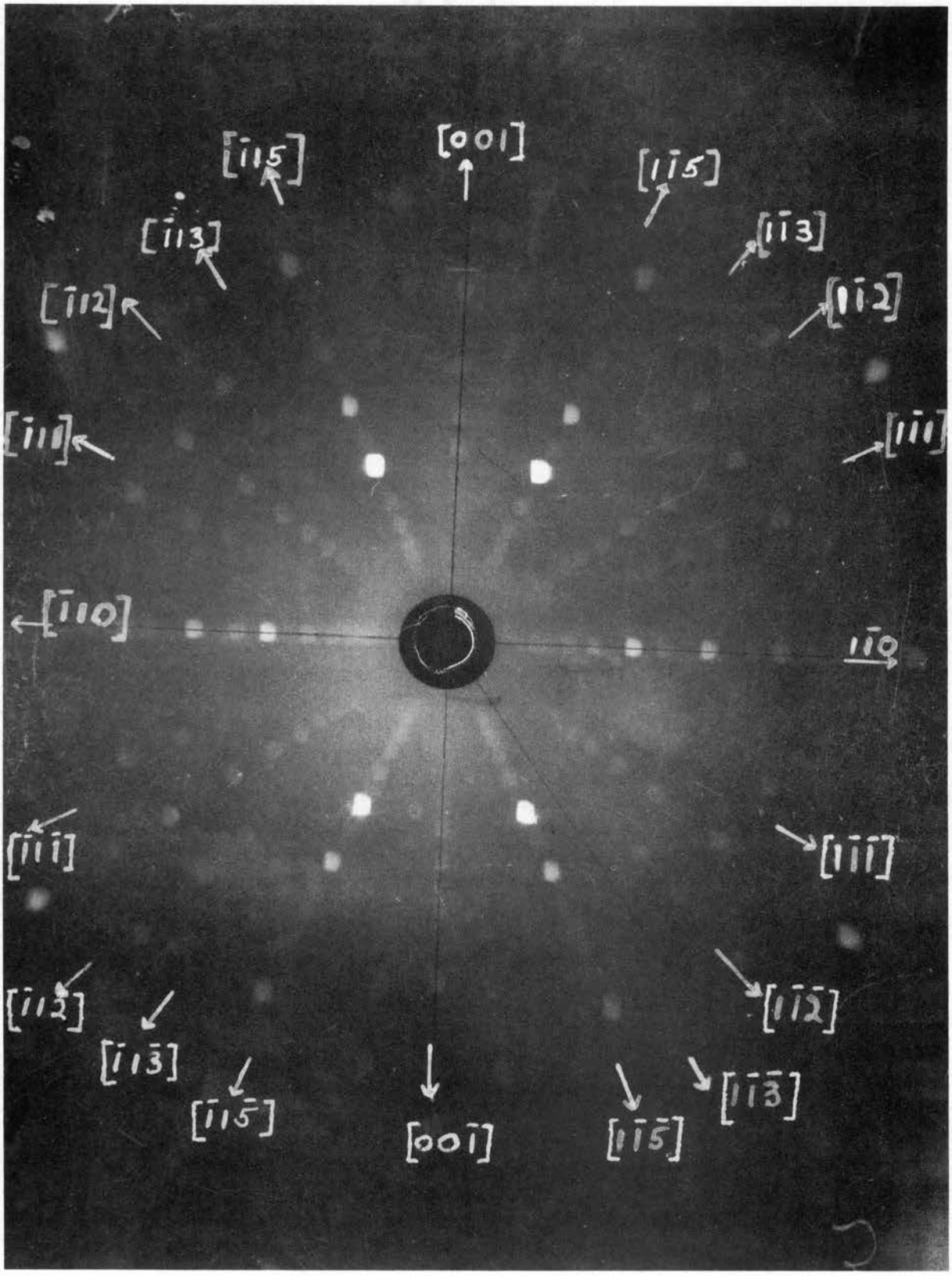

Figure 6. Laue Back-Reflection Photograph Taken in the [110] Direction.

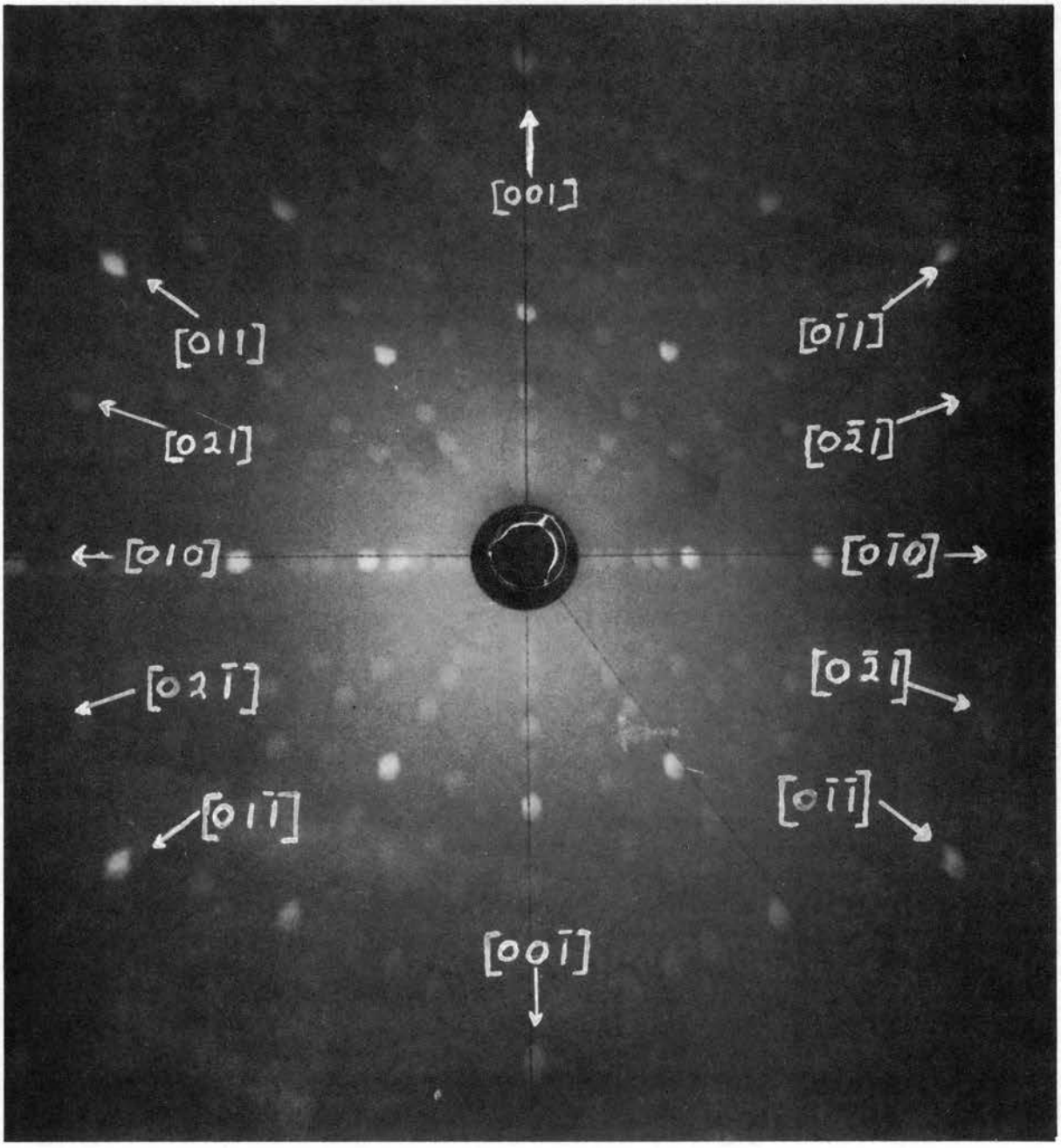

Figure 7. Laue Back-Reflection Photograph Taken in the [100] Direction.

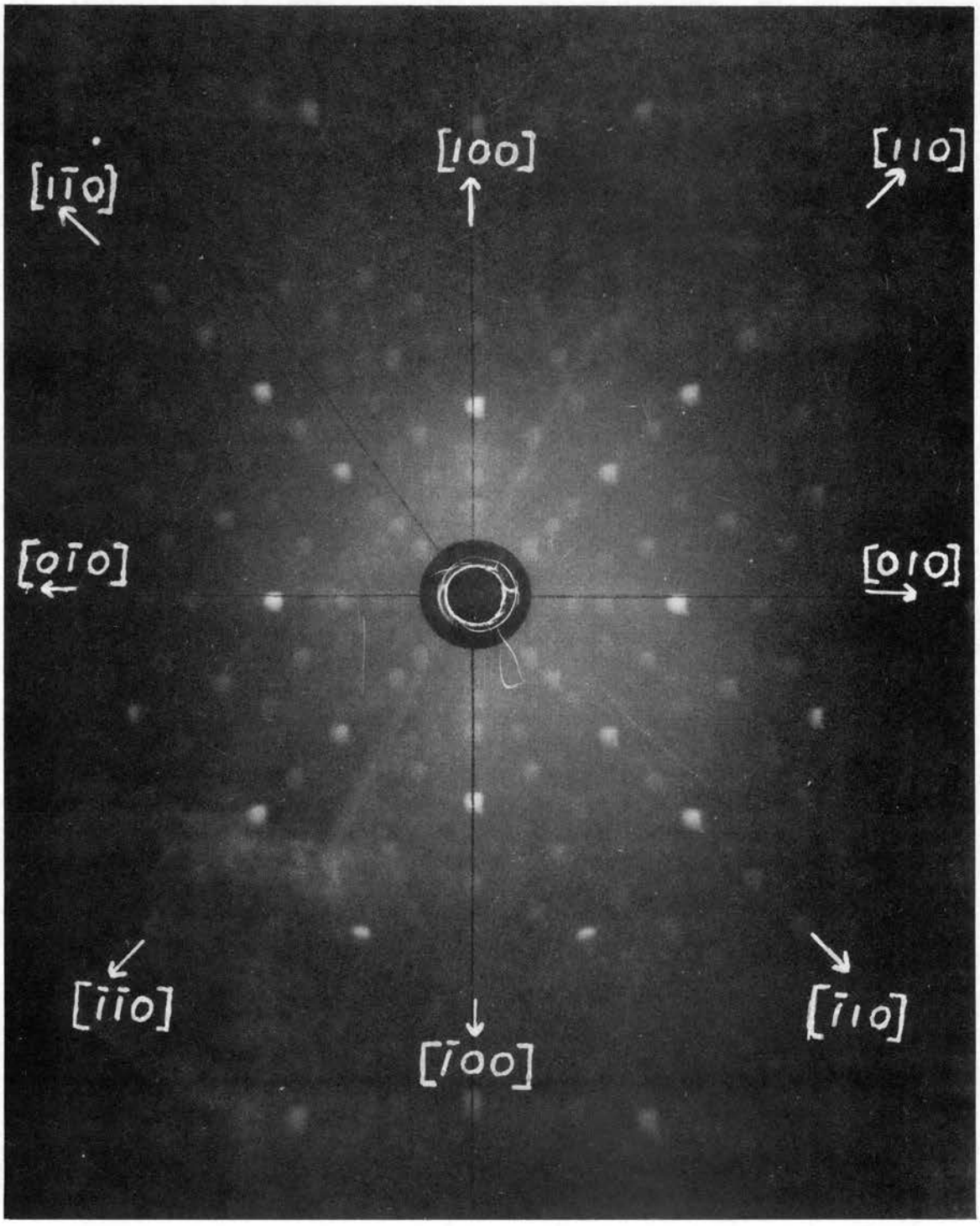

Figure 8. Laue Back-Reflection Photograph Taken in the [001] Direction.

TABLE V

LATTICE DIRECTIONS INDICATED ON FIGURES 6, 7 AND 8 AND THEIR ASSOCIATED ANGLES

[110] Projection

Measured from the [001] direction		Measured from the [00$\bar{1}$] direction	
Zone Axis uvw	Angle	Zone Axis uvw	Angle
1$\bar{1}$5 , $\bar{1}$15	22°48'	1$\bar{1}\bar{5}$, $\bar{1}\bar{1}\bar{5}$	22°48'
1$\bar{1}$3 , $\bar{1}$13	35 1	1$\bar{1}\bar{3}$, $\bar{1}\bar{1}\bar{3}$	35 1
1$\bar{1}$2 , $\bar{1}$12	46 24	1$\bar{1}\bar{2}$, $\bar{1}\bar{1}\bar{2}$	46 24
1$\bar{1}$1 , $\bar{1}$11	64 34	1$\bar{1}\bar{1}$, $\bar{1}\bar{1}\bar{1}$	64 34

[100] Projection

Measured from the [001] direction		Measured from the [00$\bar{1}$] direction	
0$\bar{1}$1 , 011	56° 5'	01$\bar{1}$, 0$\bar{1}\bar{1}$	56° 5'
0$\bar{2}$1 , 021	71 25	02$\bar{1}$, 0$\bar{2}\bar{1}$	71 25

[001] Projection

Measured from the [100] direction		Measured from the [$\bar{1}$00] direction	
110 , 1$\bar{1}$0	45°00'	$\bar{1}\bar{1}$0 , $\bar{1}$10	45°00'

CHAPTER III

THEORETICAL BACKGROUND

In this chapter a review of the general principles of semiconductors is presented as ground work for a model to explain the conduction process in SnO_2 flux-grown crystals. It will consist of the energy band picture in its relationship to the surface of semiconductors and insulators. This picture will be used in Chapter VI to explain the surface controlled electrical properties.

It must be remembered that processes such as thermoelectric power, electrical conductivity, and optical absorption involve transitions between energy states in the crystalline solid. For an impurity-free material these transitions occur between two quasi-continuous bands, the valence or filled band and the conduction or empty band. These are separated by the forbidden energy gap.

Electrical Conductivity

In processes such as conductivity which depends on the electron mobility, the energy states responsible for conduction must be dense enough as to allow electron transfer from one energy level to another. Besides the two groups of states already mentioned there can be others residing in the forbidden energy gap. These are associated with lattice imperfections, foreign atoms and ions in the bulk, surface discontinuities and surface states due to foreign ions. In many cases these states are sparse enough so that interaction does not occur causing the electrons in

them to be immobile. This means that only when electrons have energies placing them in the conduction band or have been excited into acceptor states leaving holes in the valence band will a mobility result. The conductivity is then dependent upon the respective densities, i.e.,

$$\sigma = e(\mu_e n + \mu_h p) \tag{5}$$

where σ is the conductivity, e the electronic charge, μ_e and μ_h are the electron and hole mobilities respectively (drift velocity per unit field strength) and n and p are the densities of free electrons and free holes.

The semiconductor or insulator is now to be considered as a two-band conductor with an energy gap. These bands contain a number of states about which more must be known. The question arises as to how electrons are distributed in the states and is best answered by equilibrium thermodynamics. The distribution is mathematically described by the traditional Fermi-Dirac function

$$f(E) = \frac{1}{1+\exp[(E-E_f)/kT]} \tag{6}$$

and is the probability that any particular level with associated energy E (measured from a fixed reference), will be occupied by an electron. E_f is the Fermi energy, k the Boltzman constant and T the absolute temperature. Using this and the knowledge of the states density distribution function N(E), a value of the mobile electron density can be obtained. Accounts of the methods used for obtaining the distribution function can be found in Blakemore[42]. It is expressed for the conduction band electrons as

$$N(E) = 4\pi(2m_n/h^2)^{3/2}(E-E_c)^{1/2} \tag{7}$$

where m_n is the electronic effective mass and E_c is the energy at the bottom of the conduction band. The number of conduction band electrons is obtained by integrating over the conduction band states as follows

$$n = \int_{E_c}^{\infty} f(E)N(E)dE \quad . \tag{8}$$

A similar integration can be performed for holes in the valence band by considering the probability for lack of electrons (1-f(E)), and the valence band density of states.

By letting

$$\epsilon = \left[\frac{E-E_c}{kT}\right] \text{ and } \eta = \left[\frac{E_f-E_c}{kT}\right]$$

Equation 8 becomes

$$n = 4\pi\left[\frac{2m_n kT}{h^2}\right]^{3/2}\int_0^{\infty}\frac{\epsilon^{1/2}d\epsilon}{1+\exp(\epsilon-\eta)} \tag{9}$$

which is expressed as $N_c F_{\frac{1}{2}}(\eta)$ where N_c is termed the effective conduction band density of states. $F_{\frac{1}{2}}(\eta)$ is one of the members of the set of functions known as the Fermi-Dirac integrals which have the general form

$$F_j(\eta) = \frac{1}{\Gamma(j+1)}\int_0^{\infty}\frac{\epsilon^j d\epsilon}{1+\exp(\epsilon-\eta)} \quad . \tag{10}$$

If $\eta \ll 0$ then $F_{\frac{1}{2}}(\eta)$ approaches the classical value, exp (η), and Equation 9 can be expressed as

$$n = N_c \exp[E_f/kT] \tag{11}$$

if the bottom of the conduction band is taken as the reference of energy i.e., $E_c = 0$. Likewise for holes in the valence band the equation becomes

$$p = N_v \exp[-(E_f+E_g)/kT] \tag{12}$$

where $N_v = 2(2\pi m_v kT/h^2)^{3/2}$, E_g is the magnitude of intrinsic energy gap and m_v is the hole effective mass.

For the intrinsic case where a hole-electron pair is created by thermally exciting an electron from the valence band into the conduction band, Equation 11 and 12 can be equated to get an expression for the Fermi level which is

$$E_f = \frac{-E_g}{2} + \frac{3kT}{4}\ln\left(\frac{m_v}{m_n}\right) \quad . \tag{13}$$

Substituting this into Equation 11 gives for the density of intrinsic electrons or holes

$$n_i = p_i = 2(2\pi kT/h^2)^{3/2}(m_n m_v)^{3/4}\exp[-E_g/2kT] \quad . \tag{14}$$

When imperfection states are present in the forbidden gap, the Fermi level is more difficult to describe mathematically. Consider, however, the idealized example of a wide gap semiconductor with a donor level very close to the conduction band. Let it have N_d levels per unit volume at energy E_d below the conduction band. Also suppose $N_d >> n_i$ so that the intrinsic electrons may be neglected. If all of the donors are ionized, $n = N_d$ so that using Equation 11

$$E_f = kT\ln(N_d/N_c) \quad . \tag{15}$$

A more complex example that is useful in much semiconductor work is given by Smith.[43] His discussion includes consideration of the importance of degeneracy and spin in determining the occupation probability expressions for imperfection states. If a donor level is not completely ionized it will have an electron occupation number of

$$n_d = N_d\left[1+\tfrac{1}{2}\exp[(E_d-E_f)/kT]\right]^{-1} \quad . \tag{16}$$

Similarly if an acceptor level of density N_a is present it will have a lack of electrons

$$n_a = N_a\left[1+\tfrac{1}{2}\exp\left[(E_f-E_a)/kT\right]\right]^{-1} \quad . \tag{17}$$

The charge neutrality governing a semiconductor with such donor and acceptor level is

$$n+n_d+N_a = p+N_d+n_a \tag{18}$$

where each symbol has been described above. Assume that the Fermi level is between the conduction band and mid gap and is at least a few kT from the conduction band. This means one can neglect the free hole contribution as compared to n, and neglect n_a since it is small compared to N_a, so that Equation 18 can be approximated as

$$n = N_d-N_a-n_d \quad . \tag{19}$$

Substituting Equations 11 and 16 into 19,

$$n^2+n(N_a+N_c')-N_c'(N_d-N_a) = 0 \tag{20}$$

where $N_c' = \tfrac{1}{2}N_c\exp(-E_d/kT)$ where E_d is the donor ionization energy. The solution for Equation 20 is

$$n = -\tfrac{1}{2}(N_a+N_c')+\tfrac{1}{2}\left[(N_a+N_c')^2+4N_c'(N_d-N_a)\right]^{\frac{1}{2}} \quad . \tag{21}$$

When $E_d/kT \gg 1$, N_c' will be small so that expanding the second term in powers of N_c' gives an approximate solution

$$n = \frac{N_c'(N_d-N_a)}{N_a} = \frac{N_d-N_a}{2N_a}\,N_c\exp\left[-E_d/kT\right] \quad . \tag{22}$$

This form of approximation is only valid for partially compensated

semiconductors. Similarly, if $N_a \ll N_c' \ll N_d$ Equation 21 reduces to

$$n = (N_c' N_d)^{\frac{1}{2}} = \tfrac{1}{2}(N_d N_c)^{\frac{1}{2}} \exp[-E_d/2kT] \quad . \tag{23}$$

The Fermi levels for Equations 22 and 23 are given by

$$E_f = -E_d + kT \ln\left(\frac{N_d - N_a}{2N_a}\right) \text{ and } E_f = -\tfrac{1}{2}E_d + \tfrac{1}{2}kT \ln(N_d/N_c)$$

respectively. As can be seen in these equations, when compensation is a significant factor, the Fermi level lies slightly above the donor energy, $-E_d$. However, if this is not true, it lies very close to the midpoint between donor level and conduction band. Consequently, care must be taken when interpreting data of ln n or $\ln\sigma$ plotted against $\frac{1}{T}$. In inspecting Equations 22 and 23 it is seen that the slope of the ln n versus $\frac{1}{T}$ curves, if straight lines, can be indicative of either E_d or $E_d/2$.

It must be emphasized that the simple picture thus far is one of a flat band nature, i.e. the assumption is made that donor and acceptor densities are homogeneous throughout the crystal. Two other pertinent possibilities exist that could affect experimentally determined conductivity slopes. The first is an inhomogeneous donor or acceptor density with distance from the surface and the second a charge distribution at the crystal surface. In both of these cases the band edge energies would not remain constant spatially in the crystal.

The treatment in one dimension of the bent band picture is outlined below for two cases: 1) a space charge region set up by charges fixed at the surface and 2) a donor density that is distance dependent. The formalism of Seiwatz and Green[48] has been adopted for the sake of generality. Restricted treatments have been given by Garrett and Brattain[44], Kingston and Neustadter[45], Dousmanis and Duncan[46], and Young[47]. All of these

considered only the case where the donor densities are constant with distance.

In most situations band bending is not considered to extend throughout the total crystal but is treated as confined to a few hundred angstroms distance from the surface. Now consider an n-type semiconductor with donor and acceptor densities N_d and N_a. Their respective ionization energies E_d and E_a measured from the appropriate band edge are taken to be constant throughout the crystal. Also n and p are the free electron and hole densities respectively. The electric field in the semiconductor at the surface $\mathcal{E}_s$, is obtained by using Poisson's equation. For this equation it is necessary to have expressions for the mobile and bound charge densities in the bulk.

It is convenient to define an energy E_i such that (E_c-E_i) is a constant throughout the crystal where in the neutral bulk E_i is the value E_f would take if the crystal were intrinsic. Therefore at any point the potential difference is

$$\phi = (E_f-E_i)/e$$

and $(\phi_b-\phi_s)$ is the potential difference between the bulk and the surface. For convenience the following are defined:

$$u = e\phi/kT \text{ and } w_{pq} = (E_p-E_q)/kT \quad .$$

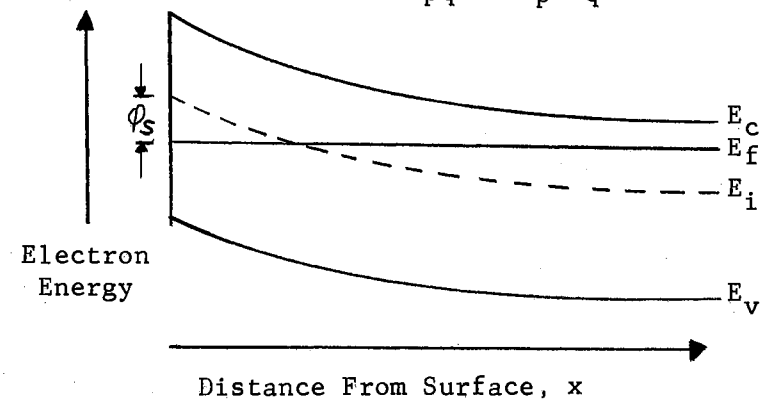

In the bulk there are four contributions to the charge density. The first arises from the ionized donor levels which make up a positive bound charge and is given by $(N_d-n_d) = N_d(1-f(E))$ where $f(E)$ in this case has a pre-exponential $\frac{1}{2}$ if one considers each donor to have only one electron which can be of either spin.

Therefore

$$\rho_d = eN_d\left[1+2\exp\left[(E_f-E_d)/kT\right]\right]^{-1} \quad . \tag{24}$$

In the same sense an ionized acceptor is a bound negative charge and so the occupation density of the acceptor level is $n_a = N_a f(E)$ where now $f(E)$ contains a pre-exponential factor of 2, considering each acceptor state must have two paired-spin electrons, therefore

$$\rho_a = -eN_a\left[1+2\exp\left[(E_a-E_f)/kT\right]\right]^{-1} \quad . \tag{25}$$

In the above notation Equation 24 and 25 can be written

$$\rho_d = eN_d\left[1+2\exp(u-w_{di})\right]^{-1} \tag{26}$$

$$\rho_a = -eN_a\left[1+2\exp(w_{ai}-u)\right]^{-1} \quad . \tag{27}$$

The conduction band electron and valence band hole densities are given by Equations 11 and 12 which can be written

$$n = 4\pi\left[\frac{2m_n kT}{h^2}\right]^{3/2}\left[F_{\frac{1}{2}}(u-w_{ci})\right] \tag{28}$$

and

$$p = 4\pi\left[\frac{2m_v kT}{h^2}\right]^{3/2}\left[F_{\frac{1}{2}}(w_{vi}-u)\right] \quad . \tag{29}$$

Combining these into the total charge density $\rho = \rho_d+\rho_a+e(p-n)$ which

is the expression needed for Poisson's equation

$$\frac{d^2u}{dx^2} = -e\rho/\epsilon\epsilon_o kT \tag{30}$$

where ϵ and ϵ_o are the dielectric constant of the material and the permittivity of free space, respectively. Substituting gives

$$\frac{d^2u}{dx^2} = -\frac{e^2}{\epsilon\epsilon_o kT}\left\{\frac{N_d}{1+2\exp(u-w_{di})} - \frac{N_a}{1+2\exp(w_{ai}-u)}\right.$$

$$+ 4\pi\left[\frac{2m_v kT}{h^2}\right]^{3/2}\left[F_{\frac{1}{2}}(w_{vi}-u)\right]$$

$$\left. - 4\pi\left[\frac{2m_n kT}{h^2}\right]^{3/2}\left[F_{\frac{1}{2}}(u-w_{ci})\right]\right\} . \tag{31}$$

By integrating Equation 31 once from the field-free bulk to the surface, the surface electric field $\mathcal{E}_s$ is obtained as

$$\mathcal{E}_s = -\frac{kT}{e}\left(\frac{du}{dx}\right)_s = \pm\frac{kT}{e}\frac{1}{L_d}\left\{\frac{N_d}{n_i}\ln\left[\frac{1+\frac{1}{2}\exp(w_{di}-u_s)}{1+\frac{1}{2}\exp(w_{di}-u_b)}\right]\right.$$

$$+\frac{N_a}{n_i}\ln\left[\frac{1+\frac{1}{2}\exp(u_s-w_{ai})}{1+\frac{1}{2}\exp(u_b-w_{ai})}\right] - \frac{1}{F_{\frac{1}{2}}(w_{vi})}\left[\frac{2}{3}F_{3/2}(w_{vi}-u_b) - \frac{2}{3}F_{3/2}(w_{vi}-u_s)\right]$$

$$\left. + \frac{1}{F_{\frac{1}{2}}(w_{ic})}\left[\frac{2}{3}F_{3/2}(u_s-w_{ci}) - \frac{2}{3}F_{3/2}(u_b-w_{ci})\right]\right\}^{\frac{1}{2}} \tag{32}$$

where $L_d = (\epsilon\epsilon_o kT/2e^2 n_i)^{\frac{1}{2}}$ and n_i is given by Equation 14. The net space charge per unit surface area, N_s, is given by

$$N_s = (\epsilon\epsilon_o kT/e)\left(\frac{du}{dx}\right)_s . \tag{33}$$

In these expressions one can additionally allow N_d and N_a to vary with x. This requires either an experimental knowledge of the functional re-

lationship or solution using assumed relationships and curve - fitting with experimental results. Considering the present state of the understanding of the conduction mechanism in the material being studied, an extension of the theory in this direction would seem to be premature.

Thermoelectric Power

By subjecting a specimen to a temperature gradient, a thermoelectric voltage is produced across its ends. Experimental measurements of the thermoelectric power -- defined as thermoelectric voltage/temperature gradient -- may be used to gain information about the density of charge carriers in the material. The sign convention used is positive when the conventional current would tend to flow from semiconductor to metal at the cold end. This convention leads to a negative thermoelectric power for n-type semiconductors and a positive one for p-type. Pertinent equations for thermoelectric power are contained in a review article by Johnson[49]. The expression given for the transition range and the intrinsic range of operation is

$$Q = \frac{-k}{e(nc+p)}\left[2(nc-p)-nc\ln\left(\frac{nh^3}{2(2\pi m_n kT)^{3/2}}\right)+p\ln\left(\frac{ph^3}{2(2\pi m_v kT)^{3/2}}\right)\right] \qquad (34)$$

where c is the electron to hole mobility ratio and e is the magnitude of the electronic charge.

By neglecting p as compared to n Equation 34 reduces to

$$Q = -\frac{k}{e}\left[2-\ln n+3/2\ \ln T+\ln\left(\frac{2(2\pi m_n k)^{3/2}}{h^3}\right)\right] \qquad (35)$$

which is the classical equation for thermoelectric power of a n-type semiconductor with lattice scattering assumed. Another equation is obtained from Equation 34 by equating p and n and substituting Equation 14 for n

which then expresses the intrinsic behavior for the lattice scattering model as

$$Q = -\frac{k}{e}\left[\frac{c-1}{c+1}\frac{E_g}{2kT} + \frac{2(c-1)}{c+1} + \frac{3}{4}\ln\left(\frac{m_n}{m_v}\right)\right] \quad . \tag{36}$$

If the forbidden gap is written as $E_g = E_o + aT$ where E_o is the gap width at absolute zero and a is the constant determing the gap change with temperature, Equation 36 can be written

$$Q = -\frac{k}{e}\cdot\frac{c-1}{c+1}\left[\frac{E_o}{2kT} + \frac{a}{2k} + 2+3/4\ \frac{c+1}{c-1}\ln\left(\frac{m_n}{m_v}\right)\right] \quad . \tag{37}$$

According to this equation a plot of Q vs $\frac{1}{T}$ can yield the mobility ratio if E_o is known or vice versa. The intercept can be used to determine a if a rough estimate of m_n/m_v is available. Alternatively, if the behavior is extrinsic, Equation 31 will give values for donor activation energies when used in conjunction with Equations 18 or 19, if it can be determined which one provides an appropriate describption of the situation.

CHAPTER IV

SAMPLES, APPARATUS AND EXPERIMENTAL TECHNIQUE

Samples

Two types of samples were used in this investigation, small rectangular rods of SnO_2 grown locally from a Cu_2O flux and similarly-shaped vapor grown samples*. The vapor-phase samples were used mainly for optical transmission studies in the visible wavelength region. As mentioned previously the rod-like crystals usually grow with a square cross-sectional area having from 0.5 to one millimeter dimensions on a side, quite adequate for measurements of the type performed.

The crystals taken from the HCl bath come in a variety of sizes. There are very large, poor quality crystal chunks apparently made up of many smaller crystals that are growing parallel to each other. These are found to contain many inclusions of veins and bubbles filled with a dark red material. Crystals intermediate in size between the chunks and the needles are the ones chosen for samples. These also have different appearances. Some have very smooth glossy surfaces and others an "embossed" surface pattern; some have veins and bubbles similar to those found in the chunks and some are essentially flaw free. Freedom from visible surface and bulk flaws provided the main criterion for choice. Due to the way the crystals are grown and cooled, much cracking of long crystals occurs under

---

*Grown by Semi-Elements, Inc., Saxonburg, Pennsylvania.

the normal stresses imposed by solidification of the melt, limiting the length. Many times during the process of facing the crystal ends in preparation for conductivity measurements, it was convenient to cut them shorter to eliminate small inclusions or surface flaws. The final length of the sample crystals usually varied from one to five millimeters.

Two varieties of color are observed in the as-grown crystals. They appear clear and transparent, some having a very faint pink tinge and others not. The crystal color will be discussed in detail later. The vapor grown samples are similar in size and surface appearance but have a deeper red color.

Sample preparation subsequent to recovery from the melt consisted of facing the ends and cleaning. The facing proceedure involved securing the crystal in the lapping holder shown in Figure 9. This was done by heating the holder and sample on a hot plate to approximately 75°C and melting optical wax around the crystal for reinforcement. After cooling, the sample ends were abraded using 600A WETORDRY silicon carbide paper on a hard flat surface. The optical wax was then dissolved in acetone using an ultrasonic cleaning apparatus.* Much care in handling had to be exercised since chipping and cracking of the crystals causes anomalous effects on electrical measurements.

Proper cleaning of the samples is imperative since the as-grown samples exhibit a very high resistance and surface films could render the electrical results erroneous. This was accomplished by four-hour baths in both hydrofluoric acid and aqua regia (75% HCl, 25% HNO_3). It was later found that the hydrofluoric acid bath could be eliminated with no

---

*Ultrasonic work done on Gulton Industries Model GT-1-10 Ultrasonic Cleaning Unit.

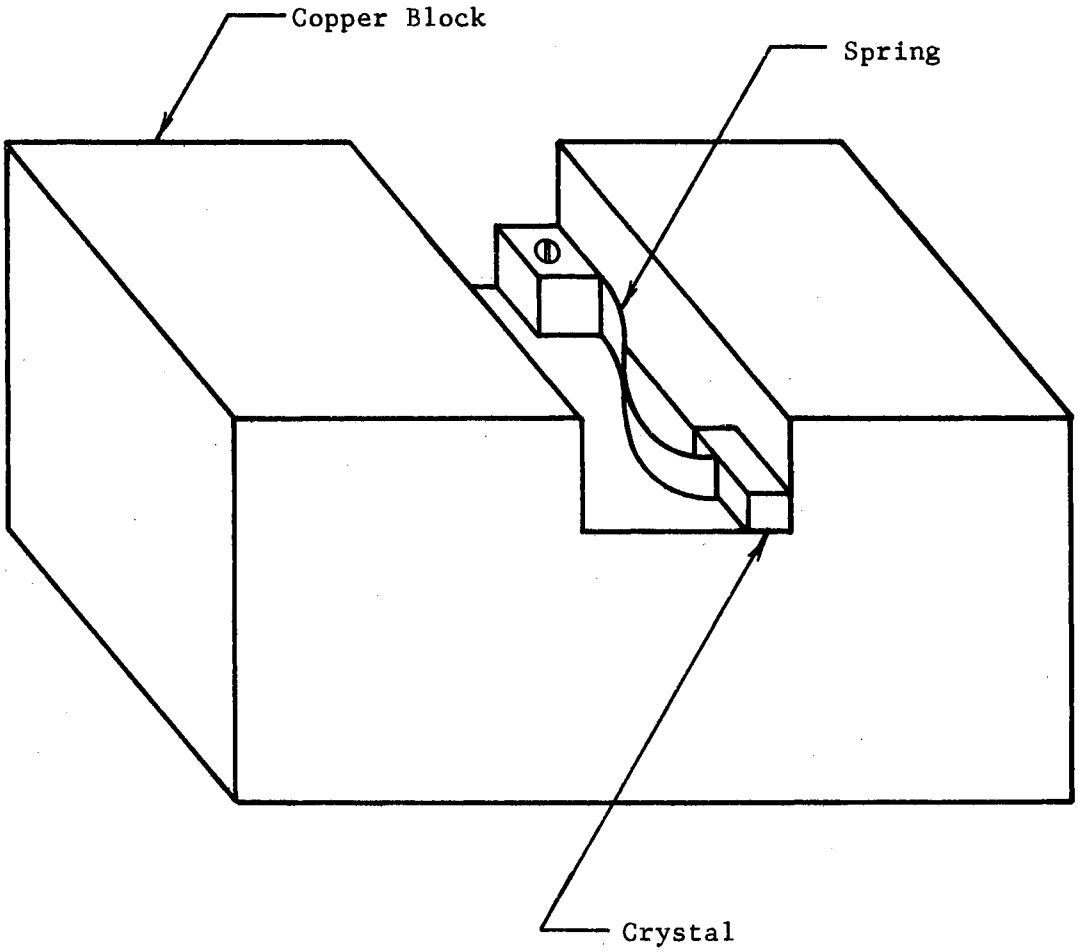

Figure 9. Holder for Lapping Ends of Samples.

adverse effects. The baths were followed by ultrasonic rinses in acetone, methanol and distilled water in that order. Particular care had to be taken to insure that the acetone was completely removed after this portion of the cleaning procedure because it can leave a film on the crystal surface which when heated produces an etching effect.

No further preparation was needed prior to experimentation. The electrical contacts, discussed later, are platinum discs pressed to the ends of the rectangular parallelopiped shaped crystals.

Apparatus

The basic design of the sample holders for conductivity and thermoelectric power measurements is very similar. The optical work on the Beckman DK-1 and IR-7 spectrophotometers used the sample holder provided with the instrument.

Electrical Conductivity - Figure 10 shows the bell jar apparatus constructed for conductivity measurements. The bell jar base was constructed to have three 3/16 inch o.d., thermocouple pass-throughs, two 1/4 inch solid conductor pass-throughs and a 3/4 inch housekeeper copper-to-glass seal for a vacuum port. It also provided support for the crystal holder system. The diameter was 12 inches and supported a C.V.C. 10 o.d. x 14 inch bell jar equipped with a Neoprene gasket. All the feed throughs were soft soldered to the base.

The crystal holder fixture and heater attached to the bell jar base are shown in Figures 11 and 12. Considerable care was required to insure a holder design having a very high leakage-resistance and also providing very little thermal conductivity in order to prevent too much heat leakage from the furnace. The arrangement also allowed crystals to be changed

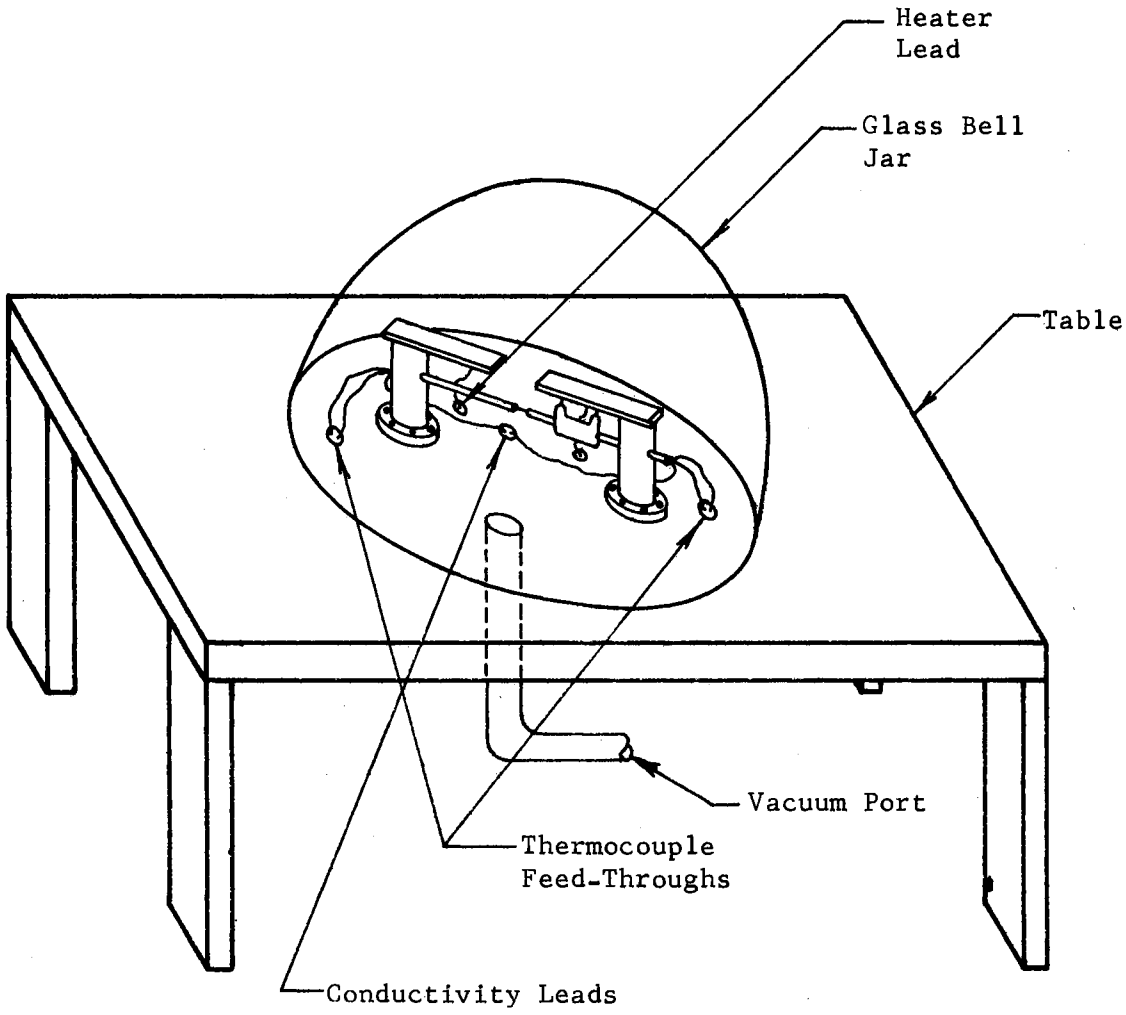

Figure 10. Bell Jar Apparatus for Conductivity Measurements.

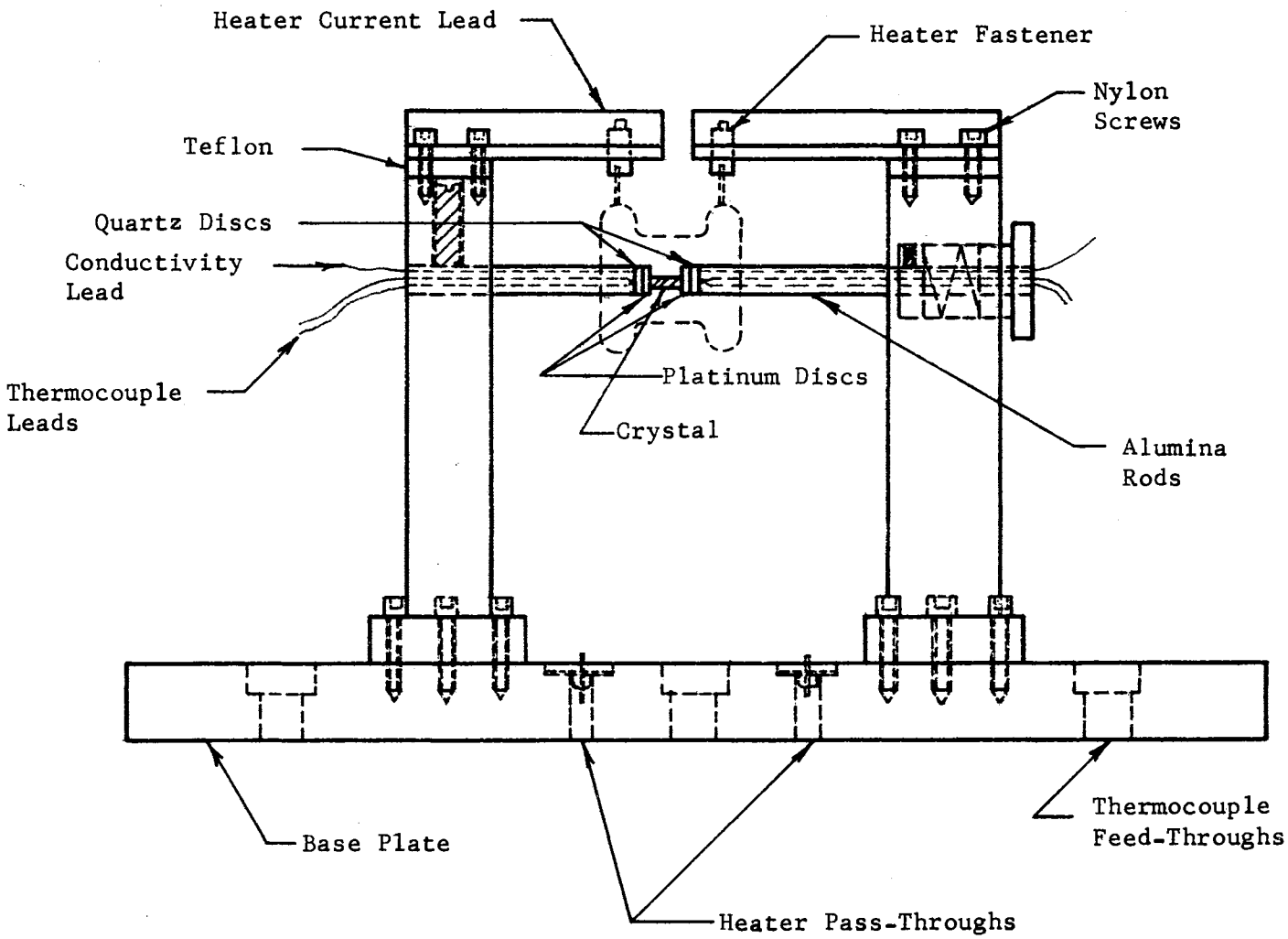

Figure 11. Crystal Holder for Conductivity Measurements.

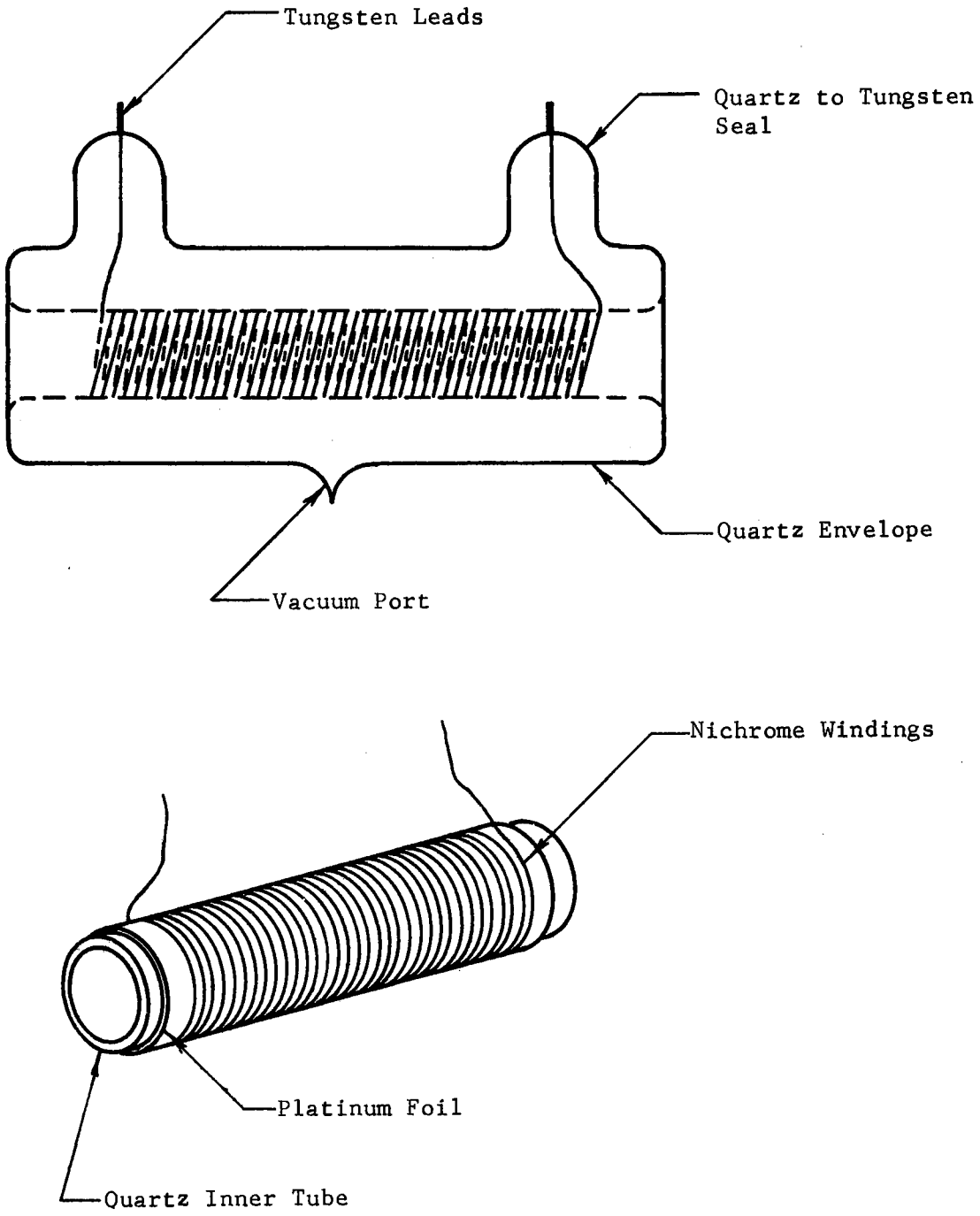

Figure 12. Quartz Furnace Design for Conductivity Measurements.

without dismantling the fixture. This was accomplished by having a heater that could slide over the crystal and be positioned out of the way. The crystal is held between two 1/4 inch o.d. alumina four-hole capillary rods. One of these is held stationary and spring tension is applied to the other. Three leads pass through the capillaries of each rod; two belong to a platinum-platinum (90%), rhodium (10%) thermocouple and the third is the conductivity current lead. The thermocouple is electrically insulated from the current lead at the crystal by a quartz disc 1/4 inch in diameter by 2 millimeters thick having a 1/2 millimeter diameter hole drilled through it for the current lead.* On the end of the current lead in contact with the crystal is a platinum disc one millimeter thick by 1/4 inch in diameter.

The heater construction is shown in Figure 12. Its laminated design consists of an inner quartz tube 3/8 inch i.d. about which platinum foil 0.002 inches thick is wrapped. On top of this are wound two layers of 28 gauge Nichrome wire coated with asbestos shielding. The platinum is used to stop hot spots from developing to cause uneven heating of the crystal. This portion of the heater is connected to an outer quartz tube having tungsten current leads through it and a port for evacuation. One lead is grounded to the platinum foil serving as an electrostatic pickup shield. The envelope is sealed to the inner portion forming a vacuum vessel. A rough pump vacuum is pulled on the furnace and the capillary sealed off reducing problems with outgassing.

A portable vacuum system was constructed for use in conductivity and thermoelectric power measurements. As seen in the schematic Figure 13, it consists of a Cenco Mechanical Hyvac 7 forepump and a C.V.C. Model GF-26

---

*Drilled with Gulton Industries Model D-10 Ultrasonic Drill.

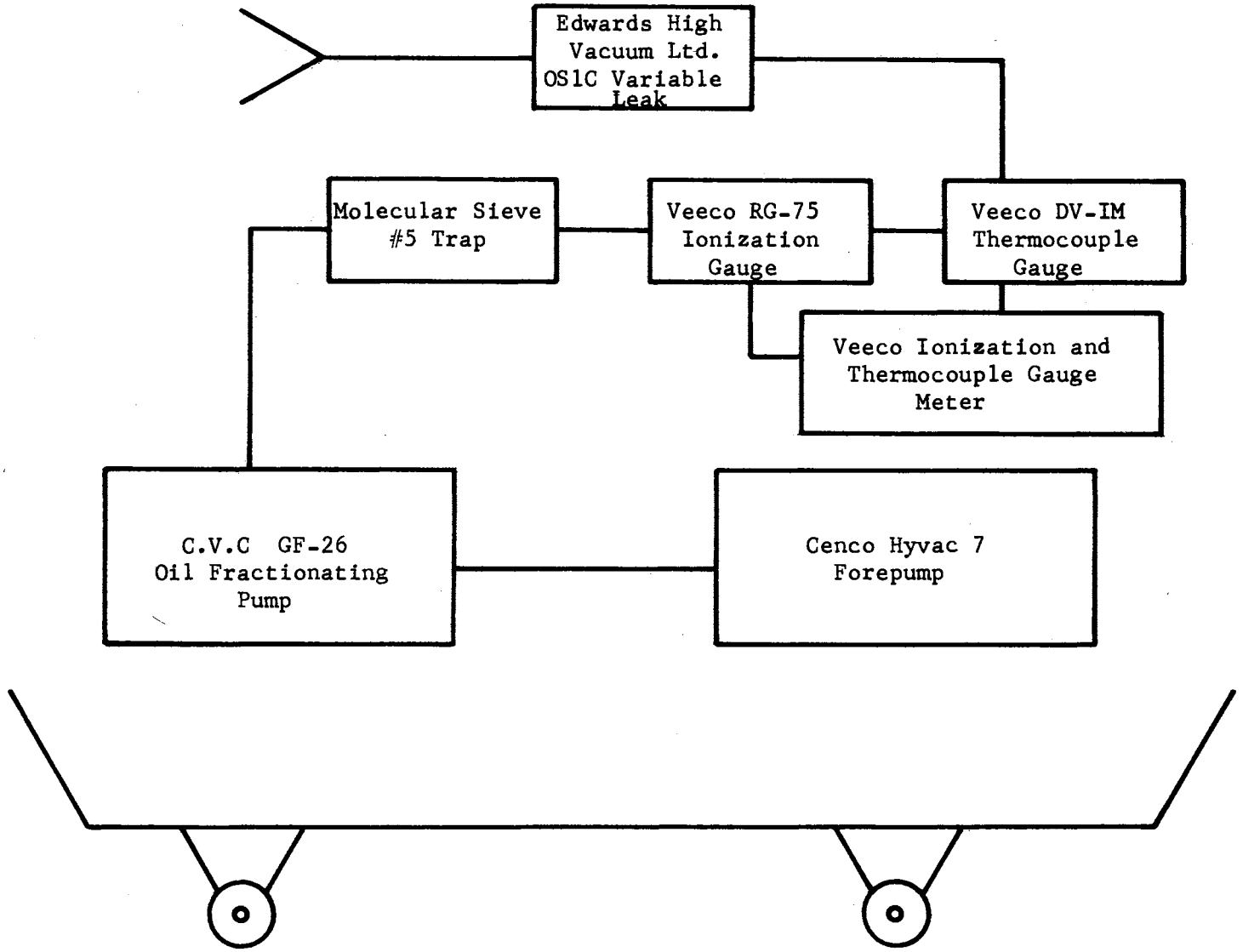

Figure 13. Portable Vacuum System Schematic Diagram.

glass oil fractionating pump. The pump is trapped using Molecular Sieve #5A in an envelope that can be contained in a Dewar Flask for low temperatures when needed. C.V.C. Octoil-S pump fluid is used and since it is an ester, no back flow of pump oil should occur at room temperature when the sieve is properly outgassed. The accessories as noted in the schematic diagram are thermocouple and ion gauge tubes which are Veeco's DV-1M and RG-75 respectively. These are controlled by a Veeco RG-31A combined power supply and meters for both gauge tubes. An Edwards High Vacuum Ltd. Model OS1C variable leak having a 360° dial produces a fairly linear flow of 420 cc/min per full turn of the dial up to 3000 cc/min from an atmospheric pressure source and can be used to vary ambient pressures. The vacuum system was sealed directly to both conductivity and thermopower apparatus to alleviate problems that might occur using vacuum grease.

Since both the conductivity and thermoelectric fixtures employed two platinum-platinum (90%), rhodium (10%) thermocouples it was necessary to compare these to each other to ascertain their reproducibility. This is especially important in the temperature gradient determination for thermoelectric power. The comparison was accomplished by using a setup as depicted in Figure 14. Each thermocouple was placed in a 1/4 inch alumina thermocouple tube that was fitted with a quartz end piece for junction protection. This was covered by a copper sleeve and inserted into a double-bore copper cylinder. The cylinder was 2 1/2 inches in diameter and 3 1/2 inches long with bores of 3/8 inches each extending to the center of the copper block. The copper block and thermocouples were placed into a muffle furnace capable of 950°C. Using an ice bath reference for both thermocouples and a Leeds and Northrup K-3 type

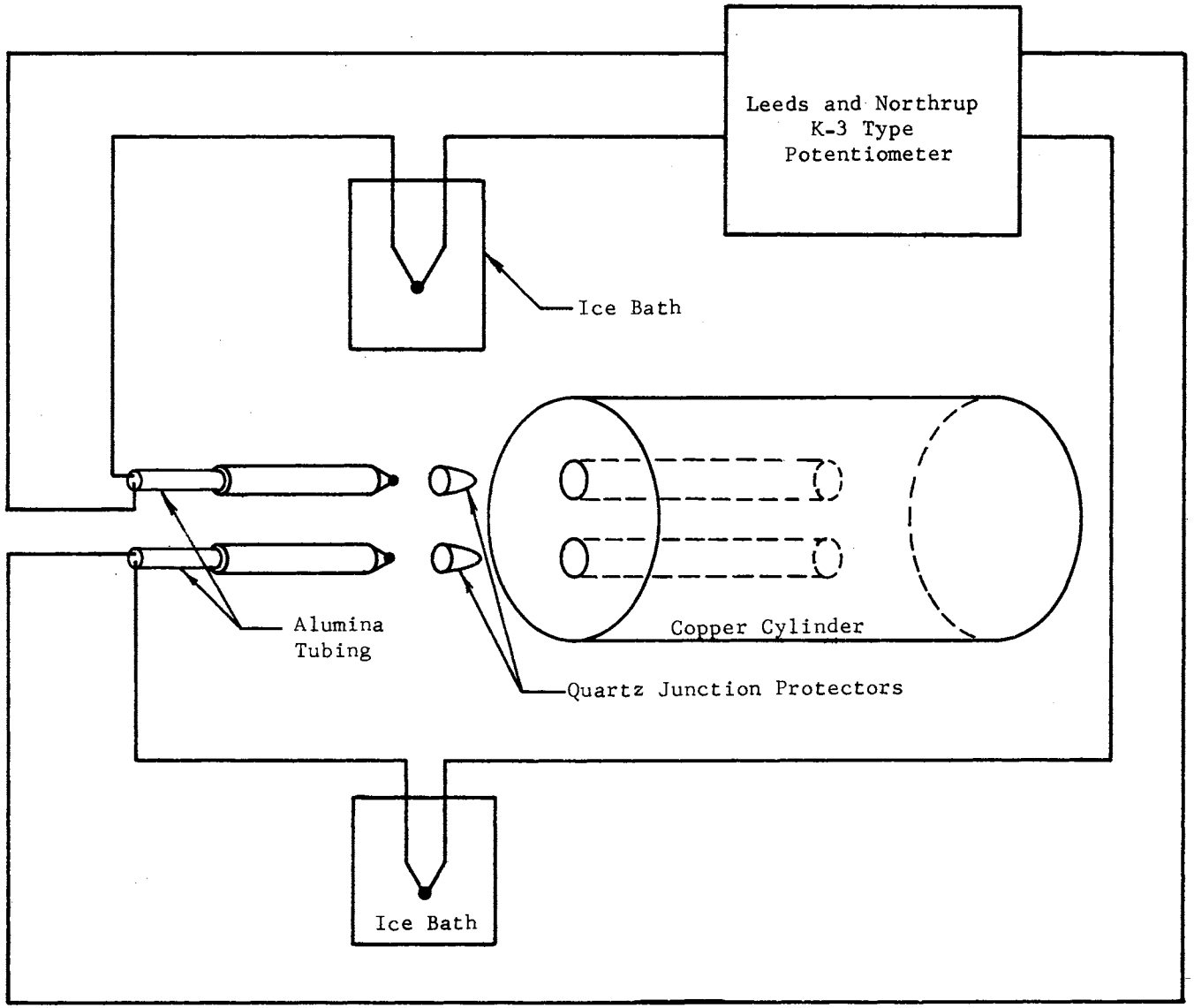

Figure 14. Apparatus for Thermocouple Comparison.

potentiometer for output determination it was found that the couples did not deviate more than 3 tenths of a degree centigrade from each other in the 20 to 900°C temperature range. The greatest difference occurred as expected at the high temperatures.

Thermoelectric Power - The thermoelectric power crystal holder and vacuum enclosure can be seen in Figure 15. Once again the crystal is supported between two alumina capillary rods under spring tension. The original design consisted of two platinum heaters wound directly on the ends of the alumina rods. These could be controlled to give the desired temperature gradient. However, this configuration was abandoned in favor of a simpler system of one quartz heater like that depicted in Figure 12 that could be positioned off-center to create the temperature gradient. It was found that the open heaters evaporated platinum onto the alumina rods causing electrical leakage from heater to crystal and giving erroneous results. The two thermocouple junction leads are contained in the rods and extended out of the system through hermetic pass throughs. As before, the end contact is a platinum disc to which the platinum (90%), rhodium (10%) lead is welded to form the couple. The platinum wires are used for the thermoelectric voltage determenation. A vacuum seal between crystal holder and enclosure is made by means of an O-ring. The enclosure and seal are water cooled with a jacket of copper tubing soldered to the can.

Optical Transmission - In the optical work two instruments were used. The Beckman DK-1 quartz prism recording spectrophotometer covered the 185 to 3500m μ wavelength range employing hydrogen (185-375 mμ) and tungsten (350-3500 mμ) lamps. The long wavelengths were covered by a Beckman IR-7 spectrophotometer provided with a Nernst glower as source for its

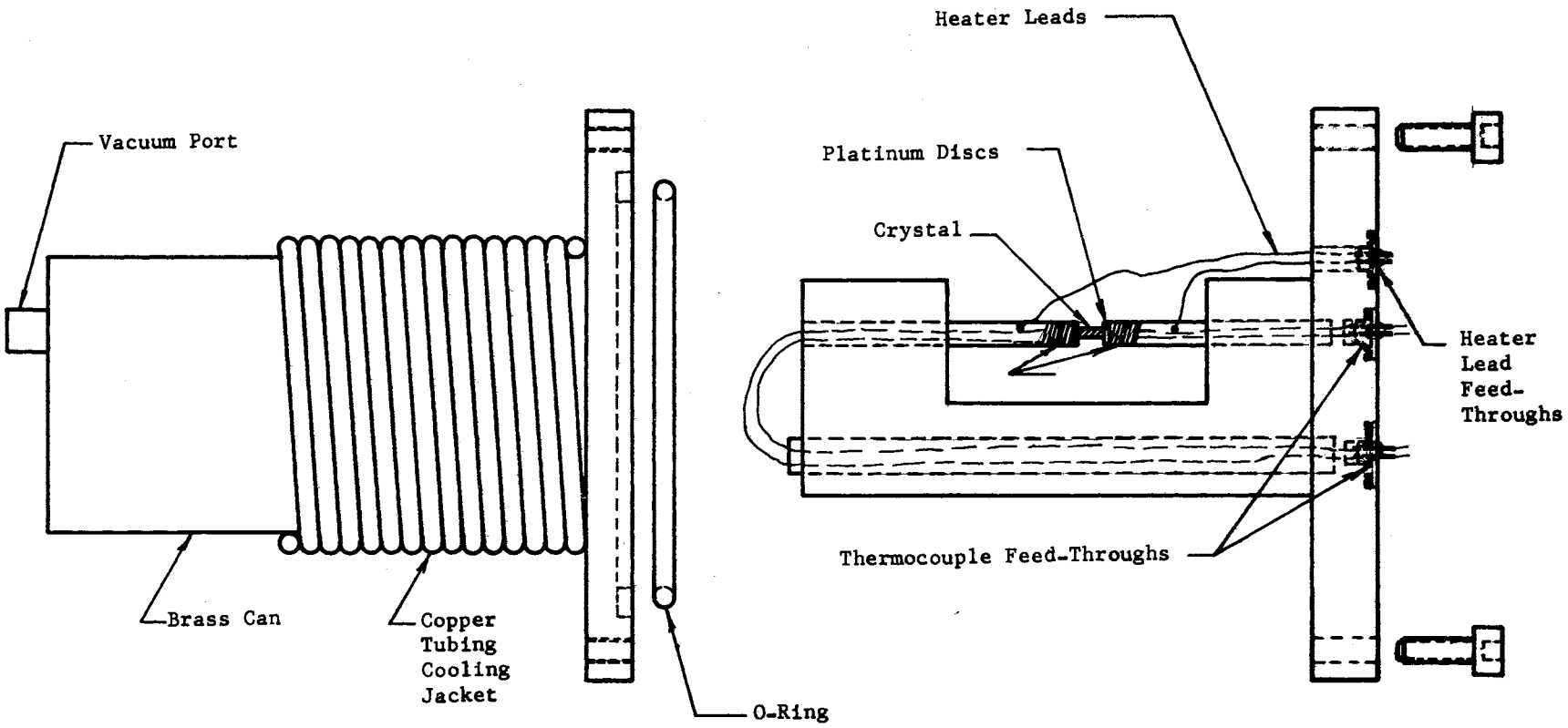

Figure 15. Crystal Holder for Thermoelectric Power Measurements.

2.5 to 15.4 μ range. In both cases the crystals were secured to a brass plate by means of optical wax. These plates had the appropriate hole size drilled in them such that the maximum area of the crystal was exposed. The plates were placed in the instrument crystal holder. In the IR-7, the standard beam condenser was used to assure that enough light would be transmitted through the crystal for detection. When measuring with double beam instruments such as these, one can insert a diaphragm in the reference beam cutting down its intensity to balance smaller signals. This type of diaphragm was used on both instruments since the size of the crystals were such that only a fraction of the instrument beam could be transmitted.

Measuring Techniques

Two-probe techniques were used in the conductivity measurements. This raises the question of contact problems due to excessive resistance at the crystal-metal interface. To justify a two-probe method, four-probe measurements were made along with V-I characteristic curves to check for rectification. Figure 16a shows the four-probe crystal holder. Its basic design added to the spring-loaded platinum contacts two point-contact probes made of the Sylvania IN21 crimped tungsten whiskers used in point-contact transistors. The four-probe measuring circuit is shown in Figure 16b. Due to the high resistance of these samples the normal potentiometer circuit could not be used and Keithley Model 621 and 610B electrometers were employed instead.

A number of preliminary experiments were performed with this basic arrangement. The first compared the effect of abraded and nonabraded contacts. If a battery and electrometer were connected in series with the two

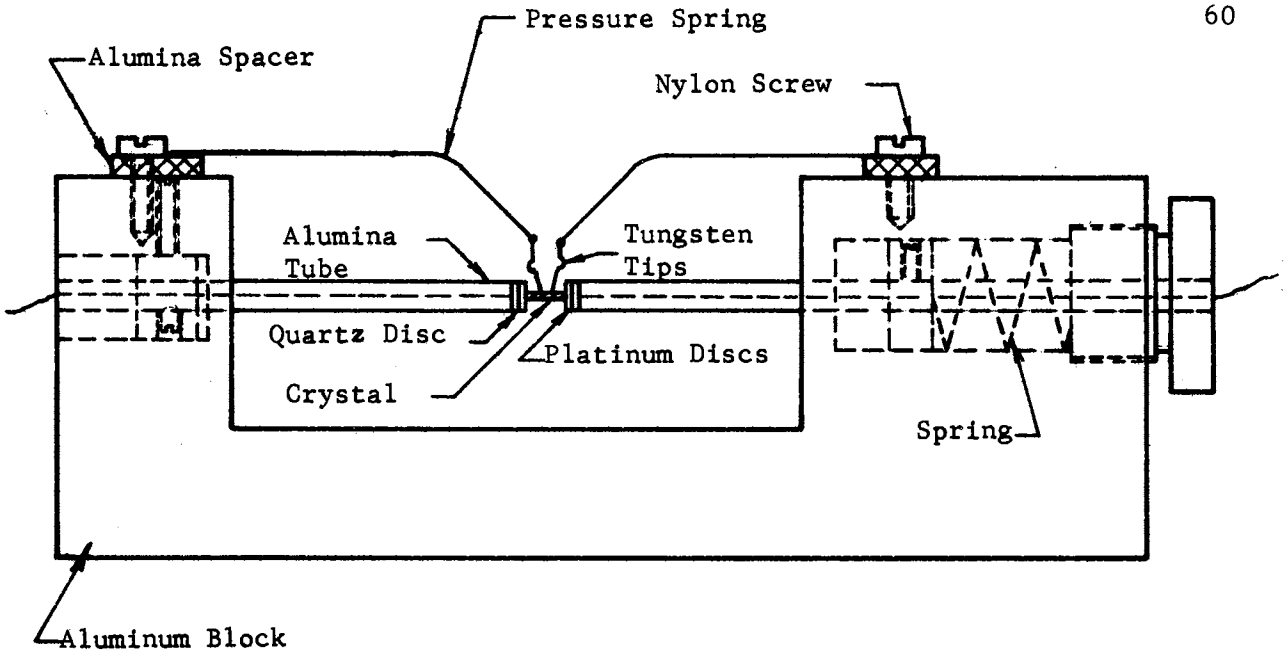

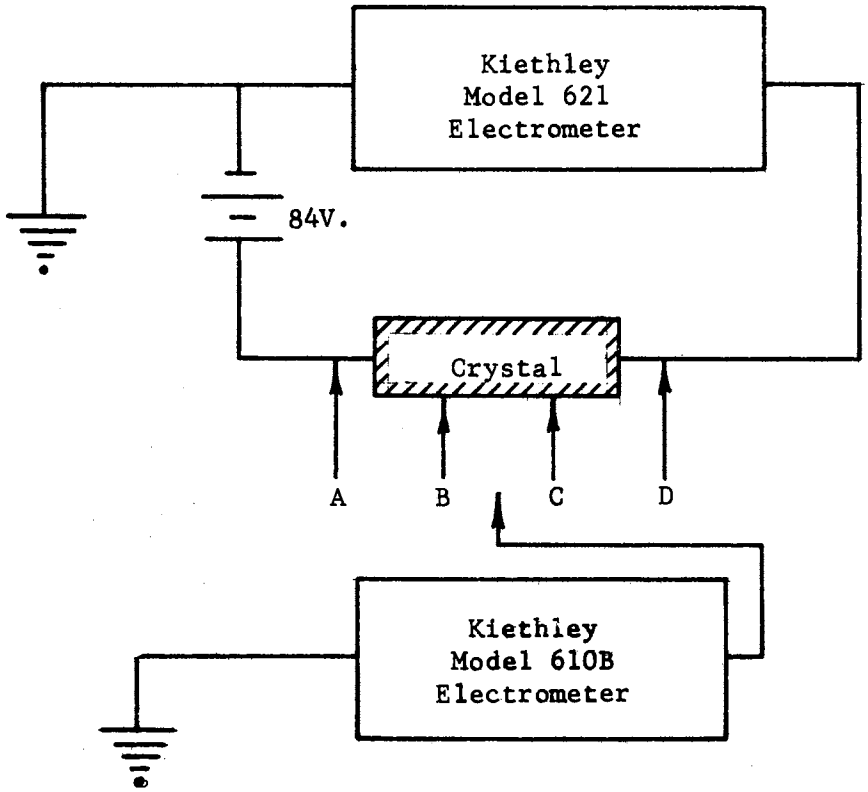

Figure 16. Crystal Holder for Measuring 4-Probe Conductivity.

point probes on the as-grown crystal surface, a very high resistance was noted. In many cases it was greater than the 10^{14} ohms input resistance of the electrometer. If, however, this experiment was performed using an abraded area on the surface under each probe, the resistance was lowered by many orders of magnitude, e.g., from 10^{14} ohms to about 10^{8} ohms. The roughened areas were prepared with the ultrasonic drill and #600 alumina grinding compound. This measurement suggested that either the as-grown surface causes a very high contact resistance or there is an insulating layer at the crystal surface.

A second configuration similar to the above used the current path from the broad abraded end contact of pressed platinum to the point contact for both the abraded and nonabraded situations. The broad platinum end contact, of course, is never made to a nonabraded crystal surface since the end is faced to make this type of contact possible. Again two results were obtained. If the point contact was made to the as-grown surface, a very high resistance was measured whereas on the roughened surface it decreased many orders of magnitude. Along with these two experiments a third was performed with point contact to one crystal end and broad pressed platinum to the other end which showed that contact size did not influence the resistance. In all experiments of this type the current was reversed to see if any rectification could be noted. None was.

It was concluded from these trials that there is a high resistance layer at the as-grown surface of the crystal. Further substantiating evidence of this is presented in the Results chapter. Similar conclusions were reached by MacAvoy and Marley[40] concerning their vapor-grown stannic oxide.

Conventional four-probe conductivity measurements were made using the arrangement in Figure 16a,b. In all cases the point contacts were made to

abraded areas. This technique involved measuring -- in the dark -- four voltages (A,B,C,D) seen in the schematic diagram. By subtracting values B from A, C from B, and likewise D from C, the voltages dropped on three sections of the crystal were determined. Similarly, data was taken with the battery reversed. In all but a few crystals examined, the sectional resistance ratios were comensurate with the respective length ratios indicating homogeneous resistivity and the sum of the sectional resistances equalled the total end-to-end resistance. Situations where one large sectional resistance occurred compared to the others could be explained by the presence of a mechanical flaw since if the crystal was reversed in the holder the voltages were also reversed, ruling out excessive contact resistance in favor of a resistivity inhomogeneity. Most of the four-probe measurements were made at room temperature although a few were taken up to 150°C by placing the crystal holder on a hot plate and checking three or four intermediate equilibrium points.

Along with the four-probe experiments, V-I characteristics were run in different sections of the crystal to check for rectification with negative results. A typical example is found in Figure 17. It must be pointed out however, that care had to be taken in placing the crystal in the holder. When rectification was observed and no visible flaw developments were apparent, it was due to placing the crystal at an angle in the holder causing uneven contact at the platinum discs. Remounting the sample was found to remedy the situation.

Reviewing these combined experiments, it has been concluded that the contact resistance is negligible in comparison to crystal resistance and that the resistivity is homogeneous along the length of visibly sound samples.

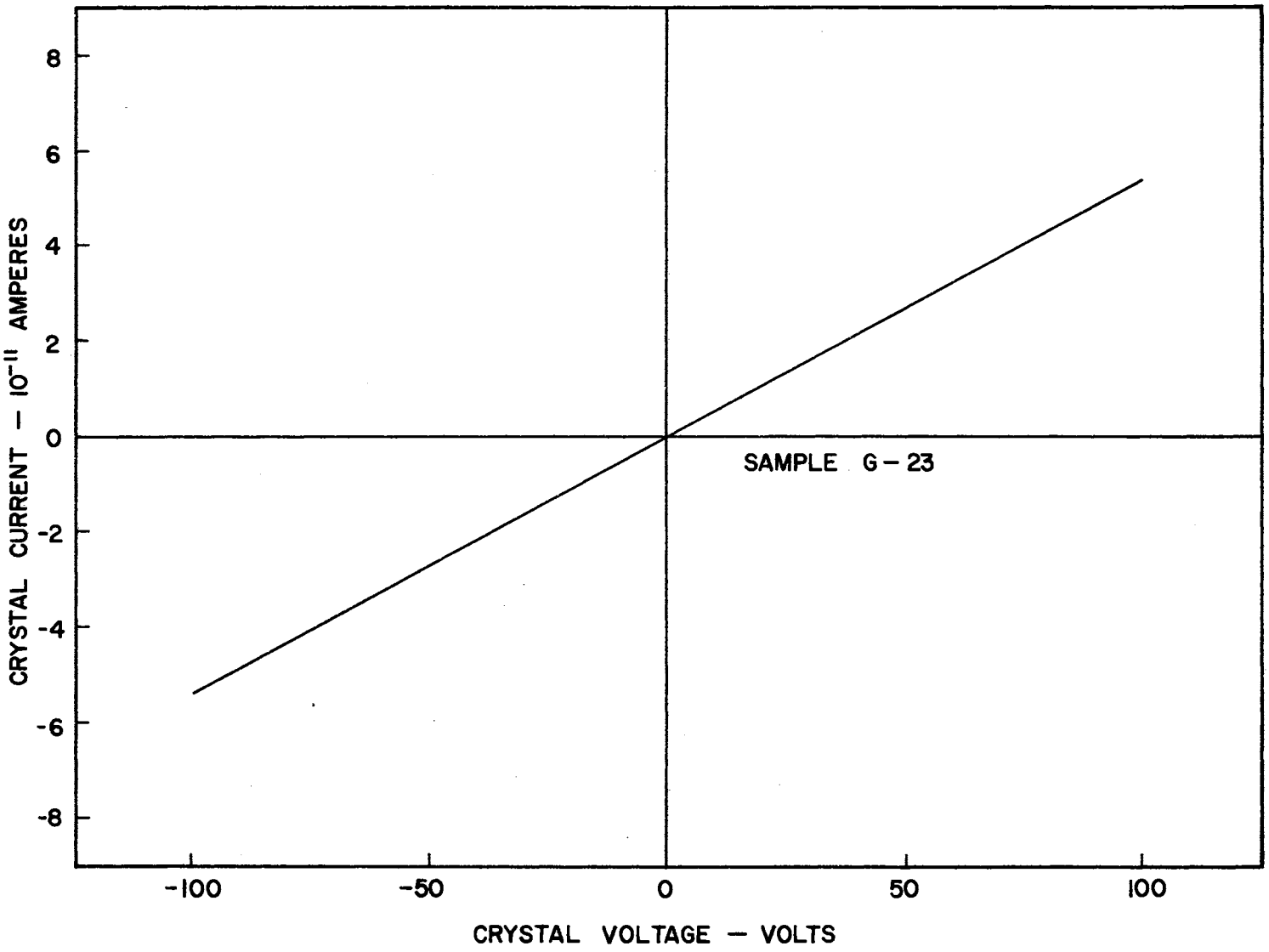

Figure 17. Typical Crystal Current as a Function of Voltage.

A schematic diagram of the conductivity measuring system is shown in Figure 18. The circuit voltage was 2.1 volts and was provided by one cell of a 6 volt automobile battery. Since data was taken point by point it was necessary to know when steady state values of crystal current had been reached. This was accomplished by using a Sargent Model SR recorder driven by the Keithley 610B. When the data was recorded continuously between steady state points, it was found that the crystal current varied closely with crystal temperature on runs made in air at atmospheric pressure. This temperature was recorded by the same type of recorder. The recorders operate on a potentiometric principle and allow the two thermocouples built into the system -- one on each side of the crystal -- to be connected directly. By means of a switch either one could be hooked into the recorder and this fact was conveniently used to check when the furnace was properly placed so as to heat the crystal evenly.

Since the basic electrometer acts as a voltage sensing device, its current ranges employ standard resistors over which voltages are measured. This being the case, when the electrometer scale is switched the voltage across the crystal changes such that the current read is not directly proportional to the crystal conductivity. Therefore a correction was made to the current so that a direct proportionality existed. This is best explained by the following equations:

$$I_a = \frac{V_k}{R_k}$$

where I_a is the actual current through the crystal and V_k the voltage read across the standard resister R_k in the electrometer circuit. The current desired is that which would pass through the crystal if a constant voltage were continuously applied. This would be $I_c = \frac{V_b}{R_c}$ where R_c is the

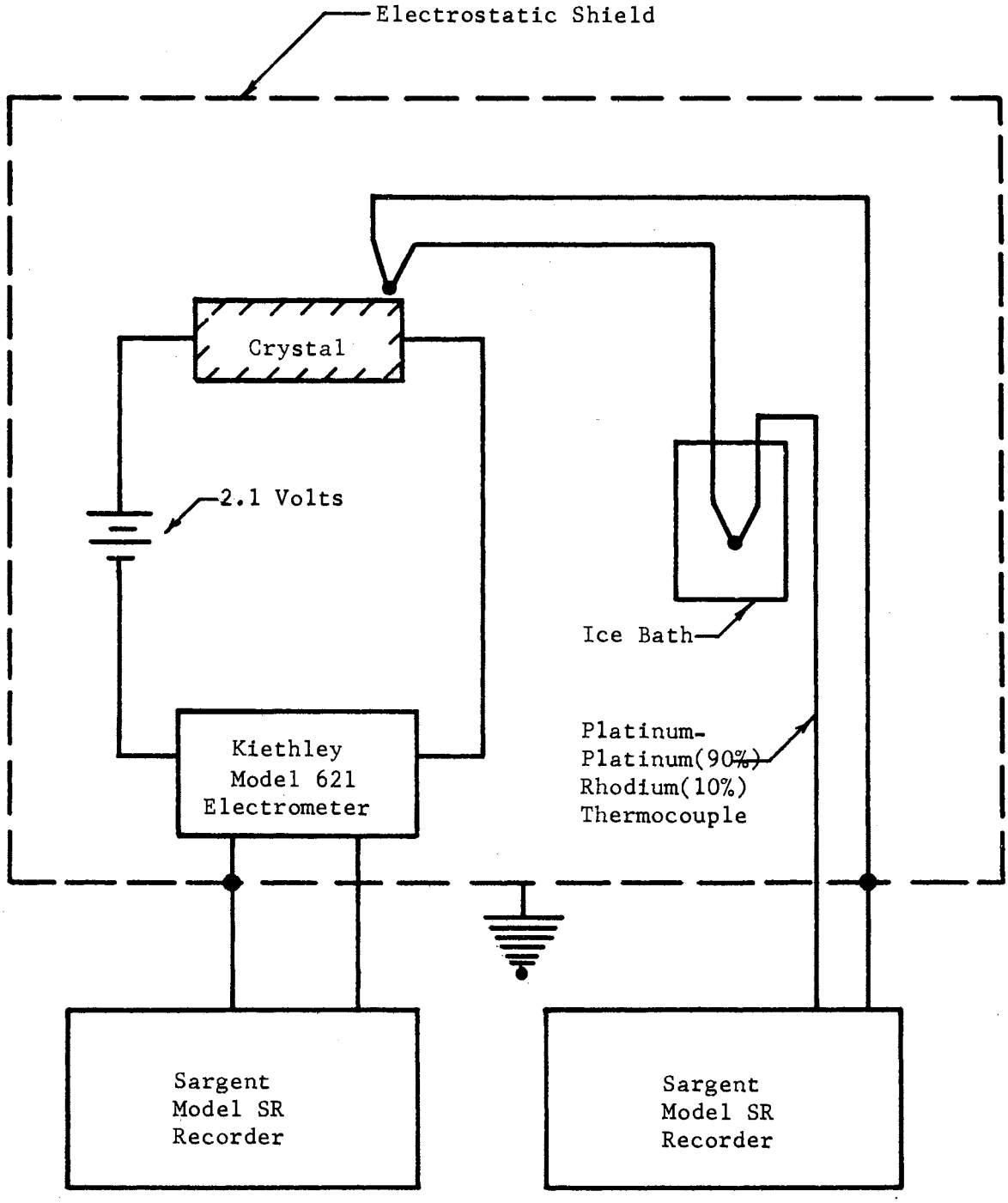

Figure 18. Block Diagram of Conductivity Measuring Circuit.

crystal resistance and V_b the battery voltage. Therefore the correction factor k is

$$k = \frac{I_c}{I_a} = \frac{V_b}{R_c} \cdot \frac{R_k}{V_k} = \frac{V_b R_k I_a}{(V_b - V_k)V_k} = \frac{V_b}{(V_b - V_k)}$$

because $R_c = \frac{V_b - V_k}{I_a}$ and $V_k = I_a R_k$. A computer program for the I.B.M. 1620 was used to obtain values of constant voltage current versus measured current from the above correction. The inputs to the program were battery voltage and voltage range on the electrometer. All the conductivity data was corrected in this manner.

A great deal of time was spent in obtaining a method of taking data that would produce consistent and reproducible results. It was found that if a crystal was heated to a given temperature, conductivity as a function of temperature was reproducible with increasing and decreasing points as long as this temperature was not exceeded. The term "fixing" is used for this procedure since it determines the conductivity versus temperature curve. A record of each specimen's past thermal history was kept to observe its effect on subsequent data.

Vacuum measurements on conductivity were taken in the same way as atmospheric pressure measurements except that the pressure could be varied from 10^{-5} torr to 10^{-1} torr by means of the variable leak. Corrections to the data were the same as above.

The thermoelectric power data taken was also dependent upon "fixing" procedure. A schematic diagram of the measuring apparatus is shown in Figure 19. Two platinum-platinum (90%), rhodium (10%) thermocouples were in contact with the crystal. The platinum leads formed the thermoelectric power or crystal voltage leads as well as one side of the thermocouple junction. A Keithley 610B electrometer measured the Seebeck voltage and a

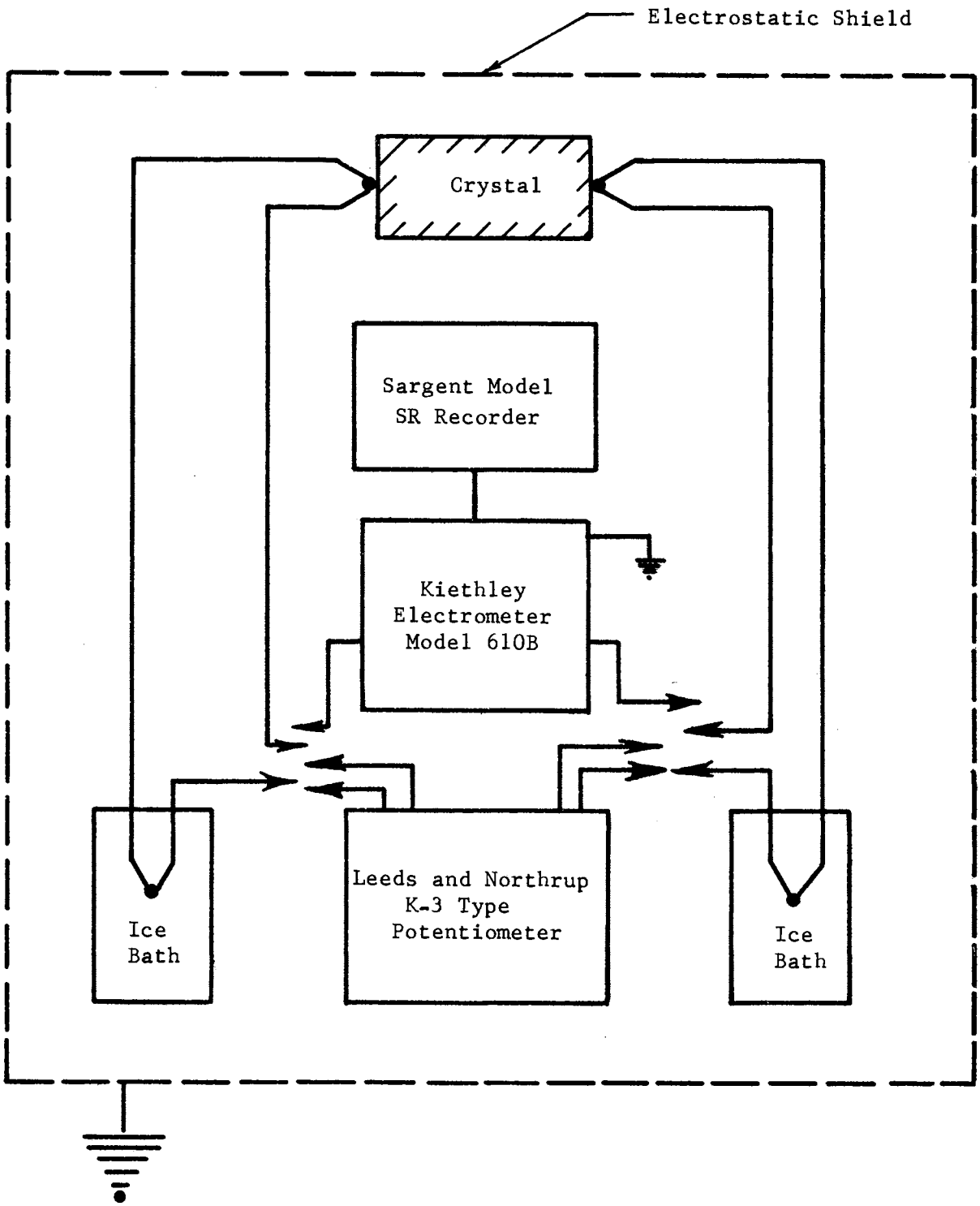

Figure 19. Block Diagram of Thermoelectric Power Measuring Circuit.

Leeds and Northrup K-3 type potentiometer measured the outputs from the two thermocouples. A Sargent Model SR recorder, provided with a signal from the electrometer, indicated when the crystal had reached equilibrium.

At each datum point the voltage was read from the electrometer and the electrometer then disconnected from the circuit. The K-3 was then connected and thermocouple voltages taken. This was done because the input impedance of the K-3 was much lower than the crystal resistance. The K-3 was then disconnected and electrometer once again inserted before the temperature was changed to verify the first voltage reading.

Two types of data were taken. Thermoelectric voltage versus temperature was measured in air following a high temperature "fix" and at several different ambient pressures varied with the vacuum system described previously. Data was taken point by point both with temperature increasing and decreasing. While at the high temperatures the gradient across the crystal was reversed to see if a polarization effect could be noticed. Measurements were taken on the way up and down without switching the gradient to check reproducibility.

Much care had to be exercised in order to get good results. High resistance electrical leaks due to dirty pass-throughs and moisture occurred frequently. Each time the system was disassembled and cleaned. The check for these leaks involved switching the heater on and off while measuring with either the K-3 or electrometer and watching for surges in meter readings which indicated their presence.

Because the single heater system was used to obtain the majority of the reported data, gradients varied from 5°C at the lower temperatures to about 30°C at the high end of the measurement range. Preliminary checks with the dual heater system indicated no significant dependence of thermoelectric power upon gradients of these magnitudes.

CHAPTER V

RESULTS

Introductory Remarks

This chapter presents the results of the experimentation described in the previous chapter. It should be noted that the measurements taken on these single crystals under similar conditions are found to be quite repeatable. Therefore the following data can be considered indicative of that gotten on a number of different crystals.

The results are broken up into three categories; electrical conductivity, optical absorption, and thermoelectric power. The conductivity data is concerned with measurements made in dry air and vacuum along with related effects noted in the process of taking data. Optical work performed on the Beckman IR-7 and DK-1 spectrophotometers as well as visual observation is included in the optical section. Measurements of thermoelectric power made in air and vacuum are presented in the final portion.

Conductivity Results - Atmospheric Pressure

As stated previously, the data presented is a consequence of a technique required to give consistent results since past thermal history is vital in interpretation of each graph. A typical example is found in Figure 20, of dark current (proportional to conductivity) versus temperature. This depicts what occurs at different "fixing" temperatures at atmospheric pressure. There are three things to note in this data. The

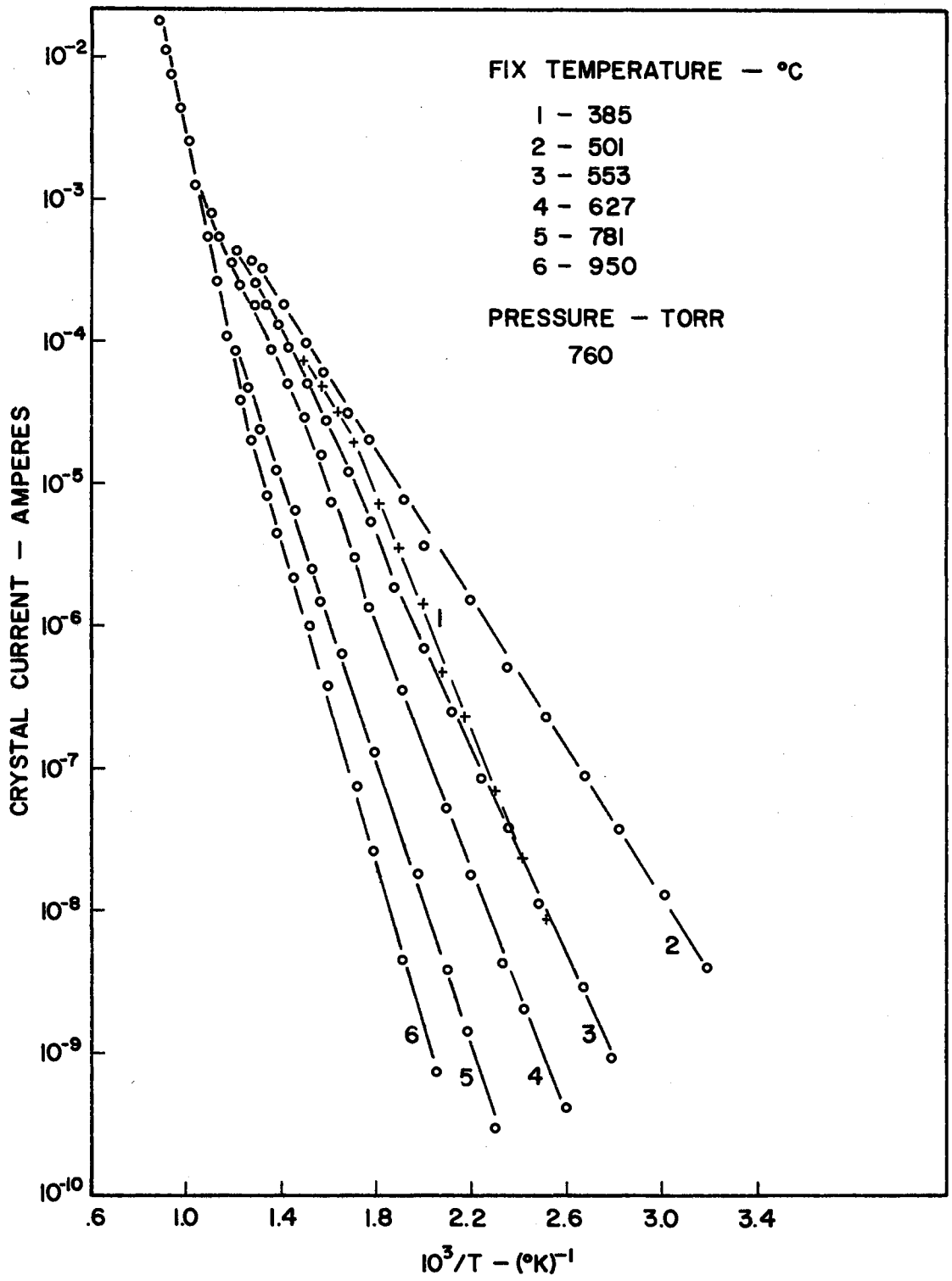

Figure 20. Crystal Current as a Function of Reciprocal Temperature for Several "Fixing" Temperatures.

first is the general increase in slope with increasing "fixing" temperature above 400°C. Temperatures of "fixing" below this cause a decrease in slope. Also, the various curves have a tendency to focus at a point which is near 560°C. At high temperatures the slopes of the curves are reproducible and independent of "fixing" temperatures.

A two slope behavior is noted as the result of fixing temperature above 560°C. The slope of this curve is reproducible following a variety of past treatment. For example, a high temperature vacuum treatment would leave the room temperature conductivity in the 10^{-5} $(ohm\ cm)^{-1}$ range. If then the system were exposed to air at atmospheric pressure and the crystal heated above 560°C, the high temperature portion of Figure 20 would be repeated. It seems that all treatments leave this piece of data unchanged unless the faces of the crystal become visibly etched. The various ways to etch the surfaces were discussed previously.

When past history is the controlling factor in measurements, one is forced to look for consistencies and reproducibility. It was found that for a given "fixing" temperature the conductivity curve is reproducible as long as the crystal is not heated above the temperature of the fix. A typical example of this reproducibility is seen in Figure 21, where two conductivity runs were made; one with decreasing temperature, the other increasing. Near the "fixing" temperature the crystal current was found to drift to lower values when this temperature is exceeded.

Figure 22 shows thermally stimulated currents associated with what were calculated by Houston[22] to be additional current carriers excited from a 0.6 ev trapping level. This is the only piece of data where a temperature rate was used in experimentation. As can be seen, the peak decreases with decreasing temperature rate and also moves to lower temperature with

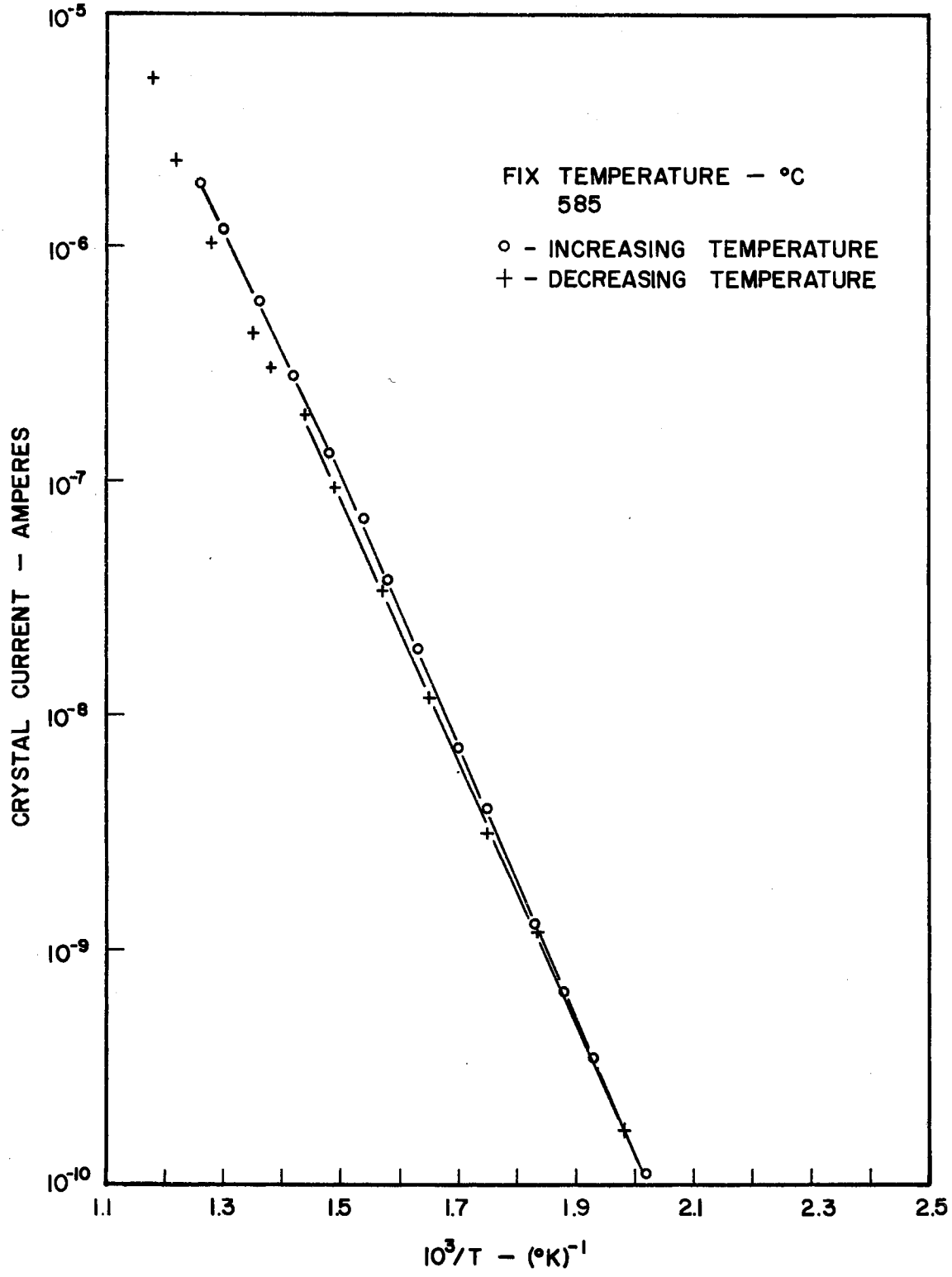

Figure 21. Crystal Current Data Showing Reproducibility Below a Fixing Temperature.

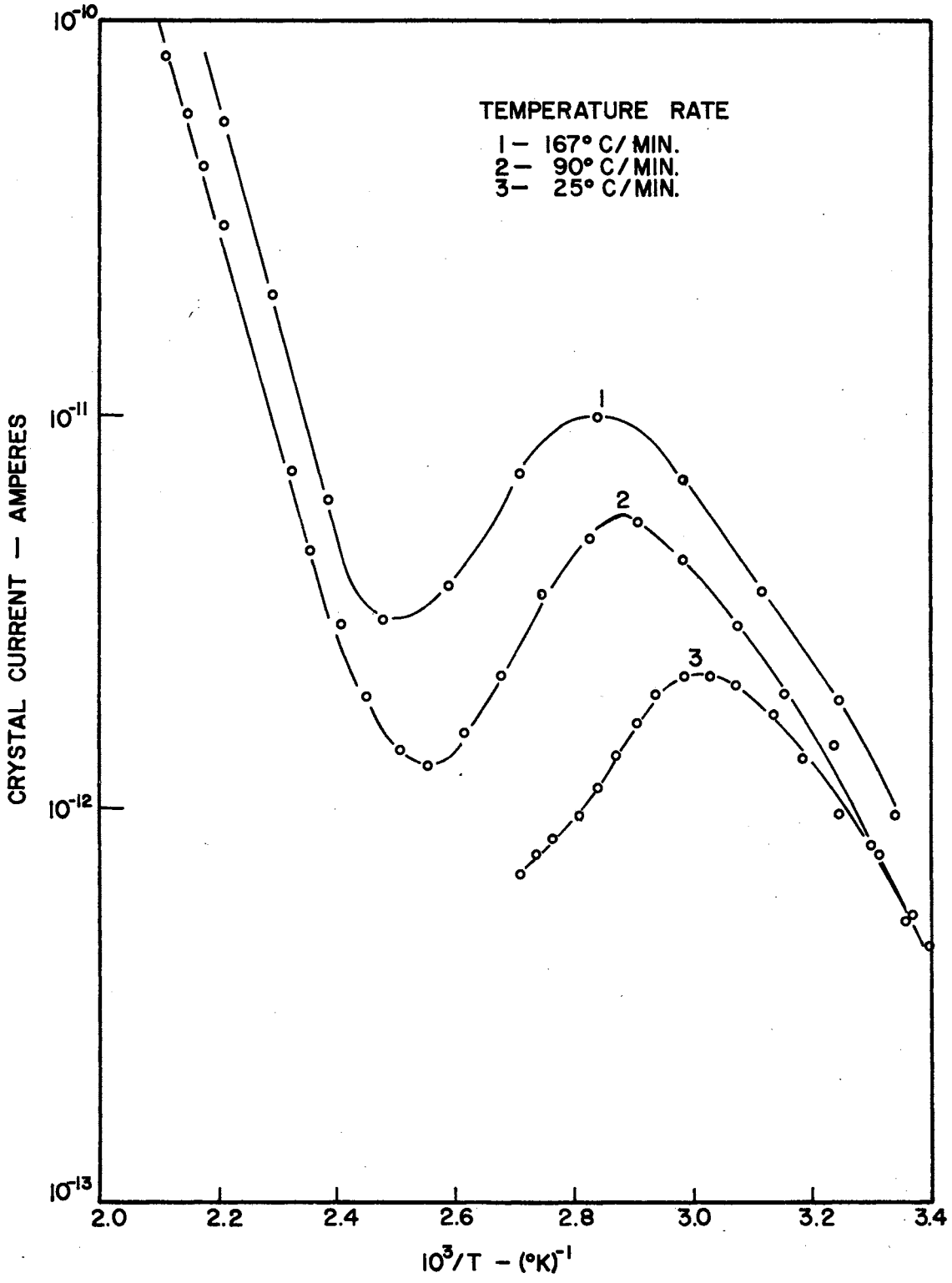

Figure 22. Thermally Stimulated Current as a Function of Reciprocal Temperature.

lower rates as found by Houston. During runs in conductivity it was found that at low temperatures there were scattered points of data due to this phenomena of photoconductivity. As it turned out although the crystal was enclosed in a furnace there was enough light leakage to the crystal that a light shield had to be used over the bell jar in order to remove these spurious effects. The data presented in this chapter was taken with care that light did not reach the crystal. At low temperatures (slightly above room temperature) a false level of conductivity can be obtained by this process. Under certain conditions the decay of photoconductivity is very slow so that it is possible to make a complete run while in the high conductivity state.

Vacuum Conductivity

The effect of a common "fixing" temperature at various pressures is exemplified in Figure 23. From atmospheric pressure to in the neighborhood of 25 microns there is little change in the slope of the curves although they are shifted to higher conductivities. However, suddenly the slopes shift to lower values exhibiting a saturation in this temperature range. From this family of curves one can take the isotherms and produce a plot as found in Figure 24, showing the short range in pressure in which a significant change in conductivity is found.

In the course of recording the data continuously for the point-by-point plots, a slow conductivity change with time at constant temperature was noted in the range below 400°C. This was produced by changing the heater voltage and recording the current as a function of time once the temperature stabilized. The direction of the change depended on the direction of temperature change. In Figure 25 the temperature was increased

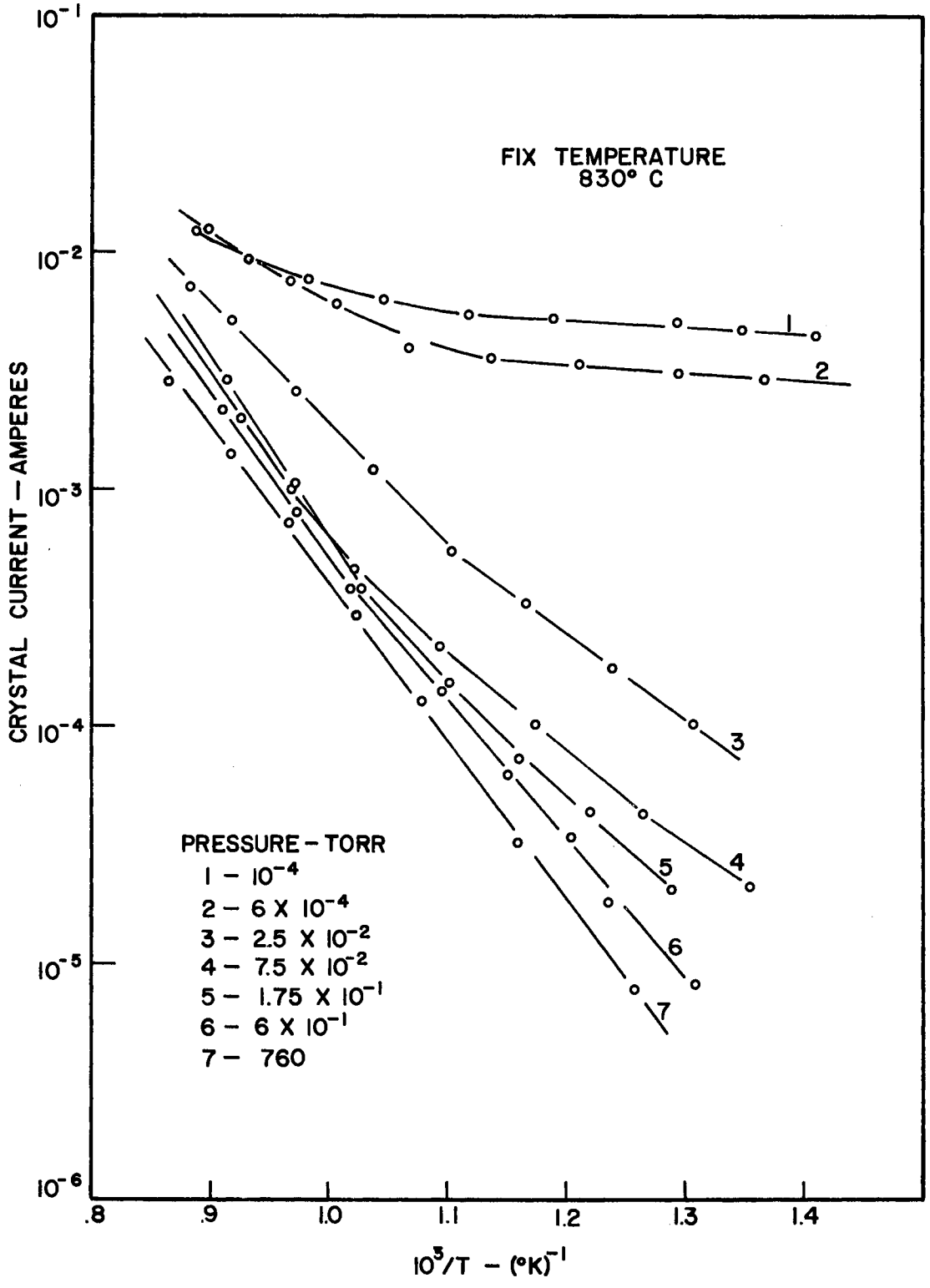

Figure 23. Crystal Current Versus Reciprocal Temperature for One Fixing Temperature at Various Pressures.

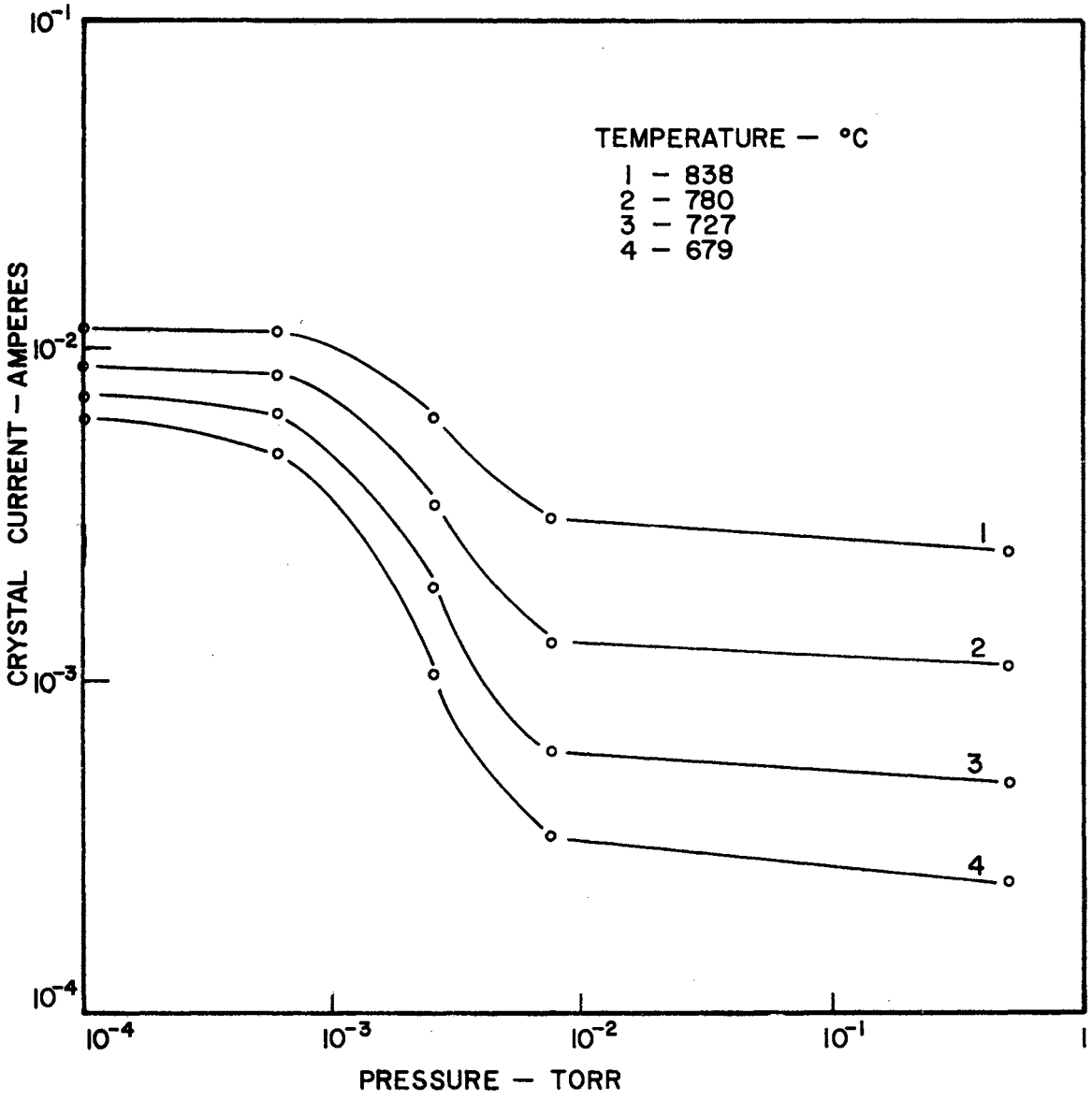

Figure 24. Crystal Current Isotherms Versus Pressure.

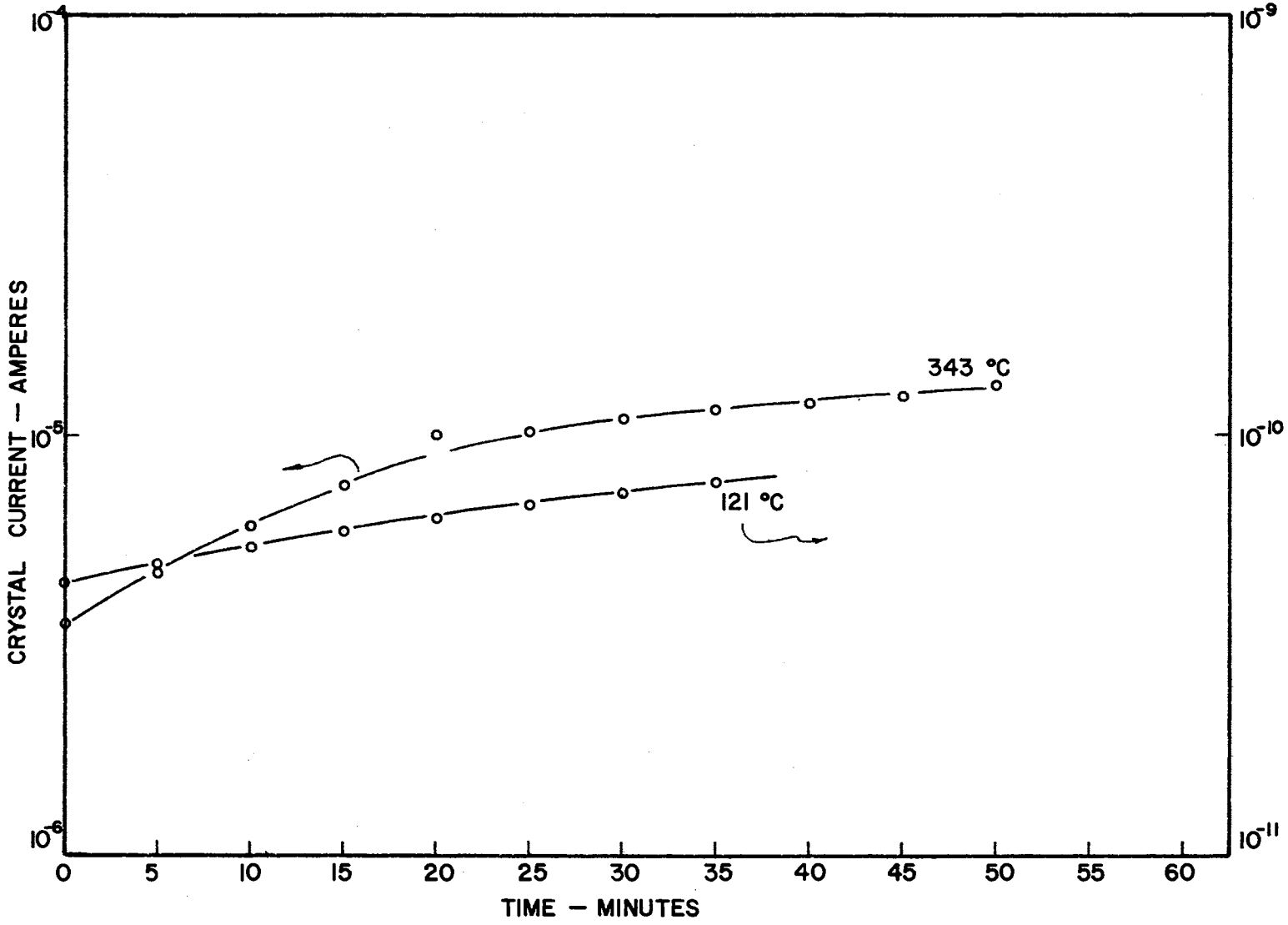

Figure 25. Crystal Current as a Function of Time from Temperature Decrease at 10^{-2} Torr.

whereas in Figure 26 it was decreased. At temperatures higher than 400°C the conductivity and temperature stabilized together.

Figure 27 is an example of what happens to a 900°C atmospheric pressure fix upon taking data under vacuum conditions. The arrows indicate the temperature direction in which the data was taken. The sequence of events was to take the crystal to 900°C in air, let it cool to room temperature, pull a vacuum on it, and start taking data with increasing temperature. At 424°C the temperature was reduced and data taken on the way down. It is noticed that on return the level of conductivity is shifted to higher values indicating more electrons in the conduction band.

In the vacuum work two factors are most important in the crystal history, the fixing temperature and fixing pressure. Very similar results are gotten when one is varied while the other is held constant and vice versa. Comparison of Figures 23 and 28 points out this fact. Again the reproducibility of this data from treatment to treatment and crystal to crystal is good.

Work done concurrently by MacAvoy and Marley[40] on the vapor grown SnO_2 involved grinding 25 microns from the width of the rectangular parallelepipeds and subsequent equilibration. This was done in order to get a homogeneous resistance across the crystal width since they noticed a resistance gradient into the crystal, the resistance being highest at the surface. Most of the work done in our laboratory was on as-grown surfaces. As stated previously, the same high resistance surface noted above is seen in the flux grown samples. Using 600 grit WETORDY silicon carbide paper the faces of a crystal were ground off and conductivity data taken. This is shown in Figure 29. Curve 1 shows the starting room temperature conductivity prior to a run in air to 900°C. The return

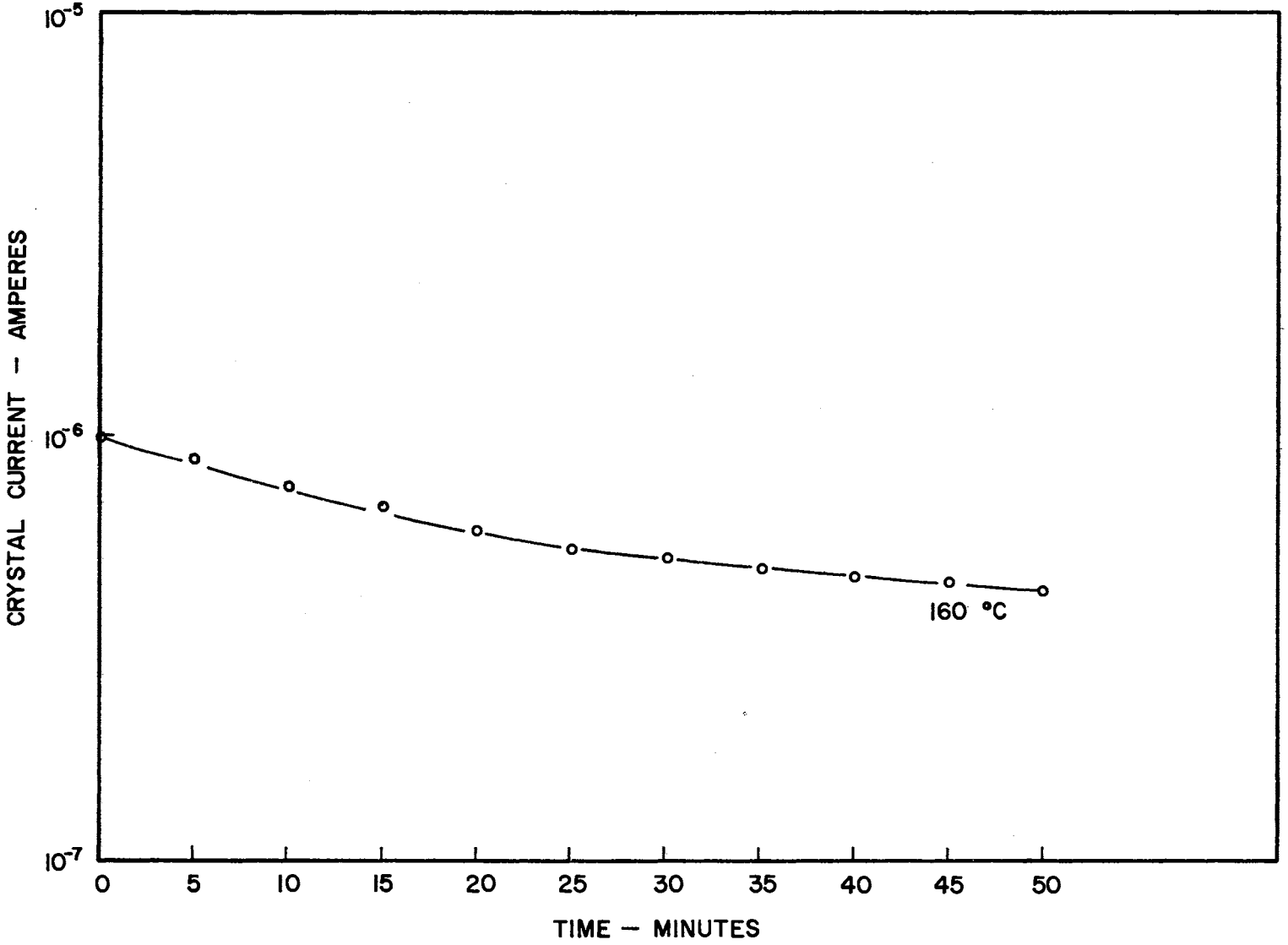

Figure 26. Crystal Current as a Function of Time from Temperature Increase at 10^{-2} Torr.

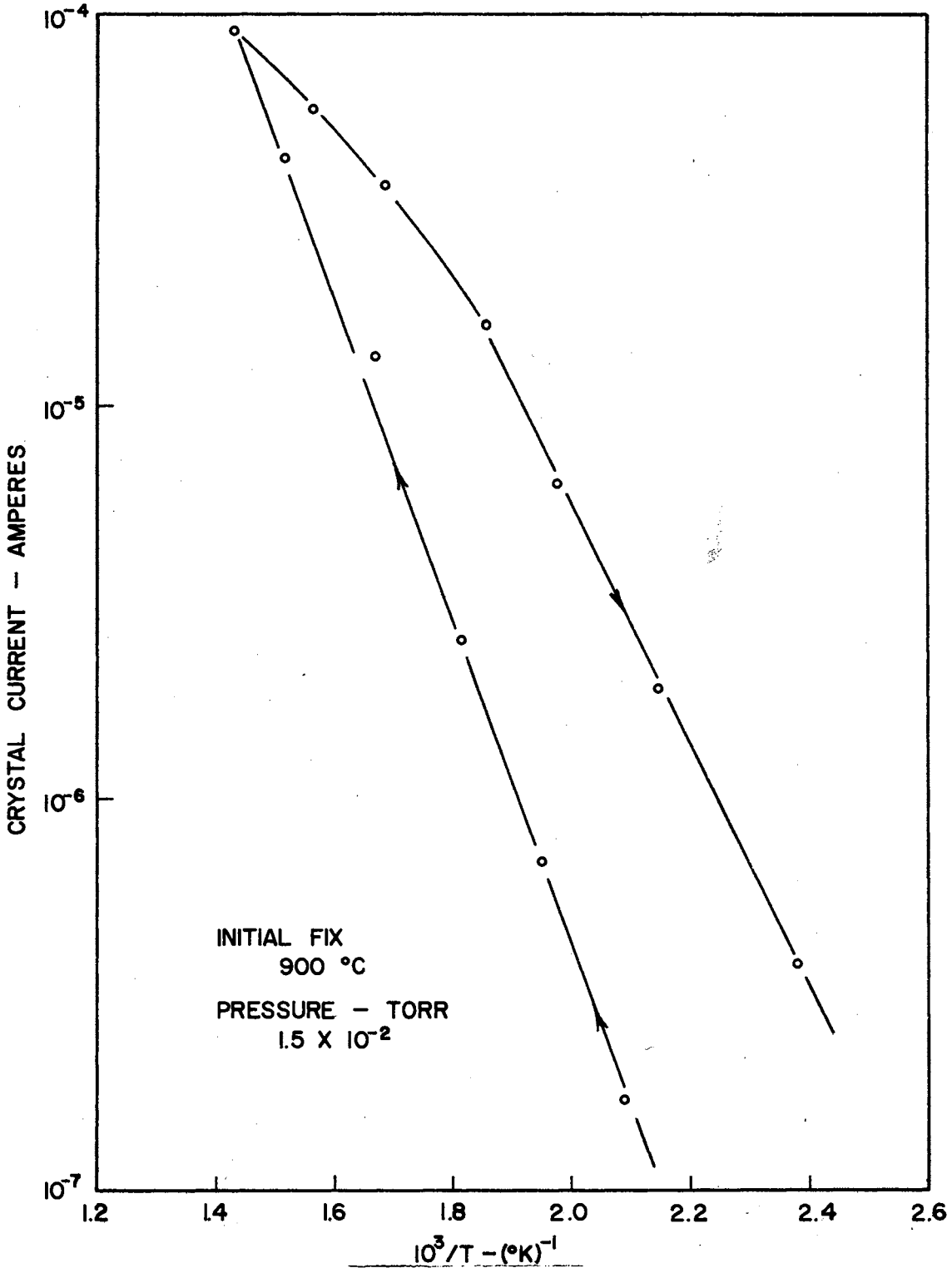

Figure 27. Crystal Current Versus Reciprocal Temperature Showing Effect of Vacuum Fixing.

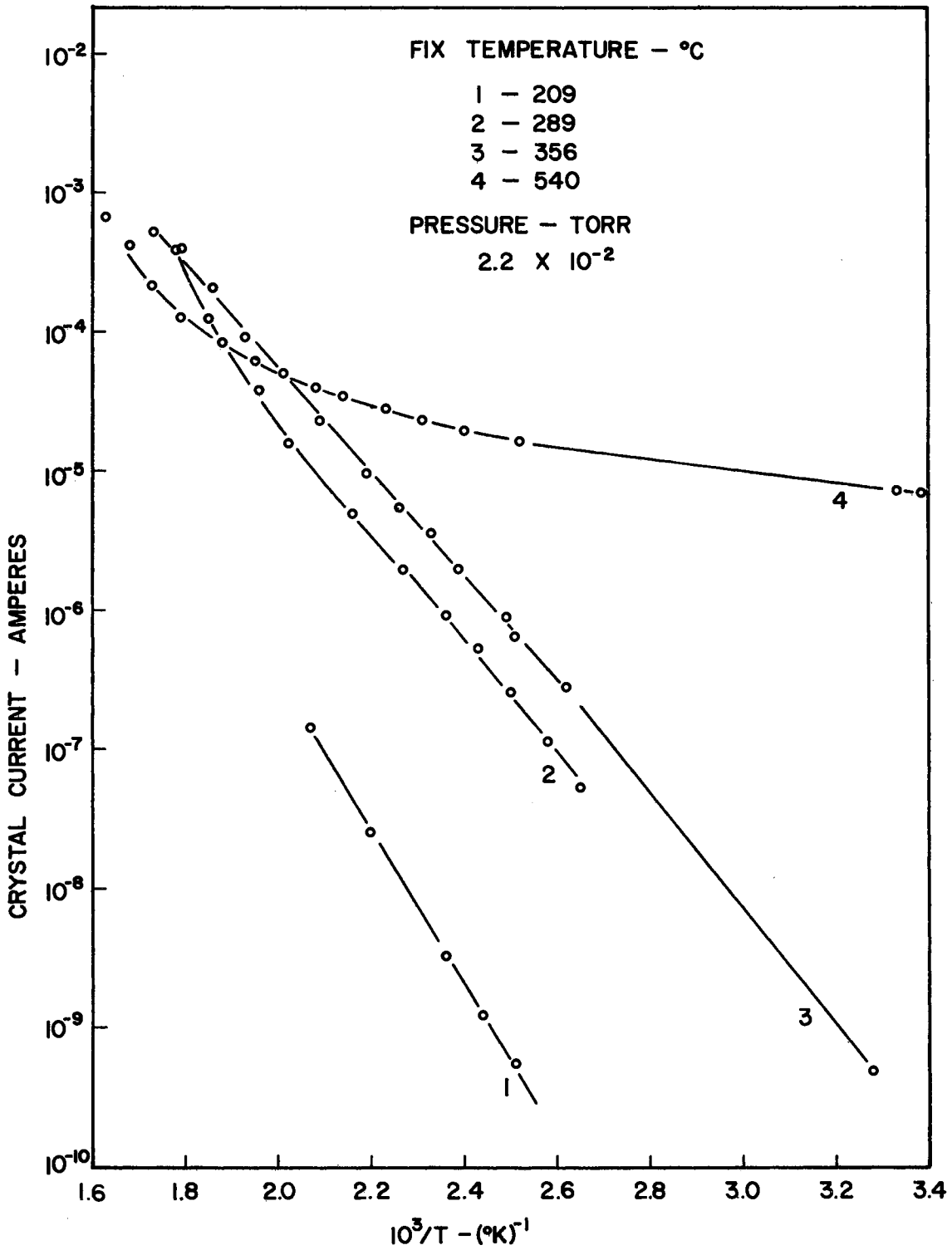

Figure 28. Crystal Current Versus Reciprocal Temperature at One Pressure for Various Fixing Temperatures.

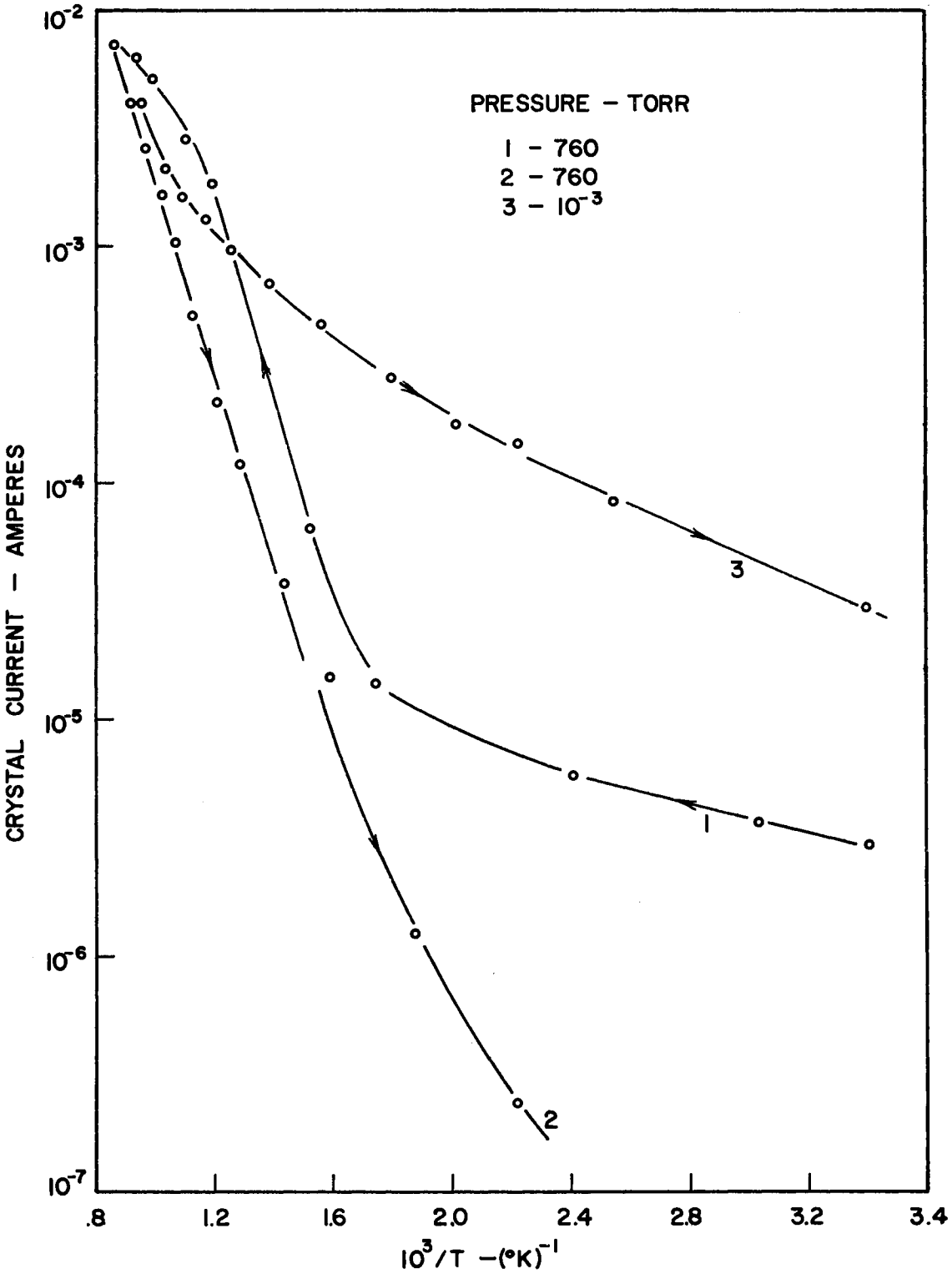

Figure 29. Crystal Current Versus Reciprocal Temperature for Abraded Surface Crystal.

run to room temperature is portrayed in Curve 2. Note the difference between Curve 2 and the high temperature fix curve of Figure 20. Normally under these conditions of fixing, the curve in Figure 20 would be reproduced with this heat treatment but as can be seen at comparable temperatures, conductivities differ by orders of magnitude. Upon heating in one micron of pressure to 800°C the conductivity versus temperature is seen in Curve 3. Note the difference between Curves 1 and 3 at room temperature. Discussions as to the reasons for this behavior will be delayed until the next chapter.

Optical Absorption

A comparison is made between the optical transmission of SnO_2 in its natural crystalline state, cassiterite, and the flux-grown artificial crystals in Figure 30. This work was reported by Kunkle and Kohnke[31]. The transmission on cassiterite is taken from work done by Kohnke[17]. It is believed that nature grows stannic oxide crystals by a hydrothermal process which is responsible for the strong absorption at 3.07 microns. It is attributed to an O-H stretching vibration as has been also reported by Soffer[50] on TiO_2 and Brunner, Wondratschek and Laves[51] on quartz. This absorption is not present, as would be expected, in the flux-grown samples. The short wavelength cutoff and long wavelength structure associated with lattice vibrations, however, remains the same.

While involved with the different air and vacuum heat treatments, measurements were made to see if these various processes changed the visible and infrared transmission spectra. Figure 31 shows the effects of four different treatments. The order in which these were gotten is as follows:

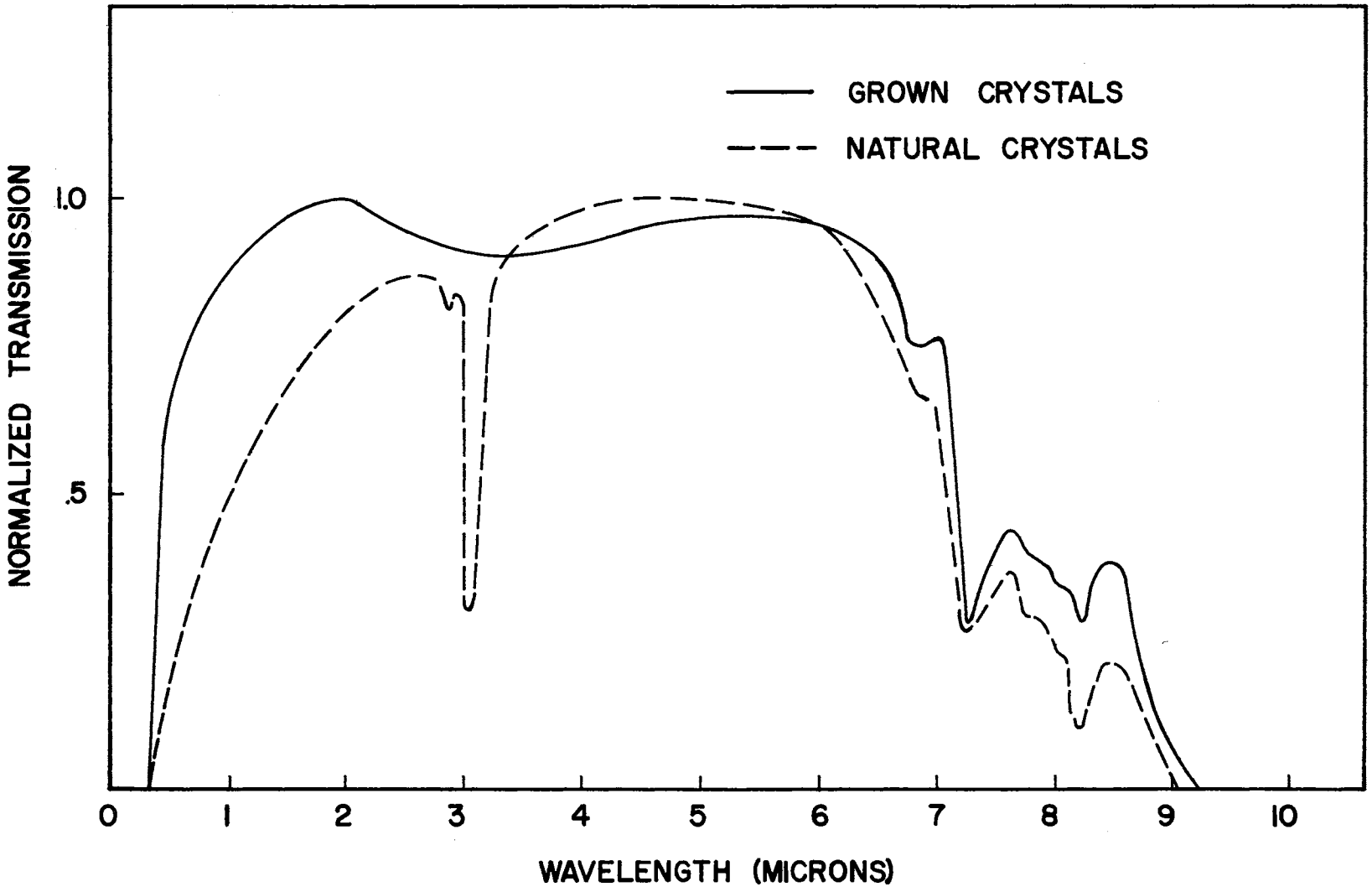

Figure 30. Optical Transmission Comparison of Natural to Flux-Grown SnO_2 Crystals.

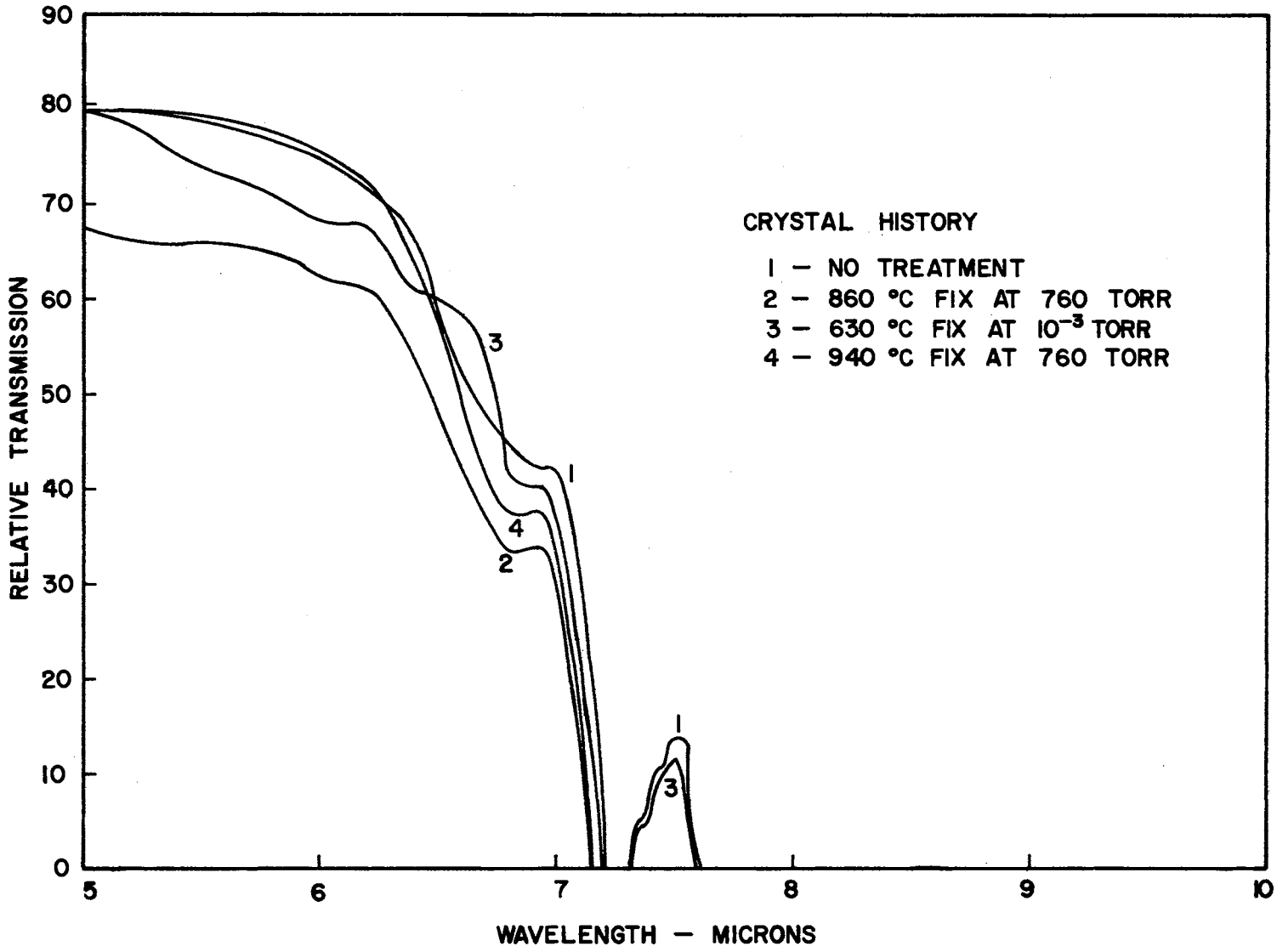

Figure 31. Optical Transmission Showing Fixing Effect on 6 to 8 Micron Structure.

Curve 1 - Taken on an as-grown sample having no treatment beyond facing and cleaning.

Curve 2 - Heated to 860°C in dry air and brought back to room temperature.

Curve 3 - Heated to 630°C in 10^{-3} torr of air and brought to room temperature.

Curve 4 - Heated to 940°C in dry air and brought to room temperature.

No attempt was made in the above to quench the crystals beyond letting them cool with the furnace. The interesting point to note is that there is definitely a reduction in the transmission at 7.5μ following high temperature fixes in air. The total spectrum was run from wavelengths of 250 millimicrons to 9.5 microns with the midrange showing no change. However, in the visible range there were weak absorptions that did not significantly change with treatment as shown in Figure 32. These small absorptions might well have been missed or ignored except for the fact that work done on very red crystals obtained from Semi-Elements, Inc. showed a strong absorption at 510 millimicrons (Figure 33) and the flux-grown samples sometimes exhibited a faint pink hue. More will be said about crystal color below.

The as-grown samples directly from the slug are colorless and transparent. After standing in a vial for extended lengths of time (e.g., one month) they take on a pale pink tinge. The pale pink can be bleached out by the following treatments: 1) Heat treatment in vacuum under one torr with temperatures greater than 500°C but not more than 850°C followed by slow cooling. Care has to be taken with very low pressures and high temperatures because this treatment tends to etch the surfaces of the crystal. 2) Heat treatment in dry air to very high temperatures, i.e., 850°C or greater, and a rapid quench to room temperature. The crystals following

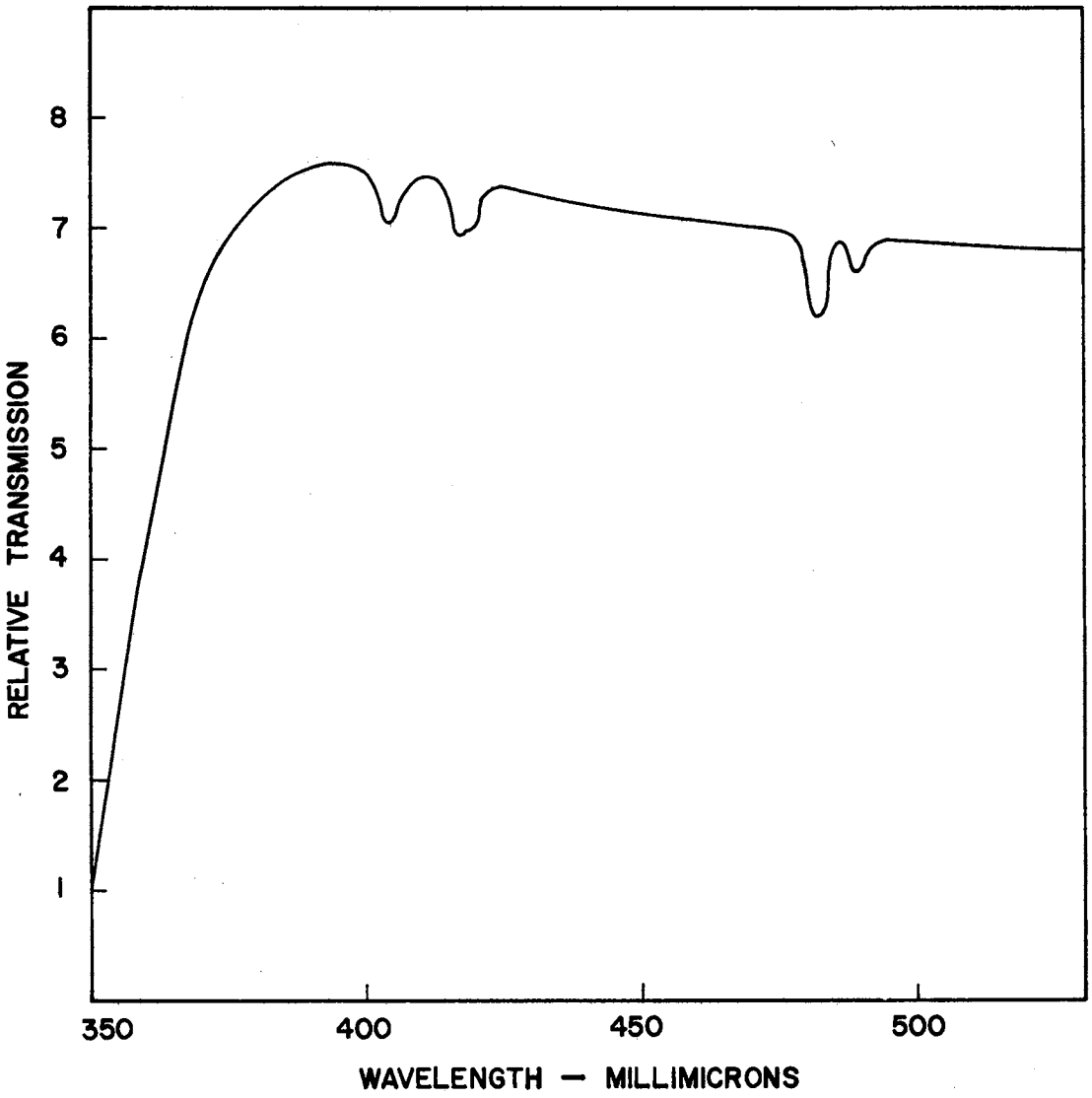

Figure 32. Optical Transmission Showing Visible Wavelength Absorptions.

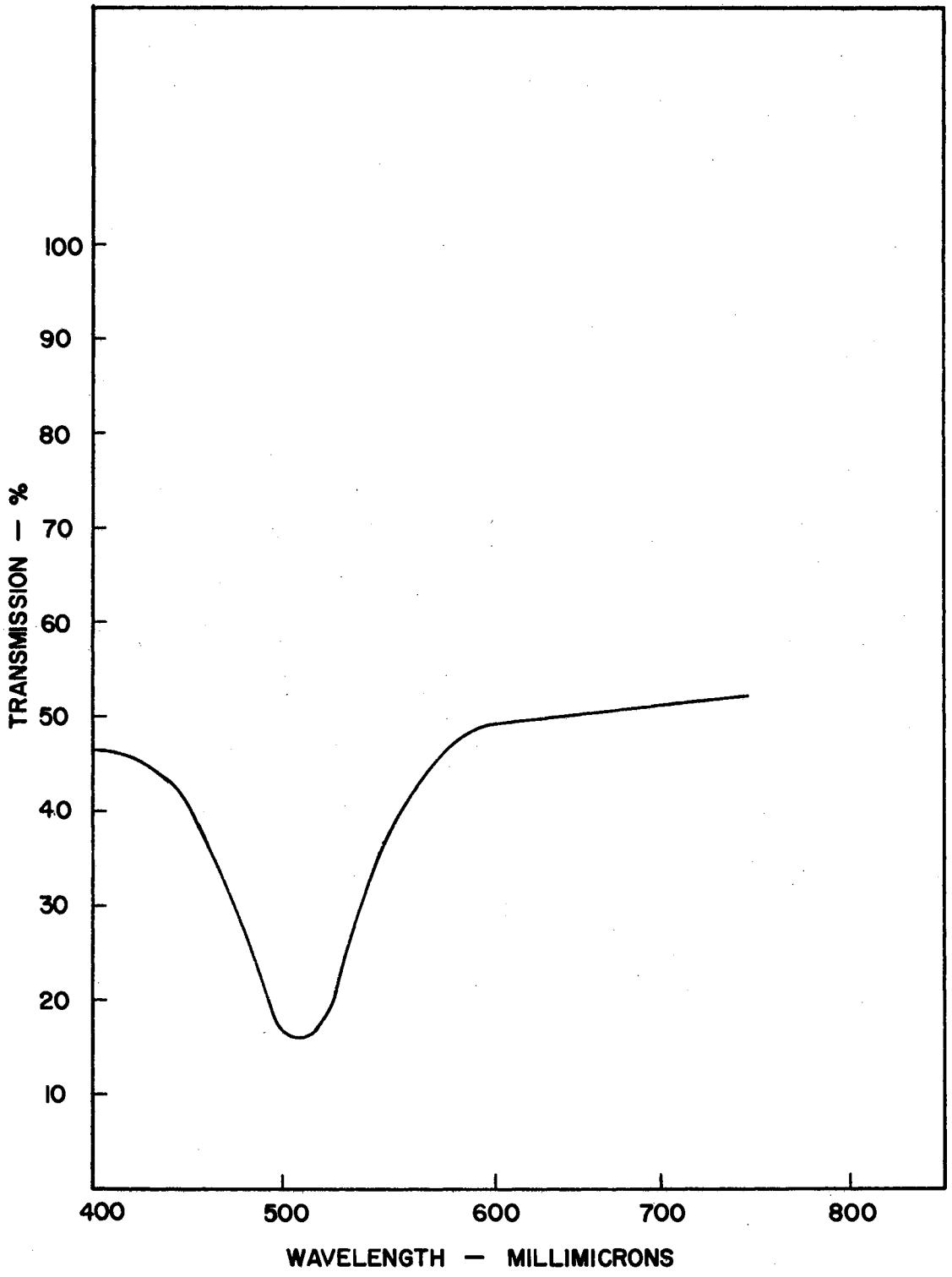

Figure 33. Optical Transmission of Vapor-Grown SnO_2 Crystal in the Visible Wavelength Range.

these treatments exhibited once again the colorless transparent character.

The pale pink tinge is produced in the following ways: 1) The crystal is exposed to light in air for extended periods of time at room temperature. 2) Heat treatment in air to temperatures above 500°C and slow cooling to room temperature. By "slow", it is meant that from 500°C to room temperature takes on the order of three quarters of an hour.

The speed with which the crystal is cooled as well as the fixing temperature is a factor determining whether the color appears or not. This pink color is not seen in the dark but only on reflected light.

A transitory yellow-green color is observed when the crystal is heated above 300°C in air or vacuum, however it again disappears upon cooling. As the temperature is increased the intensity of this color also increases until the crystal takes on the reddish glow of black body radiation. However, when this experiment is performed in the dark no yellow-green glow is seen. Only with reflected light is it observed.

Thermoelectric Power Results

Due to the problems involved in obtaining thermoelectric power results on very high resistance samples the temperature range was limited from 350°C to 850°C. Much care had to be exercised to assure that the results were directly attributable to the crystals and not to extraneous effects. Figure 34 shows the results of thermoelectric power versus temperature as the temperature was increased and decreased respectively. For this measurement the sign of the voltage was held the same on both runs. However, at the high and low temperatures the sign was reversed to see if any polarization effects could be noticed. None were. Subsequent data

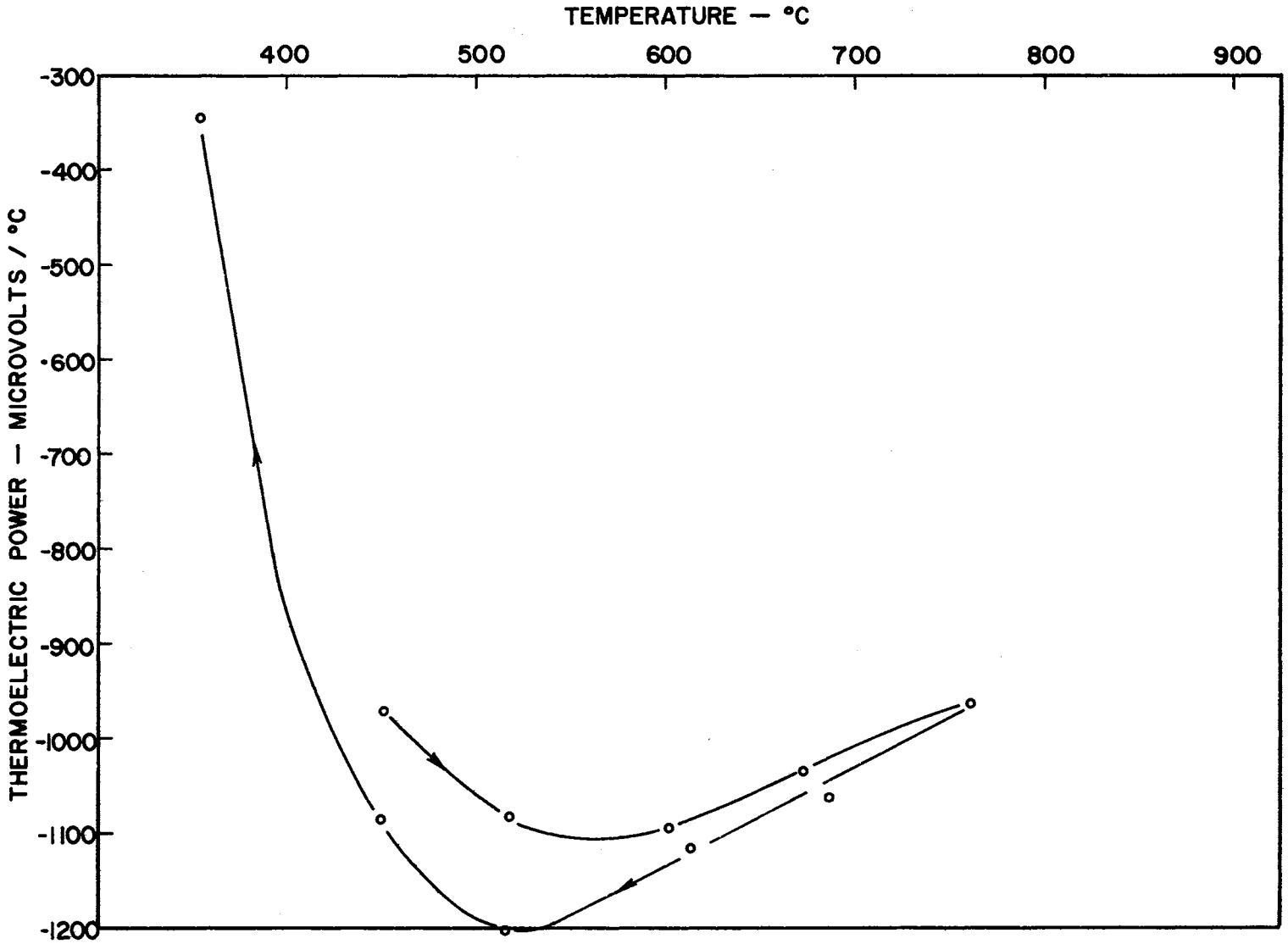

Figure 34. Thermoelectric Power Versus Temperature for a High Temperature Fix.

of a high temperature fix nature showed remarkable reproducibility in the high temperature region above the thermoelectric power minimum. However, the low temperature region showed much more scatter of points, although the trend was always the same. In other words, the shape of Figure 34 was always seen for high temperature fixes with the high temperature portion being most reproducible.

Using a rule of thumb for thermoelectric power that the higher the crystal resistance the higher the magnitude of thermoelectric power, it would be expected that vacuum work should produce lower values. This is the case as presented in Figure 35. In this data the two lower-valued curves are gotten from runs taken at the same pressure but at two different fixing temperatures. For comparison purposes representative conductivity and thermoelectric power are plotted together in Figure 36, as a function of reciprocal temperature since calculations are made with this type of data. It is to be noted that the thermoelectric power peaks in magnitude in the temperature range in which the conductivity slopes break.

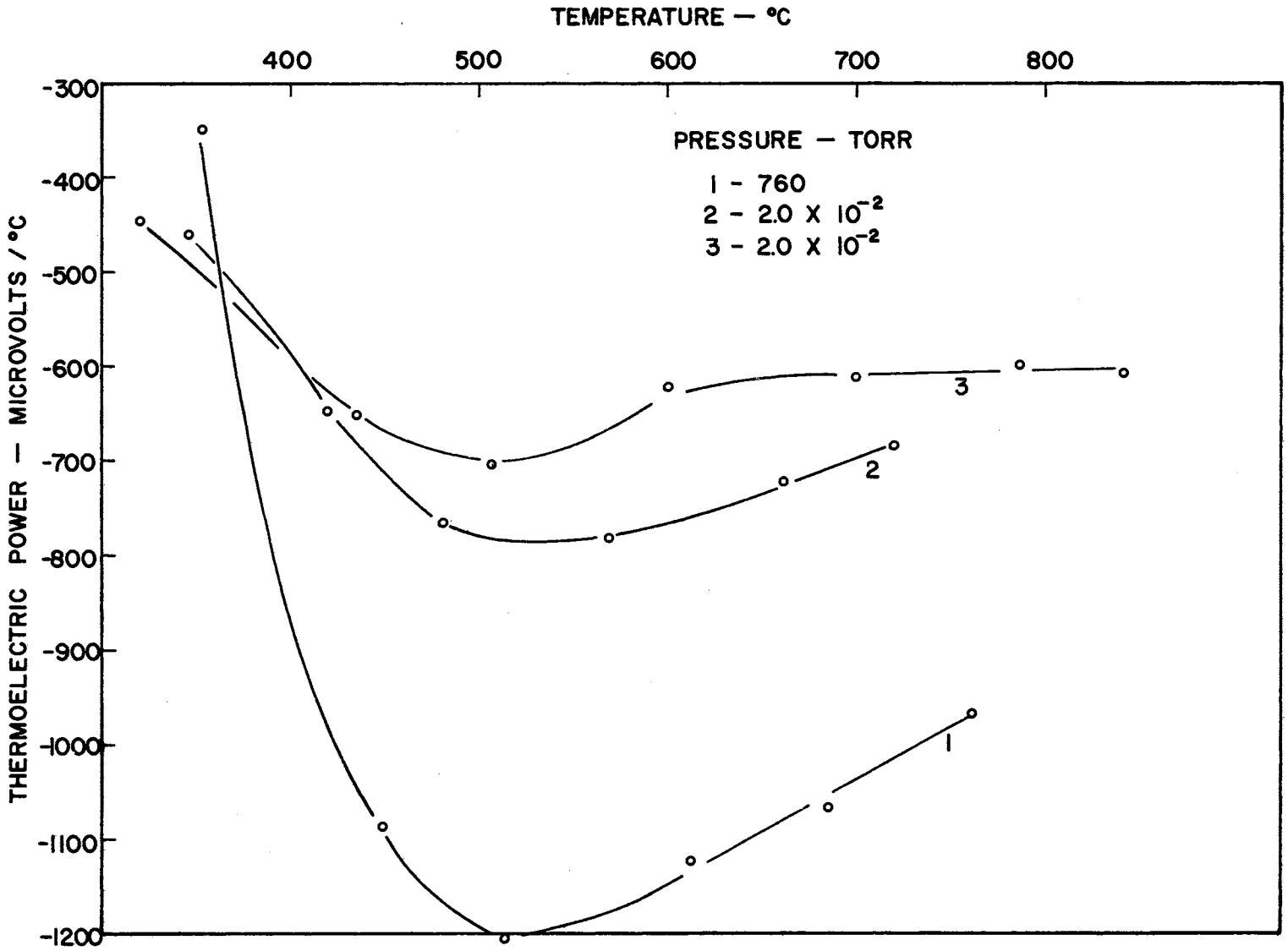

Figure 35. Thermoelectric Power Versus Temperature for Various Fixing Treatments.

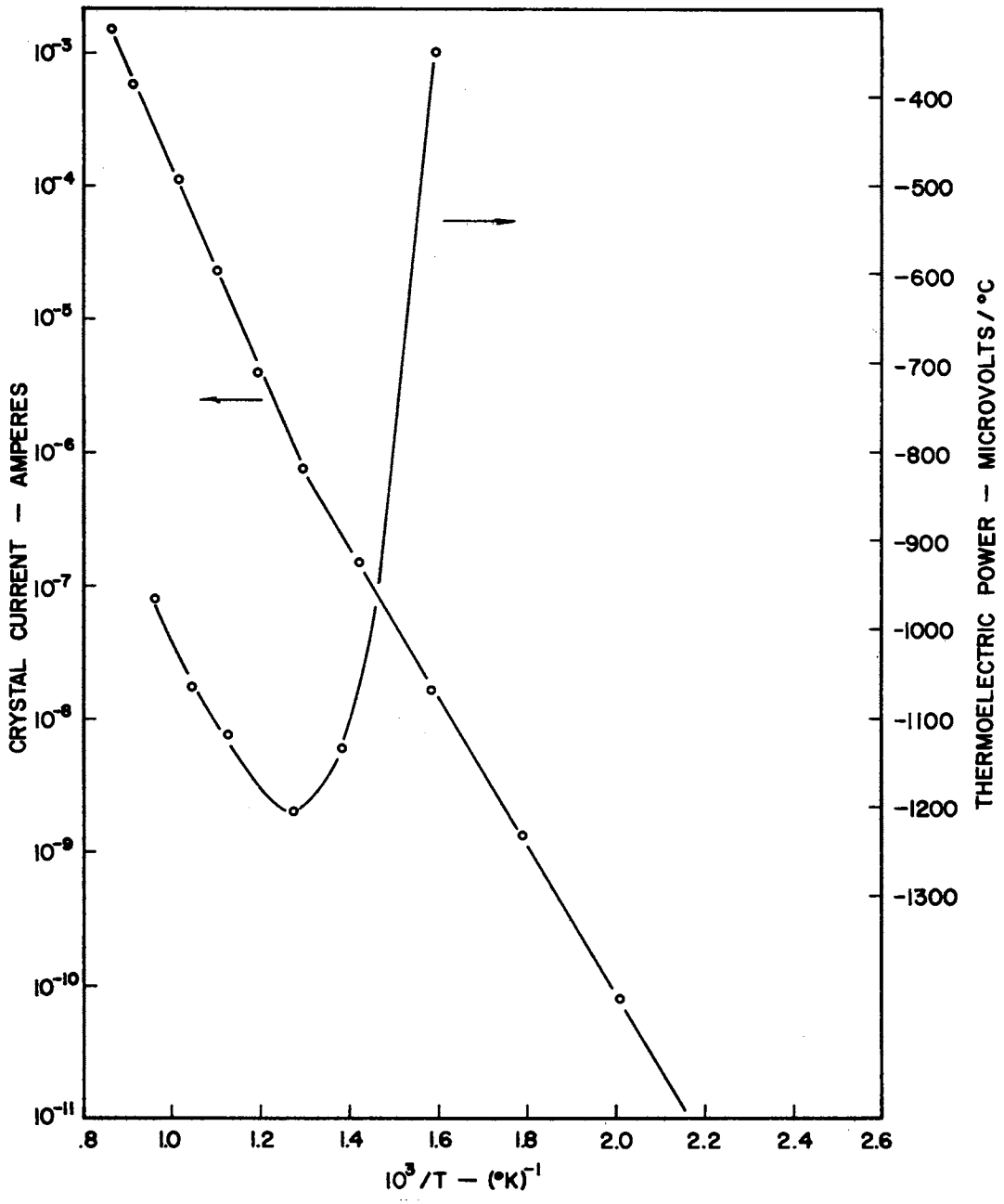

Figure 36. Comparison of Thermoelectric Power and Conductivity for a High Temperature Fix.

CHAPTER VI

DISCUSSION OF RESULTS

It is planned in this discussion to first introduce in a qualitative fashion a model explaining the general behavior noted. With this in mind, the data of the previous chapter will then be discussed in relation to the model. Since the electrical properties of SnO_2 crystals with as-grown faces have been found to be dependent on past pressure and temperature treatment even at relatively low temperatures (room temperature), surface phenomena probably play a part in conductivity control. The model which will be used for explaining the behavior is based on the conventional one-dimensional flat-band energy scheme consisting of donor levels and at least one acceptor level. To be included in the consideration is the surface double charge layer produced by immobile electrons on the surface -- associated with chemisorbed oxygen -- and a balancing distribution of positive ionized donor impurities in the bulk. This situation in itself is not unusual and appears to be the case for many n-type semiconductors, although the depth of the space charge layer may vary widely depending upon bulk properties of the material. In fact often this layer extends only a few hundred angstroms into the crystal and can be largely neglected as to effects on bulk electrical properties. For the small experimental specimens of SnO_2, however, it is believed that the space charge layer extends more deeply into the crystal even producing in certain cases a sample which is almost totally "surface". The space charge layer thickness is defined as the distance from the surface to the interior

point where the electric field becomes zero. The theory involved in this type of one-dimensional band structure was presented in Chapter III.

Space charge layers that extend deeply into the bulk of the crystal can be produced in several ways. In essence -- in n-type semiconductors with a negatively charged surface -- such a situation arises with a large forbidden gap and a very low donor density. The large gap assures almost no electronic transitions between valence band and conduction band with only a few holes created in the valence band to migrate under the influence of the surface field and free surface-trapped electrons to drop the barrier or to provide a portion of the necessary balancing positive charge density. An effective low donor density can be accomplished in a couple of different ways. The first that comes to mind is the donor density that is gotten with very pure materials. A second is one that does not necessarily involve pure materials but exists when there is a balance of bulk donor densities and bulk acceptor densities. In this case donor compensation can occur by losing electrons from the donor levels to the lower-lying acceptors completely immobilizing them at normal temperatures for thermal processes. A third situation that can occur is an extension of the other two and involves a donor density that is a function of the distance into the crystal, having a higher density in the bulk. It is reasonable then to suspect that electrons trapped at the surface would come from donors lying close to the surface but since the density there is small the effect is spread further into the crystal. An important consequence is that conductivity control by the surface can take place when the number of conduction band electrons and the number of surface traps or surface sites are comparable in magnitude.

The effect of such a space charge layer on the energy level scheme

in an n-type semiconductor is to bend the bands at the surface to higher electron energies. This is understandable if on the surface there is a high concentration of electrons. Then more energy must be supplied to an additional electron in the conduction band to move it to the surface against the repulsive force. Very little has been said to this point about the mechanism for providing the negative surface charge.

The postulated model pertaining to flux-grown stannic oxide crystals with as-grown faces consists of three or more donor levels and at least one acceptor level with fairly high density. There is adsorption of oxygen at the surface by electron transfer (chemisorption) such that the space charge region extends into the bulk of the crystal and the surface barrier to electron transfer is able to be raised or lowered by heat and pressure treatment. The donor densities are assumed to be functions of the distance into the crystal and to have a constant ionization energy as measured from the bottom of the conduction band.

It has been observed for ZnO by Morrison and Miller[52], inferred for NiO by Haber and Stone[53], and for numerous oxides studied by Bevan, Shelton and Anderson[7] in the compressed powder form that oxygen adsorption as a function of temperature reaches a maximum and then decreases with increasing temperature above this point. Some authors refer to "reversible" and "irreversible" ranges of surface properties which seem to follow this pattern of adsorption. Morrison[54] states that one is in the region of irreversible adsorption at temperatures less than T_m as on the sketch below and in the reversible range above this temperature. It seems reasonable to extrapolate this behavior to single crystal oxides. In fact, since it is a practical impossibility to measure adsorbed gas volumes directly for small crystals, it might be hoped that electrical

conductivity measurements could provide a sensitive technique for providing this type of information.

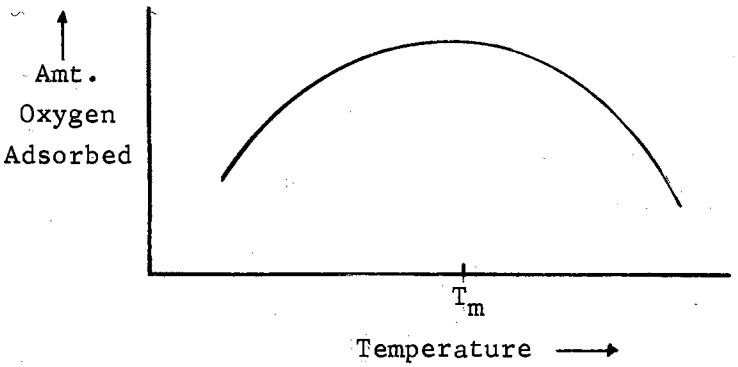

Turning now to the experimental results given in Chapter V, it appears that the behavior seen in the lower temperature region of Figure 20 can be explained by an oxygen adsorption mechanism and its effect on the space charge region. Note the general increase in slopes with increasing "fixing" temperature. The assumed effect of the fixing temperature is to determine the amount of oxygen chemically adsorbed at the surface. It can be calculated using an ionic radius that a monolayer of oxygen on the surface would produce on the order of 10^{15} electron sites/cm^2 at the surface. However, in adsorption work on various surfaces of powders and pressed compacts, maximum numbers of only 10^{12}-10^{13} oxygen atoms/cm^2 have been observed corresponding to 0.1% to 1% surface coverage. For fixing temperatures below T_m the barrier height is set by a given amount of adsorbed oxygen and this in turn indirectly determines the slope of the various electrical conductivity curves as found in Figure 20.

The mechanism visualized here is that at each fixing temperature a certain number of higher energy electrons in the conduction band can surmount the surface barrier thus enabling them to be trapped by an oxygen atom which is then chemically adsorbed on the surface. Successively

higher fixing temperatures thus produce higher surface barriers since more conduction electrons now have higher thermal energies allowing more of them to reach the surface. Simultaneously, however, what Morrison[54] terms "pinch-off" is occurring. Initially the electron transfer rate to the surface may be high but as the barrier builds it "pinches off" this rate, reducing it to zero when there are no longer free electrons with sufficient energy to get over the barrier. Subsequent reduction of the temperature will leave the barrier height at its pinch-off value since the electrons bound on the surface have no way of returning to the bulk unless some additional desorption mechanism (e.g. photodesorption) is brought into play. Temperatures above T_m provide an amount of adsorbed oxygen characteristic of the temperature, not because of a pinch-off effect but because in this temperature range the surface is apparently in equilibrium with the ambient gas (reversibility). A consequence of this is that on a conductivity run where fixing is above T_m and the data is taken as the temperature decreases, pinch-off occurs at T_m such that below it the barrier is again fixed by adsorption of the T_m amount. In Figure 20 a general increase in slope occurs with fixes between 400 and 600°C. For fixes above 600°C the slopes show only a slight increase although the general level of conductivity may change.

The equation governing the lower-temperature slope behavior is Equation 22 which gives the normal free election density expression when compensation is present. Two types of compensation may be considered in this case. First, that due to high copper content in substitutional tin lattice sites and secondly that due to the surface adsorption acceptor sites. The bulk compensation has the effect of completely depleting the highest lying donor levels of electrons as observed in recent photoelectric

measurements on these crystals[55]. As higher fixing temperatures are used, lower donor levels become increasingly compensated by the surface states and the conductivity slopes show further increase. A possible additional reason for the increase in slopes is that the pre-exponential term in this equation may have an activated temperature dependence. This would lead to a fixing temperature dependence as well as the normal temperature relationship. The effect then would be to add to the active normal donor level ionization energy the activation portion of the pre-exponential term giving an artifically large donor activation energy. Reasons for such behavior are not clear as yet, however.

The typical crystal dimensions were such that the $\frac{\text{Length}}{\text{Area}}$ factor was $\sim$30 cm^{-1}, and in relation to the plot, $\sigma = I$ (crystal) L/AV where V is 2.1 volts. Using a free electron density calculated from I at 450°C and employing a reasonable value of 100 cm^2/volt-sec for the mobility it can be seen that to completely immobilize this number of free electrons in surface states associated with oxygen adsorption would require less than 0.1% of a monolayer of adsorbed oxygen. This makes plausible significant compensation by surface acceptors.

A possibility which should also be considered is that when adsorption occurs at the surface it may cause such a high degree of compensation that space charge region extends effectively throughout the crystal. This of course would lead to a free electron density which is dependent on the depth into the crystal and as the bands are bent to higher values a smaller portion of the crystal would be responsible for the conduction process. A naive way to express this is to say that the effective cross sectional area of the crystal is decreasing with higher fixing temperatures. For progressively higher fixing temperatures, this would

produce successively lower conductivities as is observed. It is not obvious, however, why this should provide an exponential temperature dependence as is seen in the plots of Figure 20.

The reasons for the initial increase in slopes for low fixing temperatures (below 350°C) are not evident in light of the above mechanisms. Perhaps as suggested by Shear, Hilton and Bube[59] in their work on CdS and CdSe layers, thermal desorption effects may outweigh adsorption processes in this region of low conductivity.

The high temperature slopes from fixing temperatures above 560°C, (if calculated by Equation 14 assuming a lattice scattering mobility proportional to $T^{-3/2}$), are indicative of an energy of $\sim$2.7 ev. This is tentatively identified as the intrinsic thermal gap energy with justification to be provided later in this section. The reason that intrinsic behavior might be seen at high temperatures lies in the high degree of compensation. The transition temperature from compensated-donor and surface-controlled conduction to primarily intrinsic behavior is at the focal point of the various low temperature curves. A slight increase of conductivity level with increased fixing temperature is observed in the intrinsic range although this is not evident in terms of the scale chosen for Figure 20. This is presently attributed to an annealing of the assumed inhomogeneous donor distribution near the surface with consequent reduction of the remaining space charge layer thickness and an increase of the effective cross sectional area for conduction.

The vacuum conductivity results shed more light on the above discussion. Figure 23 portrays the effect of one fixing temperature at different pressures. It is noticed that as the pressure is decreased from one conductivity run to another that the level of conductivity

becomes higher as expected if the decreased pressure is responsible for decreasing the compensation due to surface adsorption. However, in the 10^{-3} to 10^{-2} torr range there is a sharp change of conductivity level with pressure. This is best seen when plotting isotherms from Figure 23 on Figure 24. Once this sharp change has taken place the conductivity saturates which is taken to mean that the electrons in the conduction band have originally come from donor levels having small enough activation energies such that in this temperature range they are completely ionized. Also acceptor levels at the surface have apparently been removed so that this saturation remains. If all of the electrons responsible for conductivity saturation were contained in surface traps prior to vacuum heat treatment then a calculation similar to that described above would again show that from 0.1% to 1% of a monolayer of oxygen coverage could provide all the necessary sites. A mobility had to be assumed and the number employed in this calculation was of the order of 100 cm^2/volt-sec, a reasonable assumption in the light of work done by Marley and Dockerty[56] on vapor-grown SnO_2 and on cassiterite by Kohnke[17]. It is further interesting to note that this saturation starts at the temperature where the transition between intrinsic and compensated conductivity occurs on the atmospheric pressure data described above.

A further implication obtained from Figure 24 is that this is not a donor defect production mechanism as opposed to a desorption process since at pressures below 10^{-3} torr, the conductivity again becomes pressure independent. Defect production as noted by Rudolph[57] and Yahia[58] is present at these temperatures on other metal-excess oxides but would continue to increase until complete reduction of the crystal occurred instead of leveling off.

Figures 25 and 26 might be considered further substantiation of the adsorption-desorption model. It is noted while taking data below 400°C in vacuum that a slow change of conductivity with time occurs subsequent to a temperature change. This occurs at temperatures at which diffusion of ions in and out of the lattice should be extremely low. Figure 25 is essentially saying that it takes on the order of one hour before "pinch-off" is completed causing the conductivity to level off whereas Figure 26 shows slow conductivity rises associated with desorptions. The very interesting implication of these results is that the adsorption versus temperature curve described at the beginning of this chapter is not only reduced in magnitude but has its maximum shifted to much lower temperatures when the ambient pressure is reduced below the 10^{-2} torr range. This obviously warrants further study.

Figure 34 shows the thermoelectric power as a function of temperature. This is the behavior noted with a high temperature fix (intrinsic temperature range). The arrows indicate the direction in temperature in which the data was taken. Note the difference in the data between temperature on the rise and decrease which is explained as incomplete high temperature fixing. Due to the fact that the crystal was taken to the high temperature and quenched to room temperature before the data was taken the fix may not have been complete since the irreversible range in adsorption was traversed too quickly. After this initial set of measurements, the higher temperature portion of the curve showed excellent reproducibility, both with temperatures increasing and decreasing. Thus two ranges are seen in this data: 1) that on the high temperature side of the minimum corresponding to the intrinsic range of behavior, and 2) that on the low temperature side as indicative of compensated donor

behavior. In the range of temperature studied the thermoelectric power was always negative.

Several times previously the term "intrinsic" has been used to describe the highest temperature behavior of the specimens. Analysis, of thermoelectric power data will be used to justify this identification.

One might expect from the nature of the conductivity and thermoelectric power changes with temperature that the highest temperature slope is indicative of electron activation from a very deep-lying donor level in the compensated material. Considering Equations 22 and 35 to be pertinent the slope of Q vs $\frac{1}{T}$ should provide a value for E_d as should the slope of I vs $\frac{1}{T}$ (assuming lattice-scattering mobility variation with $T^{-3/2}$). However, these plots give $E_d(Q) = 1.15$ ev and $E_d(I) = 1.35$ ev, a significant difference.

If it is assumed that the behavior is intrinsic and lattice scattering applies, then Equation 36 is pertinent and the thermoelectric power slope yields a value of 2.3 ev for the intrinsic gap in the range of measurement. Here a value for $\frac{c-1}{c+1} \sim 1$ has been used to place a lower limit on the gap energy. A high mobility ratio is consistent with results to be presented shortly. The conductivity slope, on the other hand, yields a value of 2.7 ev for the intrinsic gap at absolute zero.

Using a linear variation of forbidden gap with temperature, $E_g = E_o + aT$ as suggested by Pearson and Bardeen[60], a value of -3.5×10^{-4} ev/°K is indicated for the coefficient, a, by these two pieces of data. This agrees very well with values of -6×10^{-4} and -2×10^{-4} estimated respectively by Kohnke[17] and Arai[61] from optical adsorption shifts with temperature. The room temperature gap calculated in this fashion is 2.59 ev, in excellent agreement with the indirect optical transition gap reported by Reddaway and Wright[62].

Both Foex[16] and Arai[61] have reported higher conductivity slopes than 2.7 ev on SnO_2. However, these were observable in the same temperature range as is covered in the present data and were obtained using powder or thin-film specimens. Results reported here would suggest that these higher slopes resulted from decreases of grain boundary or interparticles resistances associated with sintering or agglomeration.

Returning to the intrinsic calculation, a ratio of $\frac{m_v}{m_n} > 100$ is estimated. Although this justifies the assumption of a high mobility ratio, it seems unreasonably high. It may be indicative of the restrictive assumptions used in deriving the thermoelectric power equations or even of the fact that any space charge layer remaining at high temperatures would tend to draw holes to the surface to desorb oxygen and effectively remove them from the conduction process. A point in favor of the high ratio is that when it is used in combination with a value of $m_n = 0.12m_o$ (as obtained by Marley and Dockerty[56] on vapor-grown SnO_2) to calculate an intrinsic electron density from Equation 14, excellent agreement is obtained with density values calculated from the conductivity data.

The low temperature portion of Figure 34 which is in the range of compensation controlled conduction is harder to explain. Loch[19] notes the same trend of behavior at these temperatures on compressed powders of SnO_2 although the mechanism may be vastly different since his conductivity measurements in this temperature range show an essentially constant value. Two suggestions worthy of further investigation are 1) the introduction of a new scattering mechanism associated with the pressure of a large space charge region and 2) the possibility of p-type surface conduction in an inversion layer which is used by Cimino, Molinari and Cramarossa[63] to explain the p-type character of their Seebeck voltage data on ZnO.

In Figure 35 thermoelectric power results from different fixing procedures are shown. Note the general decrease in magnitude of the thermoelectric power with increasing fixing temperature in vacuum. As stated in the model presentation, the effect of these treatments is to introduce more electrons into the conduction band. Equation 35 shows that if this is the case one would expect such behavior at least in the high temperature region where this equation is valid as long as intrinsic behavior is still partially masked by additional electrons released from surface acceptors under vacuum conditions. These fixing procedures then show results consistent with the same procedures in conductivity data further substantiating the model proposed.

Suggestions for Further Study

Further work in addition to the suggestions specifically made in the previous section is needed to ascertain more about the electrical and optical properties of the flux-grown samples. The model in a very real sense has been presented to provide a guide to further study of the surface effects, origins and densities of the donor and acceptor imperfections, and the various optical effects.

To diversify the type of investigation that can be performed, a continued effort must be expended in the area of SnO_2 crystal growth since the size of these crystals in many cases limits the types of experimentation. Impurity control by doping is mandatory for elucidating imperfection sources and for providing a better understanding of the host lattice crystal fields. Two new possibilities for growth warrant special attention. One is growth using cuprous oxide flux, in conjunction with a pulling process instead of the simple cooling process

used in this laboratory. The second is a modification of the zone refining method where a solvent such as cuprous oxide is "drawn" through a cylinder of SnO_2 powder contained in a suitable crucible and furnace. An appropriate design for ZnO growth has recently been reported by Wolff and LaBelle[64].

It is found that when crystal surfaces are abraded, chipped or cracked along their total length, the room temperature conductivity increases approximately five orders of magnitude. Figure 29 shows conductivity measurements made on a crystal with the surfaces abraded. In this case subsequent high temperature fixes in air decreased conductivity but not to the original value characteristic of crystals with as-grown surfaces. A pressure dependence of conductivity is still observed with abraded surface crystals but it is reduced in scale. These effects are very striking and need to be integrated into the conduction model. Field Effect measurements and surface potential studies should give insight into carrier lifetimes at the surface and help describe creation and destruction of surface states with temperature and pressure treatments. Work should be done on both as-grown surfaces and abraded surfaces.

Figure 31 depicts the long wavelength structure in the optical transmission data as changed by various heat treatments. The basic structure is similar to that reported by Summit and Borrelli[65] and attributed by them to combination vibrations of lattice fundamentals found at longer wavelengths on SnO_2 crystals. It is felt that a knowledge of the mechanism for the increase and decrease of the transmission at 7.5μ would shed light on the nature of the imperfections in the crystal. Two possibilities to be investigated are whether this added

absorption is due to adsorbed oxygen and its weaker-than-lattice bond to the crystal or to lattice donor impurities that have migrated to the surface causing a lattice distortion in the surface region.

The pink hue and the effectiveness of various methods for producing and bleaching it may also be associated with the lattice structure of Figure 31. The absorptions in Figure 32, however, show essentially no change with heat treatment and may be due to ions or to oxygen vacancies in the lattice. It is interesting to note that the absorption in Figure 32 just below 500 millimicrons is of the proper wavelength to cause -- when the crystal is viewed under reflected light -- a pink color. Suggestions have been advanced (e.g. by Morrison and Miller[52], Hauffe[66] and others) that heat treatments of various kinds cause ion migration from bulk to surface and vice versa. While near the surface the ion concentration may be great enough to provide perceptible color. A study of this behavior under different heat treatments coupled with diffusion work using tin and/or copper might aid in identifying these absorptions.

As mentioned earlier, a transient yellow-green color appears when the crystal are heated above 300°C in room light although this has not been visually observed in the dark. Consideration has been given to trying a glow curve analysis which could shed light on the energy values of the impurity levels and corroborate photoelectronic data. This, however, is an experiment in which the crystal size is a distinct hindrance, since radiation detection would be very difficult with small specimens.

Conductivity measurements must be extended to higher temperatures and lower pressures to verify the distinction between intrinsic and extrinsic effects. These measurements should also identify the temperature

range in which defect production begins to play a significant role in the conduction mechanism.

BIBLIOGRAPHY

1. Verwey, E. J. W., Semiconducting Materials, ed. H. K. Henisch, Butterworths Scientific Publications Ltd., London (1951).

2. Gray, T. J., Semiconducting Materials, ed. H. K. Henisch, Butterworths Scientific Publications Ltd., London (1951).

3. Gray, T. J., Chemistry of the Solid State, ed. W. E. Garner Butterworths Scientific Publications Ltd., London (1951).

4. Grant, F. A., Rev. Mod. Phys., 31, 646 (1959).

5. Heiland, G., Mollwo, E. and Stockmann, F., Paper in Solid State Physics vol 8, Acedemic Press, New York, (1959).

6. Zhuravlev, V. A. and Kulitskii, V. N., Kinetics and Catalysis, 4, 90 (1963).

7. Bevan, D. J. M., Shelton, J. P. and Anderson, J. S., J. Chem. Soc., London, 1729 (1948).

8. Arghiropoulos, B. M. and Teichner, S. J., J. Calalysis 3, 477 (1964).

9. Wyckoff, R. W. G., Crystal Structures, John Wiley and Sons (1963).

10. Bauer, G., Ann. Physik 30, 433 (1937).

11. Fisher, A., Z. Naturforsch, 9a, 508 (1954).

12. Ishiguro, K., et al., J. Phys. Soc. Japan, 13, 296 (1958).

13. Le Blanc, M. and Sache, H., Z. Physik, 32, 887 (1931).

14. Guillery, P., Ann. Physik, 14, 216 (1932).

15. Miloslavskii, V. K. and Lyaskenko, S. P., Optics and Spectrosc., tr., 7, 154 (1959).

16. Foex, M., Bull. Soc. Chem., France, 11, 6 (1944).

17. Kohnke, E. E., J. Phys. Chem. Solids, 23, 1557 (1962).

18. Hurt, J. E. and Kohnke, E. E., Relation Between Photoconductivity and Chemisorption Kinetics for Stannic Oxide Crystals. Tech. Report #2, May 1962 - Jan. 1963, Contract #Nonr.-2595(01).

19. Loch, L. D., J. Electrochem. Soc., 110, 1081 (1963).

20. Reed, T. B., Roddy, J. T. and Mariano, A. N., J. Appl. Phys., 33, 1014 (1962).

21. Marley, J. A. and MacAvoy, T. C., J. Appl. Phys., 32, 2504 (1961).

22. Houston, J. E., Photoelectronic Analysis of Imperfections in Grown Stannic Oxide Crystals. Tech. Report #4, Feb. 1965, Contract #Nonr.-2595(01).

23. Scharowsky, El, Z. Physik 135, 318 (1953).

24. Nielson, J. W. and Dearborn, E. F., J. Phys. Chem., 64, 1762 (1960).

25. Laudise, R. A., Kolb, E. D. and Caporaso, A. J., J. Am. Ceramic. Soc. 47, 9 (1964).

26. Moore Jr., C. H., Mining Trans., 184, 194 (1949).

27. Verneuil, A. V. L., Process of Producing Synthetic Sapphires, U. S. Pat. 1,004,505, Sept. 26, 1911.

28. White, E. A. D., Nature, London, 191, 901 (1961).

29. Nielson, J. W. and Dearborn, E. F., J. Phys. Chem. Solids, 5, 202 (1958).

30. Laudise, R. A. and Ballman, A. A., J. Am. Chem. Soc., 80, 2655 (1958).

31. Kunkle, H. F. and Kohnke, E. E., J. Appl. Phys., 36, 1489 (1965).

32. Harvill, M. L. and Roy, R., Am. Ceramic Soc. Bull., 44, 297 (1965).

33. Walker, A. C. and Buehler, E., Bell Laboratories Record, Jan. (1959).

34. Reed, T. B., Private Communication.

35. Kunkle, H. F., Unpublished Master's Report, Oklahoma State University (1961).

36. Urazov, G. G., Speranshaya, E. I. J. Inorg. Chem., USSR, 1, 1413 (1956).

37. Barezak, V. J. and Insley, R. H., J. Am. Ceramic Soc. Disc. and Notes, 45, 144 (1962).

38. Mellor, J. W., Mellor's Modern Inorganic Chemistry, Longman Press (1956).

39. Greninger, A. B., Trans. Am. Inst. Mining Met. Engrs. 117, 61 (1935).

40. Marley, J. A. and MacAvoy, T. C., Investigations of the Mechanism of Single Crystal Growth in High Temperature System. Final Report, June 1961 - June 1962, Contract No. AF 19(604)-8447.

41. Swanson, H. E. and Tatge, E., Nat'l.Bur. Standards (U.S.), Circ. 539, 1, (1953).

42. Blakemore, J. S., Semiconductor Statistics, Pergamon Press, New York, (1962).

43. Smith, R. A., Semiconductors, Cambridge Press, (1959).

44. Garrett, C. G. B., and Brattain, W. H., Phys. Rev., 99, 376, (1955).

45. Kingston, R. H. and Neustadter, S. F., J. Appl. Phys., 26, 718 (1955).

46. Dousmanis, G. C. and Duncan, R. C., J. Appl. Phys., 29 1627 (1958).

47. Young, C. E., J. Appl. Phys., 32, 329, (1961).

48. Seiwatz, R. and Green, M., J. Appl. Phys., 29, 1034 (1958).

49. Johnson, V. A., Article in Gibson, A. F., Progress in Semiconductors, John Wiley and Sons, New York, (1956).

50. Soffer, B. H., J. Chem. Phys., 35, 940 (1961).

51. Brunner, G., Wondratschek, H. and Laves, F., Naturwissenschaften, 46, 664 (1959).

52. Morrison, S. R. and Miller, P. H., Jr., J. Chem. Phys., 25, 1064 (1956).

53. Haber, J. and Stone, F. S., Proc. Chem. Soc, 424 (1961).

54. Morrison, R., Article in Advances in Catalysis, Acedemic Press, New York, (1955).

55. Houston, J. E. and Kohnke, E. E., J. Appl. Phys., In Press.

56. Marley, J. A. and Dockerty, R. C., Phys. Rev., 140, 304 (1965).

57. Rudolph, J., Z. Naturforsch, 14a, 727 (1959).

58. Yahia, J., Phys. Rev., 130, 1711, (1963).

59. Shear, H., Hilton, E. A. and Bube, R. H., J. Electrochem. Soc., 112, 997 (1965).

60. Pearson, G. L. and Bardeen, J., Phys. Rev., 75, 865 (1949).

61. Arai, T., J. Phys. Soc. Japan, 15, 916 (1960).

62. Reddaway, S. F. and Wright, D. A., Brit. J. Appl. Phys., 16, 195 (1965).

63. Cimino, A., Molinari, E. and Cramarossa, F. J., Catalysis, 2, 315 (1963).

64. Wolff, G. A. and LaBelle, H. E., Jr., J. Am. Cer. Soc., 48, 441 (1965).

65. Summitt, R. and Borrelli, N. F., J. Phys. Chem. Solids, 26, (1965).

66. Hauffe, K, Article in Advances in Catalysis, Acedemic Press, New York, (1955).

APPENDIX

```
     MON$$       JOB  223340009
     MON$$       ASGN MGO,A2
     MON$$       ASGN MJB,A3
     MON$$       MODE GO,TEST
     MON$$       EXEC FORTRAN,,,,,,,XRAYPRO
      DIMENSIONITS(101),RECHTS(101),XLINKS(101),A(30,30)
      COMMONA,J
00002 FORMAT(I4,2X,F7.5,2X,F6.4,2X,I2,2X,I2,2X,I4)
00003 FORMAT(1H1,2X,7HFILM=E-,I4,6X,6HDATE= ,I2,1H/,I2,1H/,I4,6X,
     C11HWAVELENGTH=,F8.5,4X,28HSHRINKAGE COR
00004 FORMAT(F5.3,1X,F5.3,1X,I2)
00009 FORMAT(2X,25HCENTER FRONT REFLECTIONS=,F9.5,/)
00018 FORMAT(2X,4HLINE,6X,4HLEFT,6X,5HRIGHT,4X,14HTHETAS(COR)    ,
     C41HSINES    SINSQR    INTENSITIES   D-V
00020 FORMAT(2X,I2,5X,F8.3,2X,F8.3,4X,F8.4,3X,F9.6,1X,F9.6,6X,I3,
     C6X,F8.5)
00012 READ(1,2)IFILM,RAD,CORFAC,MONTH,IDAY,IYEAR
00050 IF(IFILM.EQ.0)STOP
00057 WRITE(3,3)IFILM,MONTH,IDAY,IYEAR,RAD,CORFAC
      CENTER=0.0
      TAB=0.0
      J=1
00005 READ(1,4)XLINKS(J),RECHTS(J),ITS(J)
      IF(XLINKS(J).EQ.0.0)GOTO32
      IF(RECHTS(J).EQ.0.0)GOTO39
00007 CENTER=CENTER+(RECHTS(J)+XLINKS(J))/2.0
      TAB=TAB+1.0
      GOTO39
00032 IF(RECHTS(J).EQ.0.0)GOTO8
00039 J=J+1
      GOTO5
00008 GENCEN=CENTER/TAB
      WRITE(3,9)GENCEN
      WRITE(3,18)
      JJ=J-1
      DO22M=1,JJ
      IF(XLINKS(M).NE.0.0)GOTO13
      DEGREE=5.0*((RECHTS(M)-GENCEN)*CORFAC)
      GOTO17
00013 IF(RECHTS(M).NE.0.0)GOTO15
      DEGREE=5.o*(GENCEN-XLINKS(M))*CORFAC
      GOTO17
00015 DEGREE=2.5*(RECHTS(M)-XLINKS(M))*CORFAC
00017 THETA=DEGREE*0.01745329  (Omit for Back Reflection)
00017 THETA=1.570795-DEGREE*.01745329   (Omit for Front Reflection)
```

```
      SN=SIN(THETA)
      A(M,1)=SN*SN
      DAV=RAD/(2.0*SN)
00022 WRITE(3,20)M,XLINKS(M),RECHTS(M),DEGREE,SN,A(M,1),ITS(M),DAV
      IF(J.LT.31)CALLMATRIX
      GOTO12
      END
     MON$$      EXEQ FORTRAN
      SUBROUTINEMATRIX
      DIMENSIONITS(101),RECHTS(101),XLINKS(101),A(30,30)
      COMMONA,J
00030 FORMAT(1X,I2,15(F8.5))
00035 FORMAT(2X,I2,15(F8.5))
00040 FORMAT(1H1,44H  TABLE OF DIFFERENCES FOR SIN SQUARED THETA,///)
00045 FORMAT(1H1,23H  DIFFERENCES CONTINUED,//)
      WRITE(3,40)
      JJ=J-1
      DO1011=2,JJ
      DO100K=I,JJ
      A(K,I)=A(K,1)-A(I-1,1)
00100 CONTINUE
00101 CONTINUE
      DO110L=1,15
00110 WRITE(3,30)L,(A(L,N),N=1,L)
      IF(J.LE.15)RETURN
      DO120L=16,J
00120 WRITE(3,30)L,(A(L,N),N=1.15)
      WRITE(3,45)
      DO130L=16,J
00130 WRITE(3,35)L,(A(L,N),N=16,L)
      RETURN
      END
     MON$$      EXEQ LINKLOAD
                PHASE  RAYX
                CALL XRAYPRO
     MON$$      EXEQ RAYX,MJB
```

VITA

Howard Franklin Kunkle Jr.

Candidate for the Degree of

Doctor of Philosophy

Thesis: HIGH TEMPERATURE CONDUCTIVITY OF GROWN STANNIC OXIDE SINGLE CRYSTALS

Major Field: Physics

Biographical:

Personal Data: Born at Pittsburgh, Pennsylvania, March 9, 1937, the son of Edna and Howard Kunkle.

Education: Attended elementary school in Belleview and McMurray, Pennsylvania; graduated from Peters Township High School, McMurray, Pennsylvania, in 1955; received the Bachelor of Arts degree from Washington and Jefferson College, Washington, Pennsylvania, with a major in Physics, in June, 1959; received the Masters of Science degree from Oklahoma State University, with a major in Physics, in August, 1961.

Professional Experience: After receiving the Master of Science degree, worked the summer of 1962 with Westinghouse, Astronuclear Laboratory, Pittsburgh, Pennsylvania.